UNIVERSITÉ
de Cergy-Pontoise

UNIVERSITÉ DE CERGY PONTOISE

THÈSE

présentée pour obtenir le grade de

Docteur en Sciences

Spécialité Physique Théorique

par

Sahbi El Hog

Phase Transition in Thin Magnetic Films with Competing Interactions

Soutenue le 3 Mai 2017 devant le jury composé de

Prof. Kamel Boukheddaden	Université de Versailles Saint-Quentin	Rapporteur
Prof Alexander K. Hartmann	University of Oldenburg, Germany	Examinateur
Prof. Pascal Monceau	Université Paris Diderot	Examinateur
Prof. Dominique Mouhanna	Université Pierre et Marie Curie	Rapporteur
Prof. Henri Orland	CEA	Examinateur
Prof. Pascal Viot	Université Pierre et Marie Curie	Examinateur
Prof. Hung T. Diep	Université de Cergy-Pontoise	Directeur de thèse

Abstract

In this thesis, we study the phase transition and thermodynamic properties of classical and quantum spin models in thin films using both Green's function and standard Monte Carlo simulation.

In chapter 1, we study the Blume-Emery-Griffith model in a thin film of stacked triangular lattices. The model is described by three parameters a bilinear exchange interaction between spins J, a biquadratic exchange interaction K and a single ion anisotropy D. The spin S_i at the lattice i takes three values $(\pm 1, 0)$. This model has been introduced to describe the mixing phase of superfluid He^4 ($S_i = \pm 1$) and normal fluid He^3 ($S_i = 0$) at low temperatures, such system undergoes two kinds of phase transition, first and second-order ones. Our work has been motivated by the desire, on the one hand to see if the nature of the phase transition is still conserved when we reduce the film thickness and on the other hand to verify if the cross-over from the second-order to first-order transition in the bulk is also conserved in thin films. Using Monte Carlo simulations, we show that there exists a critical value of D below (above) which the transition is of second (first) order, and that the first-order nature of the transition does not disappear when we reduce the film thickness unlike in other systems where the bulk first-order transition becomes a second-order one at a small-enough thickness. In the Helium vocabulary, we show that the film surfaces have a deficit of He^4 with respect to the interior layers of the film.

In chapter 2 we first study quantum properties of a helimagnetic thin film of simple cubic lattice with the Heisenberg spin model. Surface effects in thin films have been intensively studied during the last three decades. However, due to the complicated surface spin configurations, surface effects in helimagnetic thin films have only been recently studied. Using the Green's function method for non-collinear spin configurations, we find that the spin configuration across the film is strongly non-uniform. We show that there exist surface acoustic and optical modes which affect the surface magnetization. We also show that quantum fluctuations cause the spin contraction at $T=0$ and give rise to a cross-over between layer magnetizations at low temperatures. In

the second part of chapter 2, we are interested in the effect of an external magnetic field applied along the c-axis perpendicular to the film surface using both classical and quantum Heisenberg spins. We show that spins react to a moderate applied magnetic field by creating a particular spin configuration along the c-axis. Using Monte Carlo simulation we study the phase transition as functions of the magnetic field strength, the temperature and the film thickness. We show that the system undergoes a phase transition triggered by the destruction of the transverse (in-plane) xy spin-components ordering of a number of layers, not all layers. This partial phase transition is not usual in thin films where one observes more often the disordering of the surface layer, not an interior layer. At low temperatures, we investigate effects of quantum fluctuations using Green's function method. The results show that the zero-point spin contraction is different from layer to layer. We also find a crossover of layer magnetizations which depends on the magnitude of the helical angle.

In the third chapter, we introduce the in-plane Dzyaloshinskii-Moriya interaction (DM). This kind of interaction was proposed to explain the weak ferromagnetism which was observed in antiferromagnetic Mn compounds. It has been shown in various works that the DM interaction is at the origin of topological skyrmions and new kinds of magnetic domain walls. In this chapter, we are interested in the spin-wave properties of a system of spins interacting with each other via a DM interaction. Using the steepest descend method we find a non-collinear ground state which is due to the competition between the ferromagnetic and the asymmetric DM interactions. We use the Green's function theory to calculate the spin-wave spectrum and the layer magnetization at finite temperatures in two and three dimensions as well as in a thin film with free surfaces. We find that the spin-wave excitation in 2D and 3D crystals is stable at T=0 without the need of an anisotropy, but in the case of a thin film we need a small anisotropy to stabilize the spin-wave spectrum because of the lack of neighbors at the surface. We find also that the spin-wave energy is proportional to k^2 for a small DM interaction and is linear in k for a strong one.

Finally, in the fourth chapter we are interested in skyrmion crystals created by the competition between the ferromagnetic interaction and the DM interaction under an applied magnetic field. They arrange themselves in a periodic structure. These skyrmion crystals have been experimentally observed in MnSi compounds and in doped semiconductors. Using Monte Carlo simulations, we show that skyrmion crystals are stable at finite temperatures up to a transition temperature where the topological structure of each skyrmion and the periodic structure of the skyrmion crystal are destroyed. We also investigate the relaxation of the skyrmions in the crystalline phase and find

that the relaxation time follows a stretched exponential law which is a characteristic of slowly-relaxed systems such as spin glasses.

Chapter 5 is devoted to the general conclusion with a summary of the results of the thesis and a discussion on future developments of the present work with regard to the transport properties.

Résumé

Dans cette thèse nous étudions les transitions de phase et les propriétés thermodynamiques des couches minces en se basant sur des simulations Monte Carlo et sur le formalisme de la fonction de Green.

Dans le premier chapitre, nous étudions le modèle de Blume-Emery-Griffith pour un film mince sur réseaux triangulaires empilés. Le modèle se décrit par trois paramètres : une interaction d'échange bilinéaire J, une interaction d'échange biquadratique K et un terme d'anisotropie D. Le spin S_i dans ce modèle prend trois valeurs $(\pm 1, 0)$. Ce modèle a été conçu afin de décrire un mélange de He^3 et He^4. Ce mélange binaire montre deux types de transition de phase, une du premier ordre et l'autre du second ordre. Notre travail a été motivé par le désir de vérifier si la nature de la transition de phase se conserve quand on réduit l'épaisseur du film. En utilisant la simulation Monte Carlo, nous montrons qu'il existe une valeur critique de D où la transition change de nature. Nous montrons ainsi que la nature du premier ordre ne disparaît pas lorsque nous réduisons l'épaisseur du film contrairement à d'autres systèmes où la transition du premier ordre devient du second ordre. Dans le vocabulaire de l'hélium, nous montrons que le surface du film présente un déficit de He^4 par rapport aux couches intérieures.

Dans le deuxième chapitre, nous étudions les propriétés quantiques des couches minces hélimagnétiques pour une structure cubique en utilisant le modèle de Heisenberg. Les effets de surface dans les films minces ont été intensément étudiés au cours des trois dernières décennies, cependant en raison des configurations compliquées de spin de surface, les effets de surface dans les films minces hélimagnétiques n'ont été que récemment étudiés. Nous montrons que la configuration de spin à travers le film est fortement non uniforme. En utilisant la méthode de fonction de Green pour les configurations non-colinéaires des spins, nous montrons qu'il existe des modes de d'ondes de spin de surface qui affectent la magnétisation de surface, nous montrons également que les fluctuations quantiques provoquent la contraction des spins à $T = 0$ et donnent lieu à un croisement entre les magnétisations de couche à basse température. Dans la deuxième partie du chapitre, nous nous intéressons à

l'effet d'un champ magnétique appliqué perpendiculairement à la surface du film. Nous montrons que les spins réagissent en créant une configuration particulière. En utilisant la simulation Monte Carlo nous étudions la transition de phase en fonction de l'intensité du champ appliqué. Nous montrons que le système subit une transition de phase déclenchée par la destruction des composantes transversales xy des spins de certaines couches. Cette transition partielle n'est pas habituelle dans les films minces où on observe le plus souvent la destruction des couches superficielles, et non les couches intérieures. À basse température, nous étudions les effets des fluctuations quantiques en utilisant la méthode des fonctions de Green. Les résultats montrent que la contraction des spins à $T = 0$ est différente d'une couche à l'autre. Nous trouvons également un croisement des magnétisations de couche qui dépend de l'ampleur des angles hélicoïdaux.

Dans le troisième chapitre, nous introduisons l'interaction de Dzyaloshinskii-Moriya (DM). Ce type d'interaction a été proposé pour expliquer le faible ferromagnétisme qui a été observé dans les composés antiferromagnétiques à base de Mn. Il a été montré dans de divers travaux que l'interaction DM est à l'origine de la formation des skyrmions et de nouveaux genres de parois de domaines magnétiques. Dans ce chapitre , nous nous intéressons aux propriétés quantiques d'un système de spins qui interagissent les uns avec les autres via une interaction DM et une interaction ferromagnétique. En utilisant la méthode "steepest descend", nous trouvons un état fondamental non-colinéaire qui est dû à la compétition entre l'interaction ferromagnétique et l'interaction asymétrique DM. Utilisant la théorie des fonctions de Green, nous calculons le spectre des ondes de spin et la magnétisation, couche par couche, à température finie en deux et trois dimensions ainsi que dans un film mince avec des effets de surface. Nous constatons que l'excitation des ondes de spin dans les cristaux 2D et 3D est stable à $T = 0$ sans la nécessité d'une anisotropie, mais dans le cas d'un film mince nous avons besoin d'une faible anisotropie pour stabiliser le spectre en raison du manque de voisins à la surface. On trouve aussi que l'énergie des ondes de spin est proportionnelle à k^2 (k: vecteur d'onde) pour les faibles valeurs de DM et à k pour les interactions fortes.

Dans le quatrième chapitre, nous nous intéressons aux cristaux de skyrmions créés grâce à la compétition entre l'interaction ferromagnétique, l'interaction DM et le champ magnétique appliqué. Ces skyrmions s'organisent dans une structure périodique. Ils ont été observés expérimentalement dans les composés MnSi, FeCoSi et dans les semiconducteurs dopés. En utilisant la simulation Monte Carlo, nous montrons que les cristaux de skyrmions sont stables à des températures finies et jusqu'à la transition où la structure topologique de chaque skyrmion et la structure périodique du cristal de skyrmions sont

détruites. Nous étudions également la relaxation des skyrmions dans la phase cristalline et nous constatons que le temps de relaxation suit une loi exponentielle étirée

Remerciements

Je tiens à remercier mon directeur de thèse Hung The Diep pour son encouragement, pour le temps qu'il m'a consacré et surtout pour la patience dont il a fait preuve à mon égard. Je lui suis infiniment reconnaissant.

Je remercie Messieurs Kamel Boukheddaden et Dominique Mouhanna d'avoir accepté d'être les rapporteurs de cette thèse ainsi que Messieurs Pascal Viot, Pascal Monceau, Henri Orland et Alexander Hartmann d'avoir accepté de faire partie du jury.

Je tiens à remercier mes collègues Aurélien Bailly-Reyre et Valentin Bois avec qui j'ai passé la majeur partie de ces trois années. J'exprime ma gratitude envers Sylvie Villemin, Guy Trambly, Cédric Gérard, Fabien Piguet et Yann Costes. Mes remerciements vont aussi à Quentin Duprey et Pierre Fromholz et tous les membres du LPTM qui, de près ou de loin, m'ont soutenu dans ce travail.

Enfin, merci à ma mère et ma sœur qui ont toujours cru en moi. Merci pour avoir fait de moi ce que je suis aujourd'hui.

Contents

Introduction

Spin systems are the primary object of study in condensed matter, as well as in statical mechanics. They are capital for our understanding of thermal phase transition, critical phenomena and quantum properties.

The motivation of this thesis is to study the combined effects of the presence of a surface and the existence of a frustration due to competing interactions in thin films.

On the one hand, investigations of spin systems in unfrustrated thin films have seen a spectacular development during the last 30 years. The ability to control their properties lead to many applications in technology such as in magnetic data storage devices and spin transport [1, 2]. Thin films show fundamental magnetic and electronic properties different from those of the bulk due to the loss of the spatial periodicity. In thin films, magnetic properties are influenced by the presence of the surfaces. They destabilize bulk spin wave modes by creating localized surface modes which affect physical behaviors of thin films at finite temperature such as the reduction of the critical temperature and the low surface magnetization. Exchange interactions between spins lying on the surface are also affected due to the lack of neighbors and to various neighboring defects: they are often different from those of the interior layers. Thin films also offer a lot of opportunities to discover new microscopic phenomena leading to potential electronic applications. One has seen in recent years applications using phenomena such as giant magnetoresistance, spin transfer torque and spin valves [3, 4]. Theoretically, surface effects in thin films such as surface phonon, surface magnon, surface plasmon have been widely studied [5].

On the other hand, during the last 30 years intensive researches have been carried out to understand properties of frustrated spin systems [6]. The frustration is due to competing interactions between spins or to the crystal geometry which is incompatible with the magnetic interaction as in the antiferromagnetic triangular lattice. The frustration leads to numerous spectacular effects such as high ground state degeneracy, non-collinear ground state spin configurations, partially disordered systems, reentrance, multiple phase

transitions, order by disorder. The concept of frustration has been introduced by Villain [7] and Toulouse [8] in the context of spin glasses to describe the impossibility of simultaneously satisfying all exchange interactions. A system of spins is said to be frustrated when the energy of the ground state does not correspond to the minimum energy of each spin. In such a situation, the compromise between ferromagnetic ordering and antiferromagnetic ordering leads to a non collinear ground state spin configuration such as the helical structure or to a more complicated one, the skyrmion. As said, the frustration can have two origins:

Geometric frustration arises when the exchange interaction between spins are not compatible with the lattice geometry in the case of antiferromagnetic couplings: on a square lattice neighboring spins put themselves in opposite directions so all exchange interaction are satisfied, however on a triangular lattice, there is no way to make all interactions satisfied.

Competing interactions can give rise to a frustration. It is at the origin of very interesting phenomena in a variety of systems such as helimagnets which result from the competition between ferromagnetic and antiferromagnetic interactions. This kind of structures have been observed experimentally in rare-earth metals like Holmium, Terbium and Dysprosium. We can mention also the case of spin glasses. These interactions are generally symmetrical with respect to the permutation of two spins. This is not the case with the Dzyloshinskii-Moriya interaction. The competition between this interaction and the symmetric one gives rise to an interesting structure which is non-collinear. This kind of structure is observed in many system such as MnSi [9, 10] and FeCoSi [11].

We focus in this thesis on the study of properties of spin systems resulting from the combination of surface effects and frustration effects. To this end we study different spin models in thin magnetic films with competing interactions.

The methods we use are the Green's function method and Monte Carlo simulations. The Green's function method is suitable for calculating quantum properties for non-collinear magnets at low temperature such as the spin wave spectrum, the layer magnetization and the zero-point spin contraction. Monte Carlo simulations are used to investigate the phase transition and the surface effect with the classical Heisenberg model.

We start by investigating the effect of the competition between symmetric interactions in the Blume-Emery-Griffiths model. Such system has a phase separation, due to the competition interaction between the exchange interaction J, the biquadratic exchange interaction K and the single ion anisotropy D. Using Monte Carlo simulations, we will see that the nature of the phase transition is not altered, and that the cross-over phenomenon observed in the

bulk is conserved when we reduce the film thickness, unlike in other systems where the 3D first order transition becomes a second order transition at a very small thickness. This model has been introduced to explain the phase diagram of the mixtures He^3-He^4. Using this approach we will associate He^4 atoms to spins ± 1 and He^3 atoms to spins 0. Under this identification purely phenomenological, we will see that the film surface shows a deficit of He^4 with respect to interior layers.

In chapter II we will study properties of a helimagnetic thin film with both quantum and classical Heisenberg spin models. After determination of the ground state, we will show that this spin configuration is not uniform across the film due to the surface effect. Using the Green's function method we investigate quantum properties of the film. We will show that the existence of surface modes affects the surface magnetization and that quantum fluctuations cause a spin contraction at $T = 0$. Then we will study the effect of an applied magnetic field perpendicular to the film surface. Using Monte Carlo simulations we will show that the spin arrange themselves in a non uniform structure around the axis perpendicular to the film surface. This structure undergoes a partial phase transition triggered by the destruction of the transverse xy-spin components of some layers.

In chapter III we study quantum properties of a spin system with competition interactions between a symmetric interaction and an asymmetric interaction. As we will see the ground state is non collinear. We will show that for this system the spin wave energy is stable at $T = 0$ without the need of an anisotropy in the case of 2D and 3D crystals. However, in thin films an anisotropy is needed to stabilize the spin wave spectrum. We show that the spin wave energy is proportional to k^2 like in a ferromagnet for a small value of the asymmetric DM interaction, and that it is proportional to k as in an antiferromagnet for a strong DM interaction.

In chapter IV we focus on the study of skyrmion crystals. In our model, these structures are the result of the competition between a ferromagnetic interaction and a DM interaction in an applied magnetic field. We will show, using Monte Carlo simulations that our model can reproduce experimental results. At zero field, spins of the system form a nano-size stripe domains and when we increase the field, these stripe domains are transformed into bubbles and arrange themselves in a periodic structure, namely a crystal of skyrmions. We will show that these skyrmions are stable up to the transition temperature where the bubble structure and the periodic structure of the skyrmion crystal are destroyed. As we will see, the relaxation time follows a stretched exponential law.

The last chapter is devoted to a general conclusion of the present thesis.

Chapter I

Blume-Emery-Griffiths Model

Contents

I.1 Introduction

The Blume-Emery-Griffiths (BEG) model is a spin-1 Ising model. It was originally introduced in 1971 by Blume, Emery and Griffiths in order to explain the phase separation and superfluidity in the He^3-He^4 mixtures [12]. It has been a great success since it was able to describe such mixtures and predict the order of the phase transition. This model can also describe properties of a variety of systems such as semiconductor alloys [13] and microemulsions [14].

From a theoretical point of view, the BEG model exhibits a rich phase diagram and a multitude of critical behaviors. It has been studied with

a variety of techniques such as mean-field [12, 15], renormalization group theory [16], and Monte Carlo (MC) simulations [17, 18].

We use this model to study magnetic properties of thin films. The spin in this model has three states $(\pm 1, 0)$. A site with a value 0 represents a vacant site. The system is considered as a dilute magnetic system in which the number of vacant sites varies as a function of temperature (T). In the helium approach He^3 is associated to spin 0 and He^4 to spin ± 1 [12,17]. Other models extended from the original BEG model have been recently introduced to study the effects of vacancies and of the continuous degrees of freedom in the mixtures [19,20]. We note that this model has been studied by a number of authors in thin films of simple cubic lattice structure using the mean-field approximation, they found a very rich phase diagram with a tricritical point and a staggered quadrupolar phase [21].

The aim of the chapter is to study the BEG model in a thin film of stacked triangular lattices using Monte Carlo simulations, in order to now if results of bulk BEG model remain valid in films, and to see if transition criticality can be altered when we reduce the film thickness as we have seen in Refs. [22,23]: there is a cross-over from three dimensional criticality to two dimensional universality with decreasing thickness for a second order transition, and the 3D first-order transition becomes a second order transition at very small thickness, and to show that at finite temperature in the superfluid phase, the film thickness shows a deficit of He^4 with respect to interiors layers.

The organization of the chapter is as follows: in section I.2 we present the phase diagram of mixtures He^3-He^4, in section I.3 we present the model and the simulation method. Results will be shown and discussed in section I.4.

I.2 Phase Diagram

Helium has two stable isotopes, He^3 which is a fermion, and He^4 which is a boson, we can represent the He^4 atoms by wave-functions $\varphi = |\varphi| e^{i\theta}$. In the Blume-Emery-Griffiths approximation, it was suggested to simplify the phase of the wave-functions by plus one if $\theta \in [0, \pi[$ and minus one if $\theta \in [\pi, 2\pi]$. In this representation He^4 will be superfluid when all are aligned, like a magnetic material which becomes magnetized when all spins are aligned. Using the Blume-Emery-Griffiths model we can determine the phase diagram of the mixture He^3-He^4 where He^4 atoms are represented by $(S_i = \pm 1)$ and He^3 atoms by $(S_i = 0)$.

The mixture presents a rich phase diagram as shown in Figure I.1 which exhibits three distinct phases: a He^4-rich phase called superfluid phase, where He^4 atoms are in majority and He^3 atoms are randomly distributed between

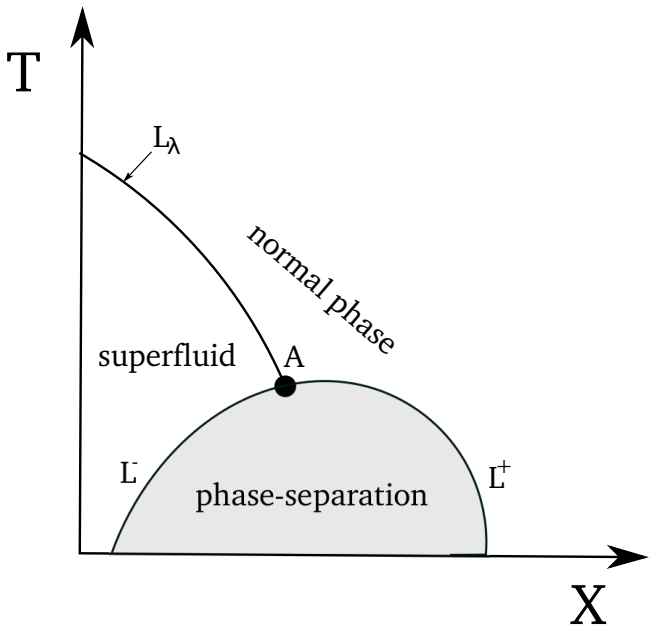

Figure I.1: Schematic phase diagram of He^3-He^4 in the $(T-X)$ plane, where X present the He^3 concentration.

them, a normal phase where He^3 and He^4 are equal in number and randomly distributed, and a phase separation where we have the coexistence of the normal and superfluid phases, namely a He^4-rich and a He^3 poor phases. In pure He^4, there is a second-order phase transition from a normal fluid to a superfluid phase. When it is diluted with He^3, the superfluid transition temperature decreases, the phase separation increases and the second-order L_λ-line terminates in the tricritical point A separating the second-order transition region from the first-order region. The order parameter for the mixture is the uniform average of the total spin M defined by

$$M = \frac{1}{N}\sum_{i}^{N}\langle S_i\rangle \tag{I.1}$$

The order parameter M is an Ising-like order parameter. In the Ising model the spin S_i takes the values ± 1 and $S_i^2 = 1$ at every site, but in the present model the spin can take the values $\pm 1, 0$ and S_i^2 can be zero or unity, we can interpret $\langle S_i^2\rangle$ as the density of He^4 atoms and $1-\langle S_i^2\rangle$ as the density of He^3 atoms. The number of He^3 and He^4 atoms are given by

$$\widehat{N_3} = \sum_{i}^{N}(1-S_i^2), \qquad \widehat{N_4} = \sum_{i}^{N} S_i^2 \tag{I.2}$$

where $\widehat{N_3} + \widehat{N_4} = N$, the total number of particles, the concentration of He^3 atoms is given by

$$X = \langle \widehat{N_3} \rangle / N \tag{I.3}$$

In the mixture He^3-He^4, experiments [24] revealed that for a concentration X of He^3 atoms below the tricritical concentration $X_{tri} = 63\%$ and above the tricritical temperature $T_{tri} = 0.87$, the mixture shows a phase transition of second order between the normal phase and the superfluid phase. If the temperature $T < T_{tri}$ a phase separation appears and the transition becomes of first order.

I.2.1 Order of the phase transition

Phase transitions are classified according to the analytical behavior of thermodynamic functions such as the free energy F. The order is given by the order from which the derivative of F is no longer continuous. A phase transition is called of first order if physical quantities such as the average energy E and the average magnetization M, which are the first derivatives of the free energy F, are discontinuous. It is called of second order if specific heat C_v and susceptibility χ, which are second derivatives of F, diverge. Figure I.2 shows schematically the magnetization observed in the first- and second-order transitions.

The mixture of He^3-He^4 shows two phase transitions, one of second order from superfluid phase to normal phase, and the other of first order from the phase-separation to both superfluid or normal phase.

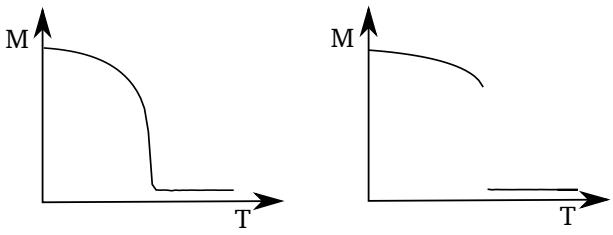

Figure I.2: Schematic of order parameter M as a function of temperature. Left: aspect of a second-order phase transition. Right: discontinuity of M at a first-order transition.

Tricritical point: The tricritical nomenclature of point A shown in Fig. I.1 comes from the fact that in a phase space, three transition lines meet [25]. In the phase diagram, the lines $L^{\pm}$ represent the first-order phase transition, they join the line L_λ which is the second-order transition line at the tricritical point A.

I.3 The BEG Model

The BEG model was proposed by Blume, Emery and Griffiths to describe a system with three states per spin. It has two terms, the first is

$$\mathcal{H}_s = -J \sum_{\langle i,j \rangle} S_i S_j \tag{I.4}$$

where the spin variable takes the value $S_i = -1, 0, 1$, $\sum_{\langle i,j \rangle}$ denotes a summation over all nearest-neighbors (NN) and J denotes the bilinear spin interaction which allows the appearance of the ferromagnetic order which is interpreted as a superfluid, such identification is purely phenomenological, when the concentration of He^3 atoms is zero the Hamiltonian $\mathcal{H}_s$ becomes an Hamiltonian for Ising ferromagnet. The presence of He^3 atoms is similar to an introduction of non magnetic impurities which affects the transition temperature T_c and the superfluidity when the concentration is sufficiently large because the mixture can support superfluid ordering by breaking into two phases (phase separation). To modulate this phase separation they added a second term which describes the isotropic interaction between the different entities which is presented by the Hamiltonian:

$$\begin{aligned} \mathcal{H}_Q = & - K_{33} \sum_{\langle i,j \rangle} (1 - S_i^2)(1 - S_j^2) - K_{44} \sum_{\langle i,j \rangle} S_i^2 S_j^2 \\ & - K_{34} \sum_{\langle i,j \rangle} [S_i^2 (1 - S_j^2) + S_j^2 (1 - S_i^2)] \end{aligned} \tag{I.5}$$

where $K_{\alpha\beta}$ represents the effective interaction between He^{α}-He^{β}. The full model is represented by the following $\mathcal{H}$ where μ_3 and μ_4 are the chemical potentials which are added to preserve the number of particles:

$$\mathcal{H} = \mathcal{H}_s + \mathcal{H}_Q - \mu_3 \langle \widehat{N}_3 \rangle - \mu_4 \langle \widehat{N}_4 \rangle \tag{I.6}$$

which is rewritten under the form:

$$\mathcal{H} = -J \sum_{\langle i,j \rangle} S_i S_j - K \sum_{\langle i,j \rangle} S_i^2 S_j^2 + D \sum_i S_i^2 - N(zK_{33} + \mu_3) \tag{I.7}$$

where $K = K_{33} + K_{44} - 2K_{34}$ is the biquadratic exchange interaction, z the coordination number and $D = \mu_3 - \mu_4 + 2z(K_{33} - K_{44})$ the single-ion crystal field. Omitting the last term of Eq. (I.7) we write

$$\mathcal{H} = -J \sum_{\langle i,j \rangle} S_i S_j - K \sum_{\langle i,j \rangle} S_i^2 S_j^2 + D \sum_i S_i^2 \tag{I.8}$$

The model is mapped over the triangular lattices stacked in the z-direction with L_z layers, where each lattice site is occupied by a spin S_i. A He^3 atom at site i corresponds to $S_i = 0$ and a He^4 atom to $S_i = \pm 1$. We have chosen the stacked triangular lattices to have a large coordination number of neighbors. Since we worked with very thin films with small quantities of matter, such a large coordination number reduces numerical errors on numerical statistical fluctuations.

Since we work at a given temperature T (canonical method) we leave the system to determine the concentration of He^3 and He^4 at equilibrium at each given T. When the concentration of He^3 is zero, all spins take the value ± 1 and Eq. (I.8) becomes an Ising Hamiltonian. On the other hand, the presence of He^3 decreases the critical temperature, and when the concentration is sufficiently large the system is broken into two phases, superfluid phase and normal phase.

The He^3 concentration depends also on the chemical potential D, where a nonzero value of D favors the proliferation of zero spins in the system and lowers the transition temperature between the superfluid and normal fluid phase. By increasing D the system can support superfluid ordering but with the appearance of a phase separation.

I.3.1 Simulation Method

We use the standard MC simulation to calculate properties of the system at finite temperatures for the size of $L \times L \times L_z$, where L_z is the film thickness. Periodic boundary conditions are used in the xy plane and two free symmetric surfaces are supposed in the z-direction . The standard MC method is used to study the phase transition. In general, we discard 10^5 MC steps per spin to equilibrate the system at temperature T before averaging physical quantities over the next 10^5 MC steps. For histograms, we record in general 10^6 MC steps per spin. The lattice sizes used in our simulations are L=20,30,...,120,300 and L_z=4,8,12,16.

The averaged energy and the specific heat per spin are defined by

$$\langle E \rangle = \frac{\langle H \rangle}{N} \tag{I.9}$$

$$C_v = N \frac{\langle E^2 \rangle - \langle E \rangle^2}{K_B T^2} \tag{I.10}$$

where $\langle ... \rangle$ indicates the thermal average. The order parameter is defined by Eq. (I.1). The susceptibility is defined by

$$\chi = \frac{\langle M^2 \rangle - \langle M \rangle^2}{K_B T} \tag{I.11}$$

I.4 Simulation Results

Let us take $J = 1$ and $K = 1$, namely ferromagnetic interaction between NN. Before showing the results for thin films, let us show the results for the bulk properties of the BEG model applied to the stacked triangular lattice. These results by symmetry argument do not bring new physics with respect to the case of simple cubic lattice [12]. However, these results provide elements for comparison with the film case which will be shown in details below.

I.4.1 Bulk case

We show in Fig. I.3 the energy E, the magnetization M, the susceptibility χ, and the specific heat C_v versus T in the bulk case for several values of D in the tricritical region. As seen, the transition is continuous for $D < D_c \simeq 7.5$ and discontinuous for $D > D_c$. The magnetization shows also a discontinuity for $D > D_c$.

We calculate the critical temperature as function of D. We keep D constant, vary the temperature, and we take the critical temperature at the peak of the magnetic susceptibility χ (see Fig. I.3). The results for the critical temperature are shown in Fig. I.4(top). The second-order phase transition starts at $D = 0$, $T_c = 5.34$ and T_c decreases as D increases. The cross-over from the second order to the first order occurs at $D_c \simeq 7.6$.

In the first-order phase transition the concentration X of He^3 atoms jumps at the value $D_c = 7.6$ from a lower to higher concentration. This behavior is observed in Fig. I.4 . Around the critical value D_c, the system jumps between the states with high and low concentrations.

I.4.2 Film case

For a given film thickness, we study in the same manner the behavior of the BEG model for different values of D by calculating the energy, specific heat, the layer magnetization and the energy histogram.

The curves E and M in Fig. I.5 present a second-order phase transition at $T_c \simeq 3.82$. With increasing D, the system undergoes a first-order transition. We show in Fig. I.6 the case of D=7.3 where one observes a discontinuity at the transition temperature $T_c \simeq 2.694$.

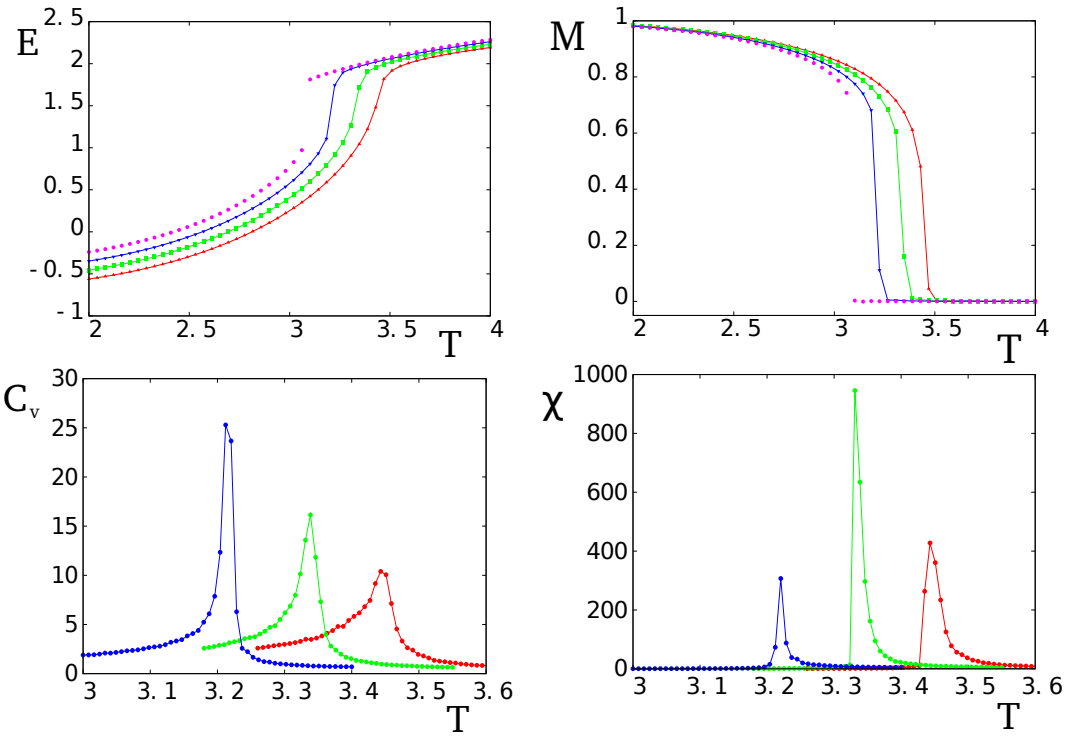

Figure I.3: Energy E, magnetization M, susceptibility χ, and specific heat C_v versus T around the tricritical D of the bulk case. From right to left: $D = 7.3, 7.4, 7.5$ and 7.6.

Using the histogram technique, we explored the transition region to search for the nature of the transition. For D=6, we obtain only a one-peak structure at the critical temperature as seen in Fig. I.7(top). The energy histogram taken at T_c in the case D=7.3 exhibits a double-peak structure as shown in Fig. I.7(bottom), thus confirming the first-order character of the transition [26].

At a first-order transition the order and disorder phases coexist. In most cases, the system has mixed domains of two phases at the same time, the energy of the system is thus the average of the energies of the two phases $(E_1+E_2)/2$. It is however possible that at the transition the system goes back and forth between the two phases during the time evolution. This is what we observe here: we show in Fig. I.8 how the energy and the magnetization evolve during the equilibration time of 10^5 MC steps/spin. There are several remarks:

(i) In a general manner, in MC simulations a trick to use to check the equilibrium time is to do two simulations one with a random initial spin

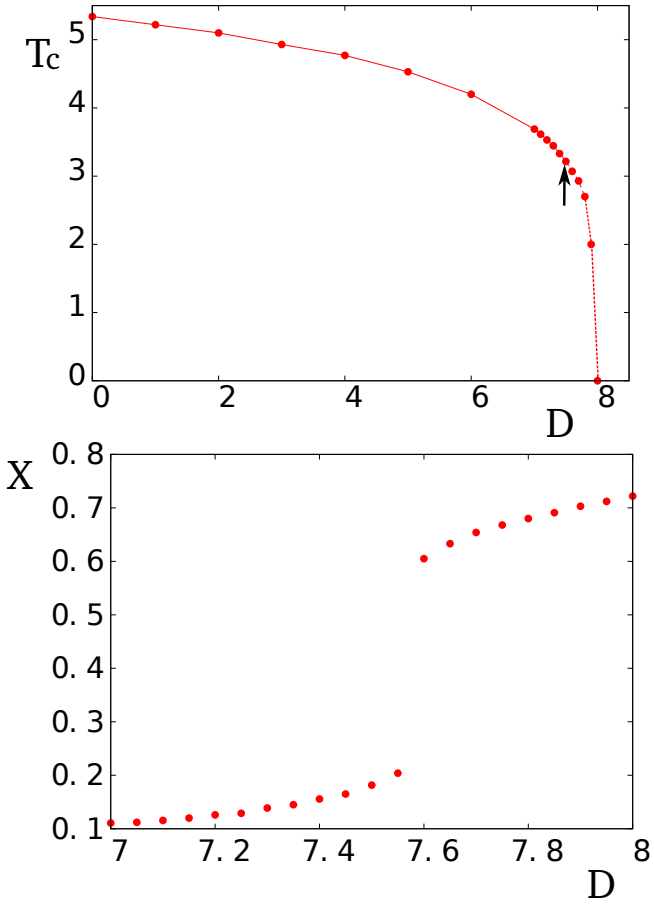

Figure I.4: Top: Phase diagram in $T-D$ plane. The solid line represents the second-order phase transition and dashed line represents the first-order transition, the arrow indicates the bulk tricritical point. Bottom: Concentration X as a function of D.

configuration and the other one with the ground-state configuration. We monitor various physical quantities with time evolution. The equilibrium is attained when two initial spin configurations give the same results. We see in Fig. I.8 that only after a few thousands of MC steps that the two initial configurations give statistically the same results.

(ii) The evolutions of E and M show bimodal distributions over periods of $\simeq 10^4$ MC steps. The time of 10^5 MC steps for equilibrating and 10^5 MC steps for averaging is thus sufficient as said above.

We have calculated the transition temperature with D from 0 to 7.5. The maximum value of D for a 4-layer film is 7.5 above which there is no transition at all. This value depends on the film thickness. It comes from the

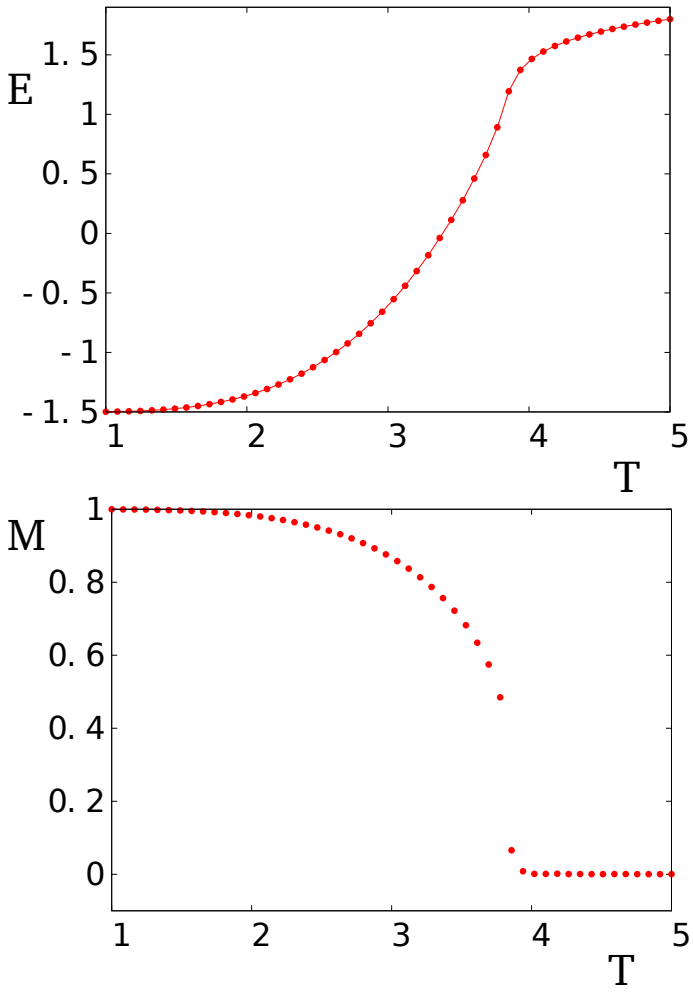

Figure I.5: Energy (top) and magnetization (bottom) versus T for $D = 6$, L_z=4 and $L = 120$.

fact that the maximum of D should cancel the energy from J and K terms. For example, with L_z=4, the energy of J and K terms is:

$$\begin{aligned} E_1 &= -(7J + 7K)2 \text{ (2 surfaces)} \\ &\quad -(8J + 8K)2 \text{ (2 interior layers)} = -30 \end{aligned}$$

where $J = K = 1$. The energy from D is $E_2 = +2D$ (2 surface atoms)$+2D$ (two interior atoms)$= 4D$. The maximum of D is determined by setting $E_1 + E_2 = 0$, from which $D = 30/4 = 7.5$. The same calculation can be done for another thickness, yielding another value of maximal D.

To determine the critical value of D, namely D_c, where the transition changes from second to first order, we follow the variation of the energy

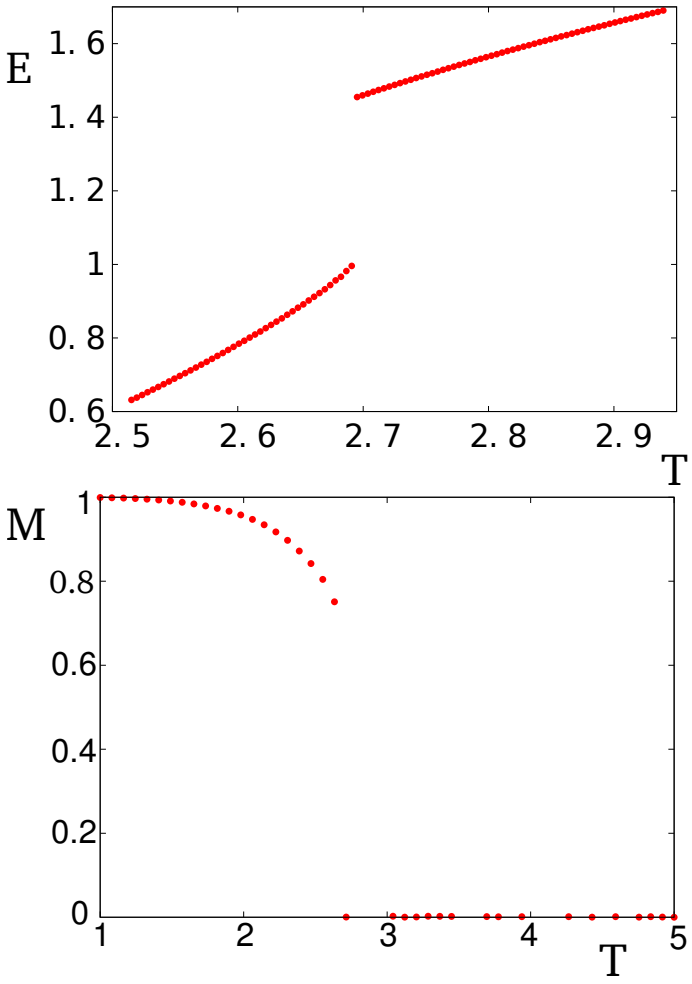

Figure I.6: Energy (top) and magnetization (bottom) versus T in the first-order region of D: $D = 7.3$, L_z=4 and $L = 120$.

gap ΔE defined as the energy separation of the two peaks in the energy distribution. This gap is zero when the transition is of second order because the energy distribution is continuous. Using the histogram method with various values of D, we show in Fig. I.9(top) the variation of ΔE versus D. As seen, ΔE is not zero for $D \in]7.2, 7.5[$. For $D \leq 7.2$ the phase transition is continuous and for $D \geq 7.5$ there is no phase transition.

We show in Fig. I.9(bottom) T_c versus D. We note that the maximal value of D and the tricritical value D_c depends on the film thickness. We can notice this by looking at the bulk maximal value $D = 8$ ($L_z = \infty$) and $D_c = 7.5$ as shown in Fig. I.4 . The four-layer film has $D_c = 7.2$. So, when L_z goes to infinity D_c goes from 7.2 to 7.5.

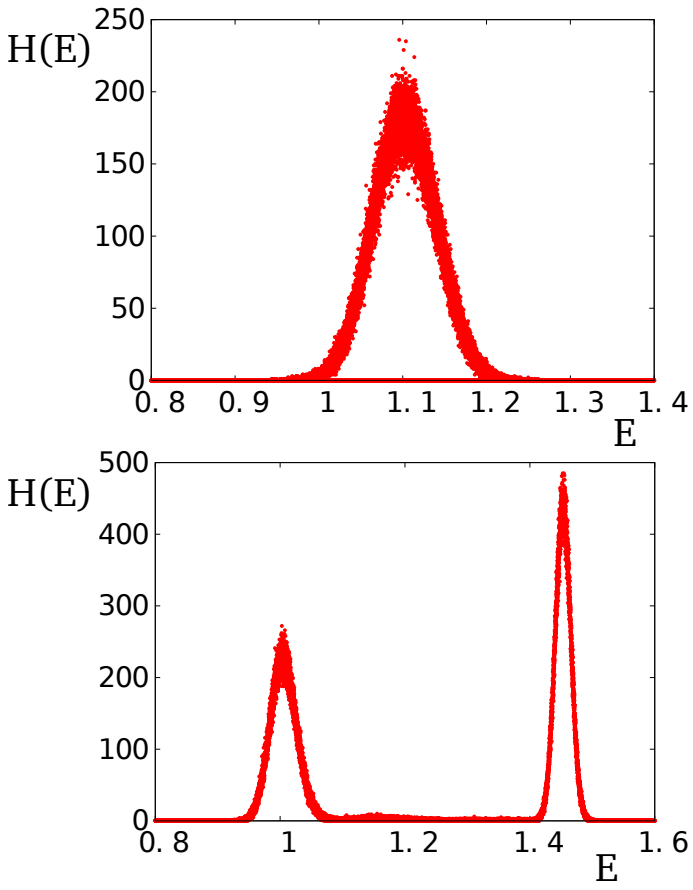

Figure I.7: Energy histograms at T_c=3.820 (top) and T_c=2.694 (bottom) for D=6 and D=7.3, respectively.

I.5 Size Effect

When the system size is infinite, in second-order phase transitions the correlation length is infinite at the critical point. However, in first-order transitions the correlation length is finite at the transition temperature where the two phases coexist and the energy is discontinuous. In simulations, in spite of the fact that we use periodic boundary conditions to mimic large systems, we cannot avoid finite-size effects on the results. The nature of the transition may not be detected at small system sizes. It is therefore very important to measure the size effects in numerical simulations. We show in Fig. I.10 the energy versus T for $L = 36$ and $L = 300$. The size effect is extremely small. The transition remains continuous though one observes a change in the slope of the curve which is steeper for the larger size. In the first-order region, the energy and magnetization are already discontinuous even for L as small as

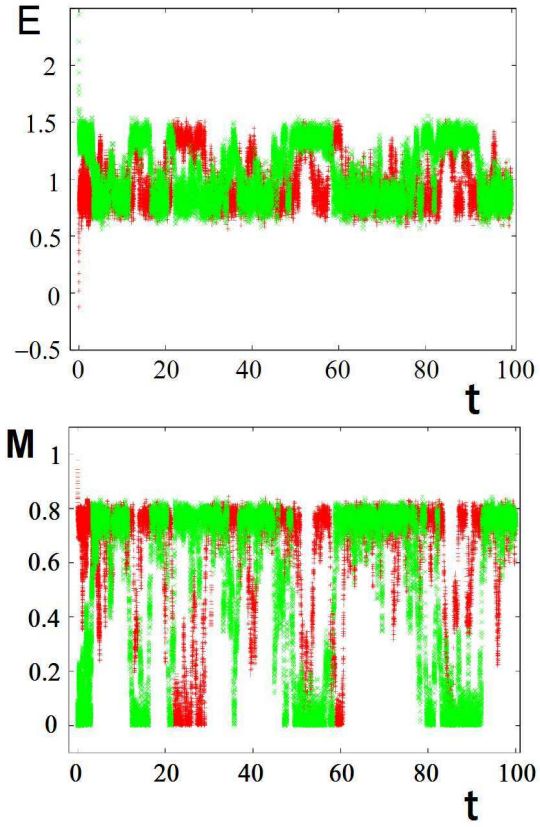

Figure I.8: Energy (top) and magnetization (bottom) versus MC time t (in unit of 10^3) at the transition temperature $T_c = 2.694$ for D=7.3. Note that the red and green curves are obtained with ferromagnetic and random initial configurations, respectively.

36.

The film thickness affects on the other hand the value of the transition temperature T_c as seen in Fig. I.11. As L_z increases, the transition temperature tends to that of the bulk. We have used the least mean-square fit with the form

$$T_c(L_z) = T_c(\infty) - \frac{A}{L_z} \tag{I.12}$$

where $A = 2.692 \pm 0.165$ and $T_c(\infty) = 4.455 \pm 0.024$. The way how T_c increases with increasing thickness is characterized by constant A in the above equation of $T_c(L_z)$. This constant is different from one material to another depending on the coupling between film layers. In some materials A is very

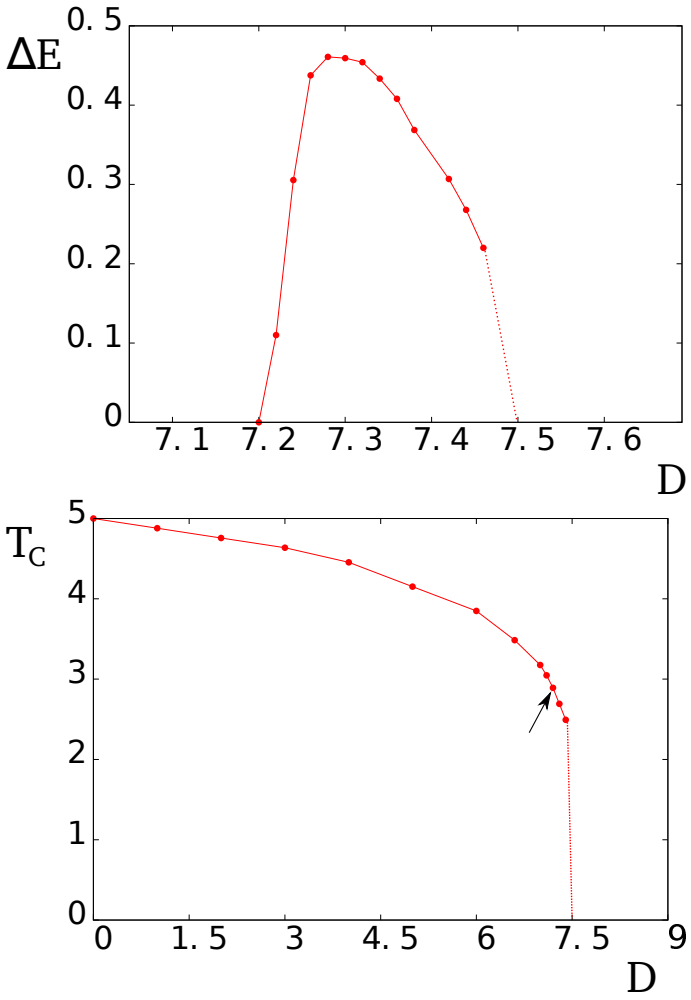

Figure I.9: Latent heat $\triangle E$ (top) and T_c (bottom) versus D, for $L_z = 4$, $L = 120$. The critical value of D ($\simeq 7.2$) is indicated by the arrow. The dotted line between $D = 7.4$ and 7.5 is extrapolated.

small, meaning that the interlayer coupling is very small. This is not the case here in spite of the fact that there are only two nearest neighbors for each interior atom on the z-axis (with only one for surface atom). Knowing how T_c varies with the film thickness can help determine the interlayer coupling.

At this stage, let us discuss about the criticality of the transition in the second order region. If we compare Eq. (I.12) with the finite-size scaling relation:

$$T_c(L) = T_c(\infty) + AL^{-1/\nu} \tag{I.13}$$

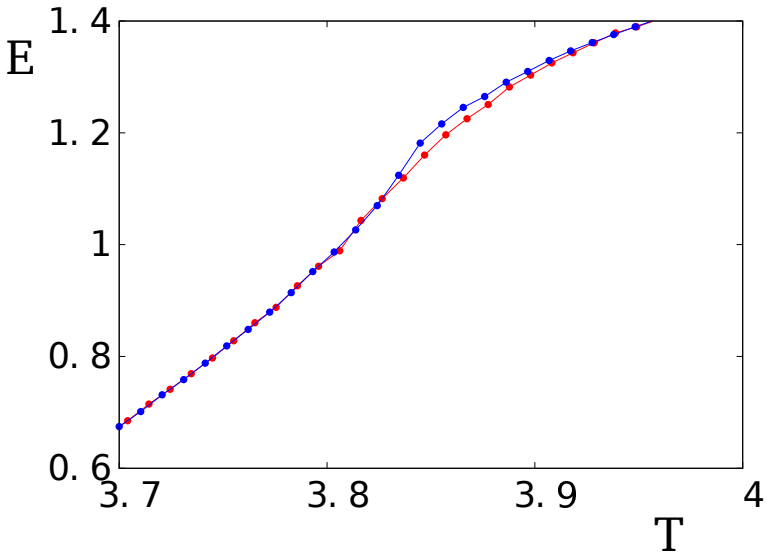

Figure I.10: Size effect on E in the transition region for L=36 (red), L=300 (blue) and D=6, and a film thickness L_z=4.

we see that ν=1 which is the 2D Ising universality exponent. This is in agreement with Ref. [22]: when the film thickness becomes small, the critical exponents tend to the 2D criticality.

I.6 Surface Effect

So far, we have supposed J=K for any NN spin pair in the film. We investigate now the surface effect due to the surface parameter K_s taken to be different from K. We write the biquadratic surface and bulk parts as follows:

$$\alpha_b \sum_{ij} S_i^2 S_j^2 + \alpha_s \sum_{i'j'} S_{i'}^2 S_{j'}^2 \tag{I.14}$$

where $\alpha_b = K/J$ and $\alpha_s = K_s/J$ denote respectively the bulk and surface interactions and $\sum_{i'j'}$ denotes the sum over NN spin pairs in the surface layer. We take $\alpha_b = 1$. Let us show the magnetization of the first and second layer in Fig. I.12 for several values of α_s. As seen, the weaker the surface interaction is, the smaller the surface magnetization becomes. Only when α_s is much larger than 1, the surface layer magnetization becomes larger than the second-layer. For the first-order region, the surface and interior layer magnetizations have discontinuities at the transition as expected (see Fig. I.13).

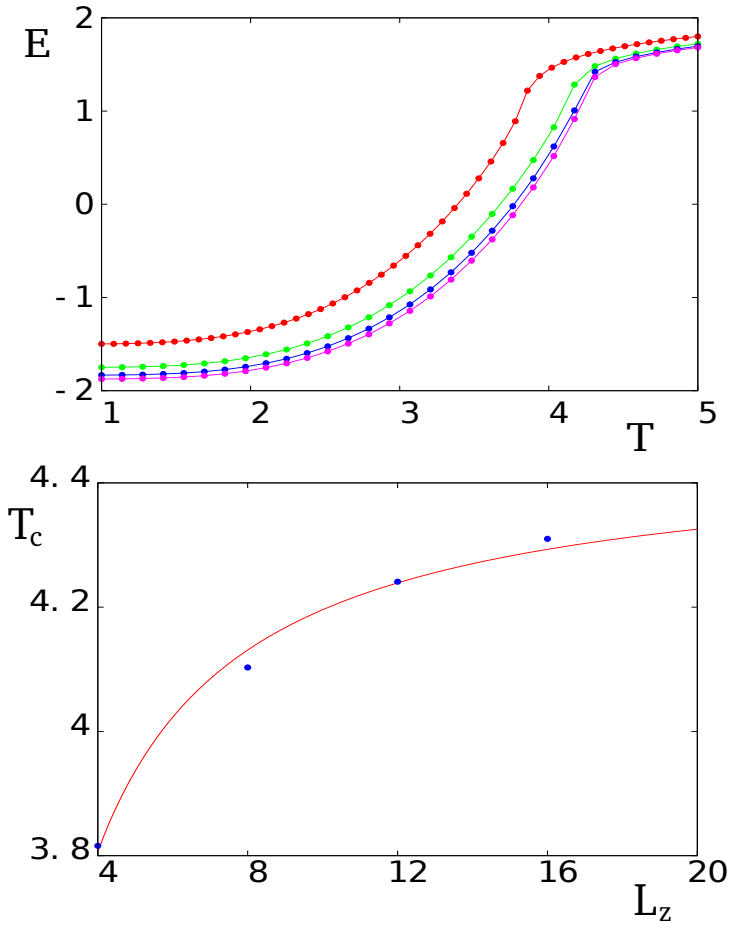

Figure I.11: Top: Energy versus T for L_z=4 (red), 8 (green), 12 (blue) and 16 (magenta), with L=120 and D=6. Transition temperature T_c (blue point) versus L_z for D=6. Bottom: The continuous red line is the least mean-square fit.

We show now the average number of spins ± 1 and the average number of spins zero in each layer versus T in Fig. I.14 at the first-order transition with $D = 7.3$. They are defined as $M_{1,2}(\pm 1) =< \sum_i [\delta(S_i, 1) + \delta(S_i, -1)] > /L^2$ where the sum is made for each layer: $M_1(\pm 1)$ and $M_2(\pm 1)$ correspond to the surface and second layers, respectively. For spins zero, $M_{1,2}(0) =< \sum_i \delta(S_i, 0) > /L^2$. Several remarks are in order:

(i) below the transition temperature, the ordering results from spins ± 1. The number of spins zero increases slowly from 0 at $T < T_c$ but becomes dominant for $T > T_c$.

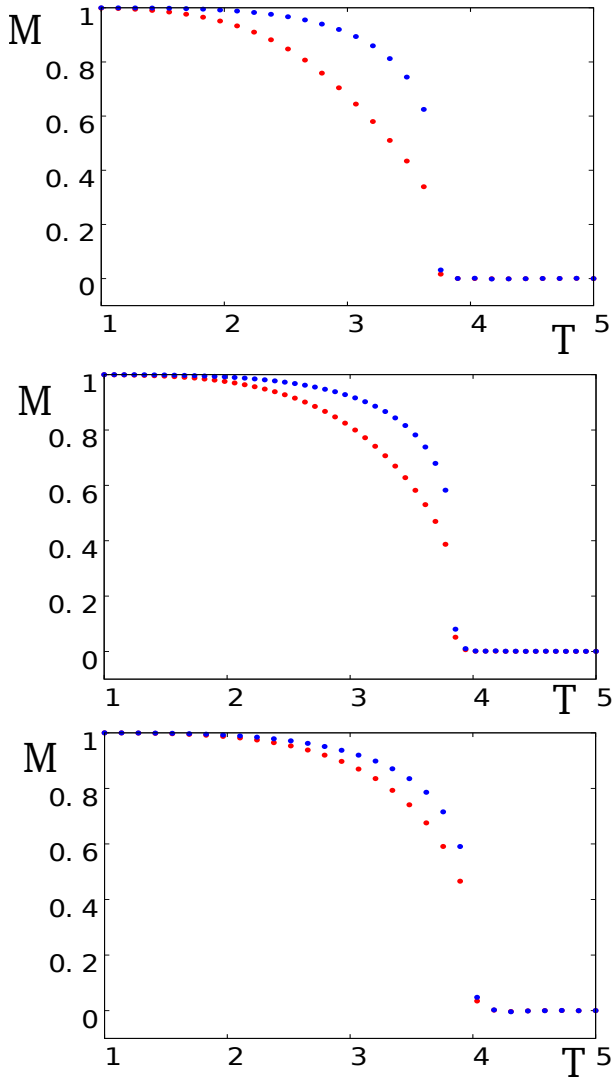

Figure I.12: Layer magnetization of the first (red) and second (blue) layers versus T, for α_s=0.8 (top), 1 (middle), 1.2 (bottom) with D=6 and $N = 120$.

(ii) At $T < T_c$ the surface has a smaller number of spins ± 1 than the second layer, namely there is a deficit of He^4 at the surface. Experimentally, it has been shown that in the mixture He^3-He^4 at low temperature, He^3 atoms are localized near the surface, giving rise to a deficit of He^4 [27].

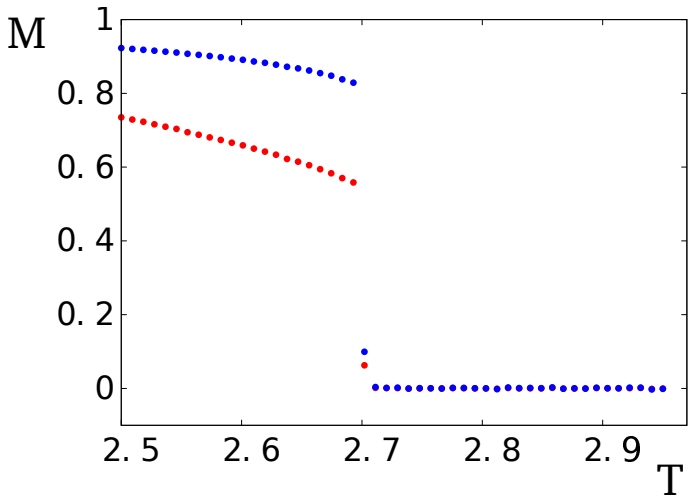

Figure I.13: Layer magnetization of the first (red) and second (blue) layers versus T, for α_s=1 and $D = 7.3$.

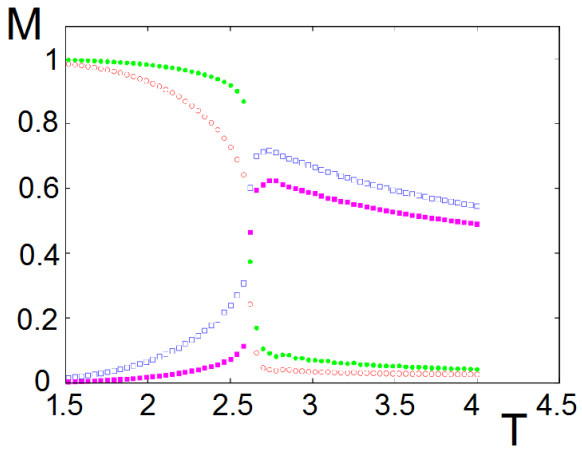

Figure I.14: The normalized numbers of spins ± 1 (He^4) and spins zero (He^3) versus T for the first and second layers. Red void circles and green circles represent the number of He^4 (spins ± 1) on the first and second layers, while blue void squares and magenta squares represent the number of He^3 (spins zero) on the first and second layers, respectively.

I.7 Conclusion

We have investigated in this chapter the BEG model used for a thin film of stacked triangular lattices with a thickness L_z. There are three important aspects of our results:

(i) The nature of the first-order phase transition in a region of the phase space (D, T) is conserved down to a 4-layer film, unlike in other systems where bulk first-order transition becomes second-order with small thickness [23],

(ii) The cross-over from second-order to first-order transition in the bulk is conserved in thin films as shown above. The anisotropy of the BEG Hamiltonian affects the nature of the phase transition as it has been observed in the bulk case of simple cubic lattice [17]: in 4-layer triangular films, for $D \leq 7.2$ the transition is continuous and for $7.2 < D < 7.5$ the transition is of first order. This has been confirmed with the histogram technique where the latent heat can be measured with precision,

(iii) The surface effect on the layer magnetizations has been shown. The surface magnetization is smaller than the interior layer if the surface interaction is not so large. If we map the BEG model into a mixing of He-3 and He-4, then near the surface there is a He-3 enrichment (normal liquid) in a film at low temperatures. This point is new with respect to the bulk properties where the mixing of two liquids is uniform over the system.

Chapter II

Helimagnetic Thin Films

Contents

II.1 Introduction

Helimagnets have been a subject of intensive investigations both experimental and theoretical, since their discovery by Yoshimori [28] and Villain

[29]. Most of experiments have been made on the rare-earth (RE) metals like Holmium (Ho), Terbium (Tb) and Dysprosium (Dy) [30–32], insulators like $NiBr_2$, Cu_2OSeO_3 [33, 34], and several others [35, 36]. In the simplest model, the helimagnetic ordering is due to the competition between nearest-neighbors (NN) and next-nearest-neighbors (NNN). This kind of structure belongs to a large family of periodic non-collinear spin structures called frustrated systems. The frustration has several origins, it can be due to the geometry of the lattice such as the triangular lattice [37], to the competition between the exchange interaction and the Dzyaloshinskii-Moriya (DM) interaction [38, 39], and the competition between exchange interactions such as in the case of helimagnets. In spite of their long history, the nature of the phase transition in non-collinear magnets has been elucidated only recently [37, 40, 41]. Helical magnets present potential applications in spin transport [42, 43]. There is a large number of experiments which has been performed on thin films to study low-temperature properties of helimagnets such as spin waves [44–47] and heat capacity [48] . Due to complicated surface spin configurations, surface effects in helimagnets have only recently studied [49].

The purpose of this chapter in the first part is to study a quantum Heisenberg helimagnetic thin film of simple cubic (sc) lattice using of the Green's function method. We will show that the spin configuration across the film is strongly non-uniform. Using the exactly determined spin configuration we calculate the spin-wave spectrum and the layer magnetizations as functions of temperature T. we will show that there exist surface-localized modes which strongly affect the surface magnetization. We also show that quantum fluctuations cause interesting spin contractions at $T = 0$ and give rise to a cross-over between layer magnetizations at low T.

In the second part of the chapter we study the effect of an external magnetic field applied along the c-axis perpendicular to the film surface of a helimagnet with both classical and quantum Heisenberg spin models. As will be seen, the applied magnetic field gives a very complex spin configuration across the film. We will show by Monte carlo (MC) simulation that the phase transition in the field is due to the destruction of a number of layers inside the film. We identify the condition under which a layer becomes disordered. This partial phase transition is not usual in thin films where one observes more often the disordering of the surface layer, not an interior layer. At low temperature, we investigate effects of quantum fluctuations using a Green's function (GF) method for non -collinear spin configurations.

The organization of the present chapter is as follows: In section II.2, the model is presented and classical ground state of the helimagnetic film is determined. In section II.3 we detail the principal steps used in the general

GF method for non-collinear spin configurations. The GF results are shown in section II.4. In section II.5 we investigate the effect of an applied magnetic field. The conclusion is given in section II.6.

II.2 Helimagnetic Thin Films

The helimagnetic order results from the competition between ferromagnetic and antiferromagnetic interactions. This screw-type structure consists of spins screwing along a crystalline axis with a spatial repetition. To generate the bulk helical structure in the c direction we take a ferromagnetic interaction ($J_1 > 0$) between NNs, and an antiferromagnetic interaction ($J_2 < 0$) between NNNs along the c-axis. The helical GS have parallel spins in the plane perpendicular to the c-axis and a turn angle α_{ij} between two NNs in the adjacent planes.

II.2.1 Model and classical ground state

We consider a thin film of sc lattice of N_z layers, with two symmetrical surfaces perpendicular to the c axis, the exchange Hamiltonian is given by

$$\mathcal{H}_e = -\sum_{\langle i,j \rangle} J_{i,j} \vec{S_i} \,.\, \vec{S_j} \tag{II.1}$$

where J_{ij} being the exchange interaction between two quantum Heisenberg spins $\mathbf{S_i}$ and $\mathbf{S_j}$ occupying the lattice sites i and j. We write the classical energy of a spin in the bulk helical GS as

$$E = -2J_1 \cos\alpha_b - 2J_2 \cos 2\alpha_b$$

where $\alpha_b = \alpha_{ij}$ is the bulk turn angle which is the same across the bulk. The bulk GS configuration corresponds to the minimum of E

$$\frac{dE}{d\alpha_b} = 2J_1 \sin\alpha_b + 2J_2 \sin 2\alpha_b = 0$$

For $\alpha_b = 0, \pi$ the GS spin configuration is ferromagnetic and antiferromagnetic respectively. The helimagnetic structure is possible for $\cos\alpha_b = -\frac{J_1}{4J_2}$, namely for $|J_2| > 0.25J_1$. The critical value of J_2 is $|J_2^c| = 0.25J_1$. The magnetic structure is seen as a chain of spins along the c-axis Fig. II.1 where each spin represents the magnetic moment per lattice site. This bulk helical stability has been experimentally observed in Holmium and MnSi films [30, 50, 51].

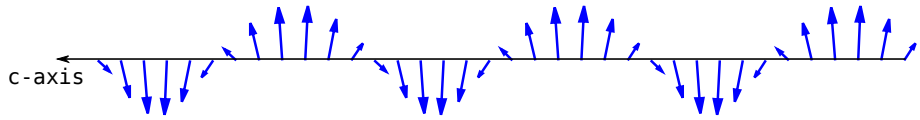

Figure II.1: Bulk helical structure with a turn angle $\alpha_b = 30°$.

In thin films the spins lie in the basal plane as in the bulk, although they are different from plane to plane, specially near the surface. The lack of neighbors for surface atoms leads to the surface reconstruction.

We assume a non-zero J_2 only on the *c-axis*, this assumption simplifies formulas but does not change the physics of the problem since including the uniform helical angles in two other directions parallel to the surface will not introduce additional effects.

II.2.2 Surface spin reconstruction

We have used here the steepest descend method [52,53] to calculate the turn angle between spins of adjacent layers. The main steps of the method are i) generate a random spin configuration, ii) update one by one all spins as follows: at each site we calculate the magnetic local field then align the spin in its direction, iii) repeat the previous steps a sufficient number of times until the convergence is reached. The results calculated for various J_2 are shown in Table II.1 for film of $N_z = 8$ layers. We note that unlike the bulk the turn angle is heavily modified near the surface with oscillation for strong $|J_2|$ and that the angle at the film center are close to the bulk value α_b (see Fig. II.2). This means that the surface reconstruction affects just a few atomic layers.

J_2/J_1	$\alpha^\circ_{1,2}$	$\alpha^\circ_{2,3}$	$\alpha^\circ_{3,4}$	$\alpha^\circ_{4,5}$	α°_b
-0.6	34,21	76,18	60,86	68,36	65,37
-0.5	29,84	65,75	58,30	60,84	60
-0.4	22,52	50,72	51,38	51,30	51,31
-0.35	17,06	39,97	44,27	44,41	44,41
-0.3	9,78	24,73	31,14	32,53	33,55

Table II.1: Values of $\alpha_{i,j}$ between two adjacent layers for various values of J_2/J_1. The last column shows the value of the angle in the bulk case.

According to the theorem of Mermin and Wagner [54] continuous spin models such as XY and Heisenberg spins do not have long-range ordering at

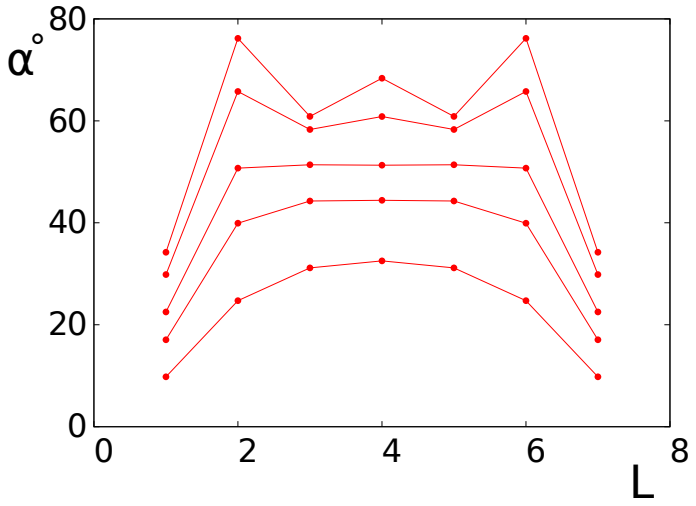

Figure II.2: Angles α_1,..., α_7 in degree across the film for J_2/J_1= -0.6, -0.5, -0.4, -0.35, -0.3 (from top) with N_z= 8.

finite temperatures in two dimensions. Since we have in our case a thin film, it is useful to add an anisotropic interaction I_{ij} to stabilize the long-range ordering at finite temperatures. We suppose that it has the following form:

$$\mathcal{H}_a = -\sum_{\langle i,j \rangle} I_{i,j} S_i^z S_j^z \cos\theta_{ij}$$

where ($I_{i,j} > 0$) is supposed to be positive, small compared to J_1 and limited to NNs. The full Hamiltonian is thus $\mathcal{H} = \mathcal{H}_e + \mathcal{H}_a$. The GS in the presence of $I_{i,j}$ is determined in the same manner. It is very slightly modified with the order of one or two degrees when $I_{i,j} \simeq 0.1 J_1$. The small anisotropy does not therefore alter the main features shown in Fig. II.2.

II.3 Green's Function Theory

The double-time Green's function developed by Zubarev [55] is a self-consistent method in quantum statistical mechanics and solid state physics. It is used for theoretical studies of spin systems and the calculation of their magnetic properties at zero and finite temperatures. We propose here to recall briefly the basic principle of this method and its application for non-collinear magnets.

II.3.1 Green's function method

We define the retarded and advanced Green's function by

$$\begin{aligned} G^r_{AB}(t-t') &= \left\langle\left\langle A(t); B(t')\right\rangle\right\rangle = -i\theta(t-t')\left\langle[A(t), B(t')]\right\rangle \\ G^a_{AB}(t'-t') &= \left\langle\left\langle A(t); B(t')\right\rangle\right\rangle = i\theta(t'-t)\left\langle[A(t), B(t')]\right\rangle \end{aligned} \tag{II.2}$$

where $A(t)$ and $B(t')$ are the Heisenberg operators at times t and t', $\langle\langle ...\rangle\rangle$ is a abbreviated notation for the Green's function, $\langle ...\rangle$ indicates the average over a grand canonical ensemble and $\theta(t-t')$ is the Heaviside step function. The quantum equations of motion for the two Green's functions are identical since $\frac{d\theta(t-t')}{dt} = -\frac{d\theta(t'-t)}{dt}$ and have the form

$$i\frac{dG}{dt} = \frac{d\theta(t-t')}{dt}\left\langle[A(t), B(t')]\right\rangle + \left\langle\left\langle i\frac{dA(t)}{dt}; B(t')\right\rangle\right\rangle \tag{II.3}$$

We take into account the relation between $\theta(t)$ and $\delta(t)$

$$\theta(t) = \int_{-\infty}^{t} \delta(t)dt \tag{II.4}$$

We can write the equation of motion (II.3) under the form

$$i\frac{dG}{dt} = \delta(t-t')\left\langle[A(t), B(t')]\right\rangle + \left\langle\left\langle[A(t), H(t)]; B(t')\right\rangle\right\rangle \tag{II.5}$$

We define the time correlation functions :

$$\begin{aligned} F_{AB}(t-t') &= \langle A(t)B(t')\rangle \\ F_{BA}(t-t') &= \langle B(t')A(t)\rangle \end{aligned} \tag{II.6}$$

These functions do not contain the discontinuous factor $\theta(t-t')$, in contrast to the Green's function they are defined also when $(t = t')$, they give then the average values of products of operators and when the the times are different $(t \neq t')$ these averages yield the time correlation functions which are essential for transport processes. They satisfy the equations :

$$\begin{aligned} i\frac{d}{dt}F_{AB}(t-t') &= \langle[A(t), H(t)]B(t')\rangle \\ i\frac{d}{dt}F_{BA}(t-t') &= \langle B(t')[A(t), H(t)]\rangle \end{aligned} \tag{II.7}$$

To solve the equations of motions of the Green's functions, we apply the Fourier transformation to have the spectral representation for the correlation functions (II.6) and the Green's function (II.2):

$$F_{BA}(t-t') = \int_{-\infty}^{+\infty} J(\omega) e^{-i\omega(t-t')} dw$$
$$F_{AB}(t-t') = \int_{-\infty}^{+\infty} J(\omega) e^{\beta\omega} e^{-i\omega(t-t')} dw \tag{II.8}$$

$$G^r_{AB}(t-t') = \int_{-\infty}^{+\infty} G^r_{AB}(E) e^{-iE(t-t')} dE \tag{II.9}$$

$$G^r_{AB}(E) = \frac{1}{2\pi} \int_{-\infty}^{+\infty} G^r_{AB}(t-t') e^{iE(t-t')} dt \tag{II.10}$$

where we have $F_{AB}(t-t') = F_{BA}(t-t'+i\beta)$, $J(\omega)$ being the spectral intensity. We replace $G^r_{AB}(t-t')$ in Eq. (II.10) by the expression (II.2) we get

$$G^r_{AB}(E) = \frac{1}{2\pi i} \int_{-\infty}^{+\infty} \big(\langle A(t)B(t') \rangle - \langle B(t')A(t) \rangle \big) e^{iE(t-t')} \theta(t-t') dt \tag{II.11}$$

Using the spectral representation (II.8) we have

$$G^r_{AB}(E) = \frac{1}{2\pi i} \int_{-\infty}^{+\infty} e^{i(E-\omega)(t-t')} \theta(t-t') dt \int_{-\infty}^{+\infty} J(\omega)(e^{\beta\omega} - 1) d\omega \tag{II.12}$$

$$G^r_{AB}(E) = \frac{1}{2\pi} \int_{-\infty}^{+\infty} J(\omega)(e^{\beta\omega} - 1) \frac{d\omega}{E - \omega + i\varepsilon} \tag{II.13}$$

Repeating the same calculation for the advanced Green's function we get

$$G^a_{AB}(E) = \frac{1}{2\pi} \int_{-\infty}^{+\infty} J(\omega)(e^{\beta\omega} - 1) \frac{d\omega}{E - \omega - i\varepsilon} \tag{II.14}$$

Combining the two functions we can obtain the spectral intensity

$$G(\omega + i\varepsilon) - G(\omega - i\varepsilon) = \frac{1}{2\pi} \int_{-\infty}^{+\infty} J(E)(e^{\beta\omega} - 1) \left(\frac{1}{\omega - E + i\varepsilon} - \frac{1}{\omega - E - i\varepsilon} \right) \tag{II.15}$$

Using now the δ function $\delta(x) = \frac{1}{2\pi i} \left(\frac{1}{x - i\varepsilon} - \frac{1}{x + i\varepsilon} \right)$ we obtain

$$G(\omega + i\varepsilon) - G(\omega - i\varepsilon) = -i(e^{\beta\omega} - 1) J(\omega) \tag{II.16}$$

$$\begin{aligned} F_{BA}(t-t') &= \langle A(t)B(t') \rangle \\ &= i \int_{-\infty}^{+\infty} \frac{G(\omega + i\varepsilon) - G(\omega - i\varepsilon)}{e^{\beta\omega} - 1} e\beta\omega e - i\omega(t-t') d\omega \end{aligned} \tag{II.17}$$

II.3.2 Green's functions applied to helimagnetic spin systems

We apply the Green's function technique to the helimagnetic system presented by the above Hamiltonian which we express in the local coordinates (ξ_i, η_i, ζ_i), we obtain

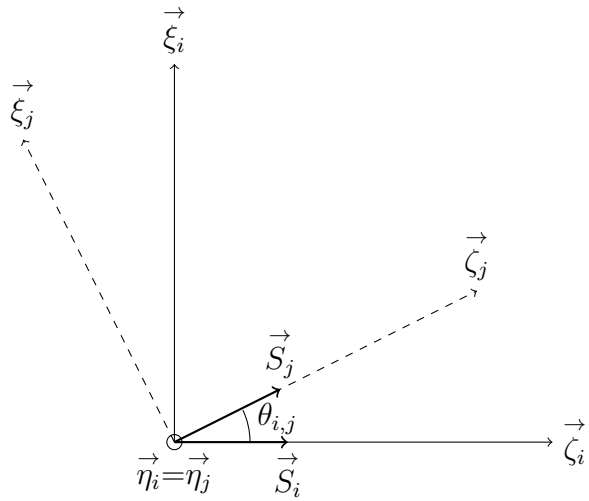

$$\vec{\zeta}_j = cos\theta_{i,j}\ \vec{\zeta}_i + sin\theta_{i,j}\ \vec{\xi}_j$$
$$\vec{\xi}_j = cos\theta_{i,j}\ \vec{\xi}_i - sin\theta_{i,j}\ \vec{\zeta}_j$$

$$\vec{S}_i = S_i^x\ \vec{\xi}_i + S_i^y\ \vec{\eta}_i + S_i^z\ \vec{\zeta}_i$$
$$\vec{S}_j = S_j^x\ \vec{\xi}_j + S_j^y\ \vec{\eta}_j + S_j^z\ \vec{\zeta}_j$$

Figure II.3: Local coordinates in plane perpendicular to the c-axis

$$\begin{aligned}\mathcal{H} = &-\sum_{\langle i,j\rangle} J_{i,j}[\frac{1}{4}(S_i^+S_j^+ + S_i^-S_j^-)(\cos\theta_{ij}-1)\\ &+\frac{1}{4}(S_i^+S_j^- + S_i^-S_j^+)(\cos\theta_{ij}+1)\\ &+\frac{1}{2}\sin\theta_{ij}(S_i^+ + S_i^-)S_j^z - \frac{1}{2}\sin\theta_{ij}(S_J^+ + S_j^-)S_i^z + S_i^zS_j^z\cos\theta_{ij}]\\ &-\sum_{\langle i,j\rangle} I_{i,j}S_i^zS_j^z\cos\theta ij\end{aligned} \tag{II.18}$$

We define the following two double-time Green's functions in the real space:

$$\begin{aligned}G_{ij}(t-t') &= <<S_i^+(t); S_j^-(t')>> = -i\theta(t-t') < [S_i^+(t), S_j^-(t')] >\\ F_{ij}(t-t') &= <<S_i^-(t); S_j^-(t')>> = -i\theta(t-t') < [S_i^-(t), S_j^-(t')] >\end{aligned} \tag{II.19}$$

We need these two functions because the equation of motion of the first function generates the function of the second type and vice versa.

II.3.3 Equation of motion

Writing the equations of motion of these functions

$$
\begin{aligned}
i\frac{dG_{ij}(t-t')}{dt} &=< [S_i^+(t), S_j^-(t')] > \delta(t-t') - << [H, S_i^+(t)], S_j^-(t') >> \\
i\frac{dF_{ij}(t-t')}{dt} &=< [S_i^-(t), S_j^-(t')] > \delta(t-t') - << [H, S_i^-(t)], S_j^-(t') >>
\end{aligned}
\tag{II.20}
$$

where the spin operators and their relations are given by

$$
\begin{aligned}
S_j^{\pm} &= S_j^x \hat{\xi}_j \pm i S_j^y \hat{\eta}_j \\
[S_j^+, S_l^-] &= 2S_j^z \delta_{jl} \\
[S_j^z, S_l^{\pm}] &= \pm S_j^{\pm} \delta_{jl}
\end{aligned}
$$

Expanding the commutators in Eq. (II.20), we have

$$
\begin{aligned}
i\frac{dG_{i,j}(t-t')}{dt} &= 2 < S_i^z > \delta_{i,j}\delta(t-t') - \langle\langle \sum_k J_{i,k}\big[S_i^z S_k^-(\cos\theta_{i,k} - 1) \\
&\quad + S_i^z S_k^+(\cos\theta_{i,k} + 1) + 2S_i^z S_k^z \sin\theta_{i,k} + \sin\theta_{i,k}(S_i^+(S_k^+ + S_k^-)) \\
&\quad - 2\cos\theta_{i,k} S_i^+ S_k^z\big] - 2\sum_k I_{i,k} S_i^+ S_k^z \cos\theta_{i,k}, S_j^-(t')\rangle\rangle \\
i\frac{dF_{i,j}(t-t')}{dt} &= \langle\langle \sum_l J_{i,k}\big[S_i^z S_k^+(\cos\theta_{i,k} - 1) + S_i^z S_k^-(\cos\theta_{i,k} + 1) \\
&\quad + 2S_i^z S_k^z \sin\theta_{i,k} + \sin\theta_{i,k}(S_i^-(S_k^+ + S_k^-)) - 2\cos\theta_{i,l} S_i^- S_k^z\big] \\
&\quad - 2\sum_k I_{i,k} S_i^- S_k^z \cos\theta_{i,k}; S_j^-\rangle\rangle
\end{aligned}
\tag{II.21}
$$

The equations of motion contain higher-order Green's functions. In order to reduce them and close the system of equations, we adopt the decoupling scheme introduced by Tyablikov [56] which is called Random-Phase Approximation (RPA) or Tyablikov decoupling:

$$
\begin{aligned}
\langle\langle S_i^z S_k^+; S_j^-\rangle\rangle &= \langle S_i^z\rangle\langle\langle S_k^+; S_j^-\rangle\rangle + \langle S_k^+\rangle\langle\langle S_i^z; S_j^-\rangle\rangle - \langle\langle\langle S_i^z\rangle\langle S_k^+\rangle; S_j^-\rangle\rangle \\
&= \langle S_i^z\rangle\langle\langle S_k^+; S_j^-\rangle\rangle = \langle S_i^z\rangle G_{k,j}(t-t') \\
\langle\langle S_i^z S_k^-; S_j^-\rangle\rangle &= \langle S_i^z\rangle\langle\langle S_k^-; S_j^-\rangle\rangle = \langle S_i^z\rangle F_{k,j}(t-t') \\
\langle\langle S_i^z S_k^z; S_j^-\rangle\rangle &= 0 \\
\langle\langle S_i^\alpha(S_k^+ + S_k^-); S_j^-\rangle\rangle &= 0
\end{aligned}
\tag{II.22}
$$

where we have considered $\langle S_k^+ \rangle = \langle S_k^- \rangle = 0$, and $\langle\langle S_k^z; S_j^- \rangle\rangle = 0$. We obtain the following general equations for non-collinear magnets

$$\begin{aligned} i\frac{dG_{ij}(t-t')}{dt} &= 2 < S_i^z > \delta(t-t') - \sum_k J_{i,k}\big[(\cos\theta_{ik} - 1) < S_i^z > F_{k,j}(t-t') \\ &+ (\cos\theta_{i,k} + 1) < S_i^z > G_{k,j}(t-t') - 2\cos\theta_{i,k} < S_k^z > G_{i,j}(t-t')\big] \\ &+ 2\sum_k I_{i,k} < S_k^z > G_{i,j}(t-t')\cos\theta_{i,k} \\ i\frac{dF_{ij}(t-t')}{dt} &= \sum_k J_{i,k}\big[(\cos\theta_{i,k} - 1) < S_i^z > G_{k,j}(t-t') \\ &+ (\cos\theta_{i,k} + 1) < S_i^z > F_{k,j}(t-t') - 2\cos\theta_{i,k} < S_k^z > F_{i,j}(t-t')\big] \\ &- 2\sum_k I_{i,k} < S_k^z > F_{i,j}(t-t')\cos\theta_{i,k} \end{aligned} \tag{II.23}$$

We now introduce the following in-plane Fourier transforms:

$$\begin{aligned} G_{i,j}(t,t') = &\frac{1}{\Delta}\int\int_{BZ} d\mathbf{k}_{xy}\frac{1}{2\pi}\int_{-\infty}^{+\infty} d\omega e^{-i\omega(t-t')} \\ &\times g_{n_i,n_j}(\omega,\mathbf{k}_{xy})\, e^{i\mathbf{k}_{xy}\cdot(\mathbf{R}_i-\mathbf{R}_j)} \\ F_{i,j}(t,t') = &\frac{1}{\Delta}\int\int_{BZ} d\mathbf{k}_{xy}\frac{1}{2\pi}\int_{-\infty}^{+\infty} d\omega e^{-i\omega(t-t')} \\ &\times f_{n_i,n_j}(\omega,\mathbf{k}_{xy})\, e^{i\mathbf{k}_{xy}\cdot(\mathbf{R}_i-\mathbf{R}_j)} \end{aligned}$$

where ω is the spin-wave frequency, $\mathbf{k}_{xy}$ denotes the wave-vector parallel to xy planes and $\mathbf{R}_i$ is the position of the spin at the site i, n_i, n_j are respectively the z-component indices of the layers where the sites $\mathbf{R}_i$, $\mathbf{R}_j$ and belong to. The integral over $\mathbf{k}_{xy}$ is performed in the first Brillouin zone (BZ) whose surface is Δ in the xy reciprocal plane.

$$\begin{aligned} \omega g_{n_i,n_j} = &2 < S_{ni}^z > \delta_{n_i,n_j} - \sum_{n_k} J_{n_i,n_k}[(\cos\theta_{n_i,n_k} - 1) \\ &< S_{ni}^z > f_{n_k,n_j} e^{i\mathbf{k}_{xy}(R_{n_i},R_{n_k})} + (\cos\theta_{n_i,n_k} + 1) < S_{ni}^z > g_{n_k,n_j} e^{i\mathbf{k}_{xy}(R_{n_i},R_{n_k})} \\ &- 2\cos\theta_{n_i,n_k} < S_{nk}^z > g_{n_i,n_j}] + 2\sum_{n_k} I_{n_i,n_k}\cos\theta_{n_i,n_k} < S_{nk}^z > g_{n_i,n_j} \end{aligned}$$

$$\omega f_{n_i,n_j} = \sum_{n_k} J_{n_i,n_k}[(\cos\theta_{n_i,n_k} - 1)$$
$$< S^z_{ni} > g_{n_k,n_j} e^{i\mathbf{k}_{xy}(R_{n_i},R_{n_k})} + (\cos\theta_{n_i,n_k} + 1) < S^z_{ni} > f_{n_k,n_j} e^{i\mathbf{k}_{xy}(R_{n_i},R_{n_k})}$$
$$- 2\cos\theta_{n_i,n_k} < S^z_{n_k} > f_{n_i,n_j}] + 2\sum_{n_k} I_{n_i,n_k}\cos\theta_{n_i,n_k} < S^z_{nk} > f_{n_i,n_j}$$

For convenience, we denote n_i=1 for all sites on the surface layer, n_i=2 for all sites on the second layer and so on, we finally obtain the following matrix equation :

$$M(\omega)h = u \tag{II.24}$$

where $\mathbf{M}(\omega)$ is a square matrix of dimension $(2N_z \times 2N_z)$, $\mathbf{h}$ and $\mathbf{u}$ are the column which are defined as follows :

$$h = \begin{pmatrix} g_{1,n'} \\ f_{1,n'} \\ \vdots \\ g_{n,n'} \\ f_{n'_n} \\ \vdots \\ g_{N_z,n'} \\ f_{n_z,n'} \end{pmatrix} \qquad , u = \begin{pmatrix} 2 < S^z_1 > \\ 0 \\ \vdots \\ 2 < S^z_n > \\ 0 \\ \vdots \\ 2 < S^z_{N_z} > \\ 0 \end{pmatrix} \tag{II.25}$$

$$M(\omega) = \begin{pmatrix} \omega{+}A_1 & 0 & B^+_1 & C^+_1 & D^+_1 & E^+_1 & 0 & 0 & 0 & 0 & 0 & 0 \\ 0 & \omega{-}A_1 & -C^+_1 & -B^+_1 & -E^+_1 & -D^+_1 & 0 & 0 & 0 & 0 & 0 & 0 \\ \cdots & \cdots & \cdots & \cdots & \cdots & \cdots & \cdots & \cdots & \cdots & \cdots & \cdots & \cdots \\ \cdots & D^-_n & E^-_n & B^-_n & C^-_n & \omega{+}A_n & 0 & B^+_n & C^+_n & D^+_n & E^+_n & \cdots \\ \cdots & -E^-_n & -D^-_n & -C^-_n & -B^-_n & 0 & \omega{-}A_n & -C^+_n & -B^+_n & -E^+_n & -D^+_n & \cdots \\ \cdots & \cdots & \cdots & \cdots & \cdots & \cdots & \cdots & \cdots & \cdots & \cdots & \cdots & \cdots \\ 0 & 0 & 0 & 0 & 0 & 0 & D^-_{N_z} & E^-_{N_z} & B^-_{N_z} & C^-_{N_z} & \omega{+}A_{N_z} & 0 \\ 0 & 0 & 0 & 0 & 0 & 0 & -E^-_{N_z} & -D^-_{N_z} & -C^-_{N_z} & -B^-_{N_z} & 0 & \omega{-}A_{N_z} \end{pmatrix}$$

where $n = 1, 2, ..., N_z$, $d_n = I_1/J^{\perp}_1$, and

$$\begin{aligned} A_n &= -8J^{//}_1 \langle S^z_n \rangle (1 + d_n - \gamma) \\ &\quad -2\left\langle S^z_{n+1} \right\rangle \cos\theta_{n,n+1}(d_n + J^{\perp}_1) \\ &\quad -2\left\langle S^z_{n-1} \right\rangle \cos\theta_{n,n-1}(d_n + J^{\perp}_1) \\ &\quad -2J_2\left\langle S^z_{n+2} \right\rangle \cos\theta_{n,n+2} \\ &\quad -2J_2\left\langle S^z_{n-2} \right\rangle \cos\theta_{n,n-2} \end{aligned} \qquad \begin{aligned} B^{\pm}_n &= J^{\perp}_1 \langle S^z_n \rangle (\cos\theta_{n,n\pm1} + 1) \\ C^{\pm}_n &= J^{\perp}_1 \langle S^z_n \rangle (\cos\theta_{n,n\pm1} - 1) \\ E^{\pm}_n &= J_2 \langle S^z_n \rangle (\cos\theta_{n,n\pm2} - 1) \\ D^{\pm}_n &= J_2 \langle S^z_n \rangle (\cos\theta_{n,n\pm2} + 1) \end{aligned}$$

Note that to use the above formulas, we have to apply the following rules: (i) if $n = 1$ then there are no $n-1$ and $n-2$ terms in the matrix coefficients,

(ii) if $n = 2$ then there are no $n-2$ terms, (iii) if $n = N_z$ then there are no $n+1$ and $n+2$ terms, (iv) if $n = N_z - 1$ then there are no $n+2$ terms.

Solving $\det|\mathbf{M}| = 0$, we obtain the spin-wave spectrum ω for each value (k_x, k_y). There are $2N_z$ eigenvalues of ω corresponding to two opposite spin precessions as in antiferromagnets.

The solution for $g_{n,n}$ is given by

$$g_{n,n}(\omega) = \frac{|\mathbf{M}|_{2n-1}}{|\mathbf{M}|}$$

where $|\mathbf{M}|_{2n-1}$ is the determinant made by replacing the $2n-1$th column of $|\mathbf{M}|$ by $\mathbf{u}$ given by (II.25). Writing now

$$|\mathbf{M}| = \prod_i [\omega - \omega_i(k_{xy})] \tag{II.26}$$

where $\omega_i(k_{xy}), i = 1, ..., 2N_z$ are poles of $g_{n,n}$. $\omega_i(k_{xy})$ can be obtained by solving $|\mathbf{M}| = 0$. In this case, $g_{n,n}$ can be expressed as

$$g_{n,n}(\omega) = \sum_i \frac{D_{2n-1}[\omega_i(k_{xy})]}{\prod_i [\omega - \omega_i(k_{xy})]} \tag{II.27}$$

where $D_{2n-1}[\omega_i(k_{xy})]$ is

$$D_{2n-1}[\omega_i(k_{xy})] = \frac{|\mathbf{M}|_{2n-1}[\omega_i(k_{xy})]}{\prod_{j\neq i}[\omega_j(k_{xy}) - \omega_i(k_{xy})]} \tag{II.28}$$

Using the spectral theorem which relates the correlation function $< S_i^- S_j^+ >$ to the Green's function, we have

$$\begin{aligned} < S_i^- S_j^+ > = & \lim_{\varepsilon \to 0} \frac{1}{\Delta} \int \int d\mathbf{k}_{xy} \int_{-\infty}^{+\infty} \frac{i}{2\pi} [g_{n,n'}(\omega + i\varepsilon) - g_{n,n'}(\omega - i\varepsilon)] \\ & \times \frac{d\omega}{e^{\beta\omega} - 1} e^{i\mathbf{k}_{xy}(R_i - R_j)} \end{aligned} \tag{II.29}$$

where ε is an infinitesimal positive constant and $\beta = (k_b T)^{-1}$, k_B being the Boltzmann constant.

Using the Green's function presented above, we can calculate self-consistently various physical quantities as a function of temperature T. The magnetiza-

tion $< S_n^z >$ of the $n-th$ layer is given by

$$\begin{aligned} < S_n^z > &= \frac{1}{2} - < S_i^- S_j^+ > \\ &= \frac{1}{2} - \lim_{\varepsilon \to 0} \frac{1}{\Delta} \int \int d\mathbf{k}_{xy} \int_{-\infty}^{+\infty} \frac{i}{2\pi} [g_{n,n'}(\omega + i\varepsilon) - g_{n,n'}(\omega - i\varepsilon)] \\ &\times \frac{d\omega}{e^{\beta\omega} - 1} e^{i\mathbf{k}_{xy}(R_i - R_j)} \end{aligned} \tag{II.30}$$

Replacing Eq. (II.28) in Eq. (II.30) and making use of the following identity

$$\frac{1}{x - i\eta} - \frac{1}{x + i\eta} = 2\pi\delta(x)$$

we obtain

$$< S_n^z >= \frac{1}{2} - \frac{1}{\Delta} \int \int d\mathbf{k}_{xy} \sum_{i=1}^{2N_z} \frac{D_{2n-1}[\omega_i(k_{xy})]}{e^{\beta\omega_i} - 1} \tag{II.31}$$

$< S_n^z >$ depends on the magnetizations of the neighboring layers via $\omega_i (i = 1, ..., 2N_z)$, therefore we should solve by iteration Eq. (II.31) written for all layers, namely for $n = 1, ..., N_z$, to obtain the layer magnetizations at a given temperature T. Note that by symmetry $< S_1^z >=< S_{N_z}^z >$, $< S_2^z >=< S_{N_z-1}^z >$, $< S_3^z >=< S_{N_z-2}^z >$, and so on. Thus, only $N_z/2$ self-consistent layer magnetizations are to be calculated.

The value of the spin in the layer n at $T = 0$ is calculated by

$$< S_n^z > (T = 0) = \frac{1}{2} + \frac{1}{\Delta} \int \int d\mathbf{k}_{xy} \sum_{i=1}^{2N_z} D_{2n-1}[\omega_i(k_{xy})] \tag{II.32}$$

where the sum is performed over N_z negative values of ω_i. For positive values, the Bose-Einstein factor is equal to zero at $T = 0$.

The transition temperature T_c can be calculated in a self consistent manner by iteration, letting all $< S_n^z >$ tend to zero, namely, $\omega_i \to 0$. Expanding $e^{\beta\omega_i} - 1 \to \beta_c\omega_i$ on the right hand side of Eq. (II.31) where $\beta_c = (k_B T_c)^{-1}$, we have, by putting $< S_n^z >= 0$ on the left hand side,

$$\beta_c = \frac{2}{\Delta} \int \int d\mathbf{k}_{xy} \sum_{i=1}^{2N_z} \frac{D_{2n-1}(\omega_i)}{\omega_i} \tag{II.33}$$

There are N_z such equations using Eq. (II.31) with $n = 1, ..., N_z$. Since the layer magnetizations tend to zero at the transition temperature with different

values, it is obvious that we have to look for a convergence of the solution of Eq. (II.33) to a single value T_c.

II.4 Green's Function Results

We consider the helimagnetic case where J_2 is negative and $|J_2| > 0.25J_1$. The GS spin configuration across the film has been determined for each value of J_2/J_1. Using the values of $\theta_{i,j}$ to calculate the matrix elements of $\mathbf{M}$, then solving $\det|\mathbf{M}| = 0$, we find the eigenvalues $\omega_i (i = 1, ..., 2N_z)$ for each $\mathbf{k}_{xy}$ with an input set of $< S_n^z > (1, ..., N_z)$ at a given T. Using Eq. (II.31) for $n = 1, ..., N_z$ we calculate the output $< S_n^z > (1, ..., N_z)$. Using this output set as input, we calculate again $< S_n^z >$ until the input and output are identical within a desired precision $P = 1\%$. Numerically we use a Brillouin zone of 100^2 wave-vector values, and use the obtained values $< S_n^z >$ at a given T as input for a neighboring T. At low T and up to $\sim \frac{3}{5} T_c$, only a few iterations suffice to get the convergence precision. Near T_c, the convergence is much harder.

II.4.1 Spin-wave spectrum

In spin systems, collective excitations are called spin waves or magnons when they are quantized. They propagate in magnetically ordered systems like phonons in crystalline solids. At finite temperatures, as long as the magnetic order exists ($T < T_c$), spin waves are the only physical process to determines the magnetic properties of the system. In the semiclassical approach the spins are treated as precessing vectors, the spin waves are illustrated schematically in Fig. II.4.

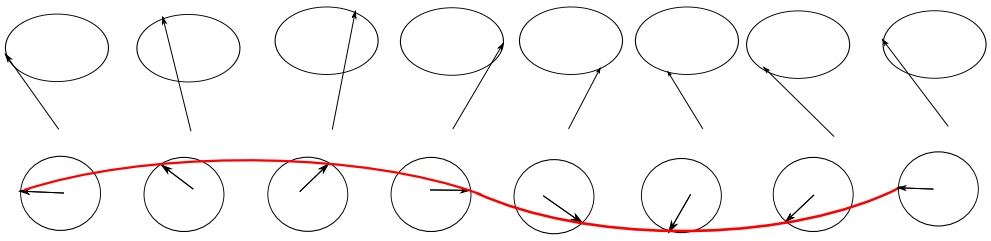

Figure II.4: Semiclassical representation of a spin wave.

In the bulk case, making a 3D Fourier transformation of Eq. (II.23) we obtain the spin wave dispersion relation in the absence of anisotropy:

$$\hbar\omega = \pm\sqrt{A^2 - B^2} \tag{II.34}$$

where

$$A = J_1 \langle S^z \rangle [8\gamma - 8 + z_2(\cos\theta + 1)\cos k_z - 2z_2 \cos\theta)] + J_2 \langle S^z \rangle [(\cos 2\theta + 1) z_2 \cos 2k_z - 2z_2 \cos 2\theta]$$

$$B = J_1 \langle S^z \rangle (\cos\theta - 1) z_2 \cos k_z + + J_2 \langle S^z \rangle (\cos 2\theta - 1) z_2 \cos 2k_z$$

where z_2=2 the number of NNN on the c-axis, and $\gamma = \frac{1}{2}(\cos k_x + \cos ky)$. We see that $\hbar\omega$ is zero when $A = \pm B$, namely, at $k_x = k_y = k_z = 0$ and at $k_z = \theta$ along the helical axis (see Fig. II.5).

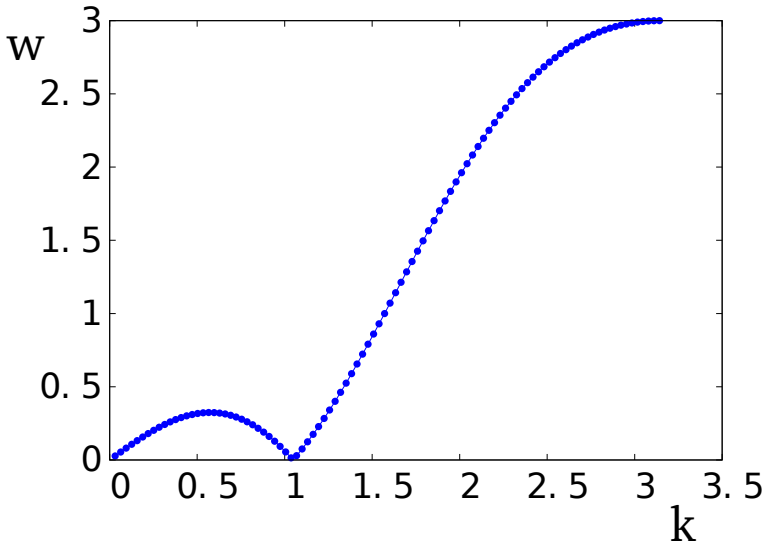

Figure II.5: Spin-wave spectrum versus k_z at T=0, in the bulk case $d = 0$, $J_2 = -0.5$, and $k_x = k_y = 0$.

The amplitude of a bulk spin-wave mode does not vary in space (see Fig. II.4), but near a magnetic perturbation such as surface, the spin waves can be spatially localized. Such modes are called "surface localized modes". Their amplitudes decay when they propagate from the surface into the bulk for an acoustic surface mode, and increases for an optical surface mode.

Let us take $J_1^{//} = J_1^{\perp} = J = 1$ everywhere except on the surface where $J_1^{//} = J_s$. We have calculated the spin-wave spectrum ω versus $k_x = k_y$ for various values of J_s. In the case of an eight-layer film with an anisotropy d=0.1, there are 8 positive and 8 negative modes corresponding two opposite spin precessions which describe the opposite circular motions of each lattice

spin. The negative sign does not mean spin-wave negative energy, but it indicates just the precession contrary to the trigonometric sense.

We can mention here the existence of two degenerate acoustic surface modes for J_s=0.6, which lie in the low energy region [Fig. II.6(middle)] and two optical surface branches which lie outside the bulk-mode energy region for J_s=1.6 [Fig. II.6(bottom)], whereas no such modes exist in the case when $J_s = 1$ [Fig. II.6(top)]. This degeneracy comes from the two symmetrical surfaces of the film. These surface modes propagate parallel to the film surface and their presence affects directly the surface magnetization: acoustic modes diminish the surface magnetization according to Eq. (II.31), while optical modes increase it (see Fig. II.7). As T increases, layer magnetizations decrease, reducing therefore the spin wave energy as seen in Fig. II.8.

II.4.2 Spin contraction at T=0

It is known that in antiferromagnets, quantum fluctuations give rise to a contraction of the spin length at zero temperature [57]. We will see here that a spin under a stronger antiferromagnetic interaction has a stronger zero-point contraction. The spins near the surface serve for such a test. In the case of the film considered above, spins in the first and second layers have only one antiferromagnetic NNN while interior spins have two NNN, so the contraction at a given J_2/J_1 is expected to be stronger for interior spins. This is verified with the results shown in Fig. II.9. When $|J_2|/J_1$ increases, namely the antiferromagnetic interaction becomes stronger, we observe stronger contractions. Note that the contraction tends to zero when the spin configuration becomes ferromagnetic, namely J_2 tend to -0.25. We show the layer magnetizations in Fig. II.10 in the case where $J_2/J_1 = -0.7$ and $N_z = 8$. Some remarks are in order: (i) The shown result is obtained with a convergence of 1%. For temperatures close to the transition temperature T_c, we have to lower the precision to a few percents which reduces the clarity because of their close values, (ii) The surface magnetization, which has a large value at T=0 as seen in Fig. II.9, crosses the interior layer magnetizations at $T \simeq 0.6$ to become smaller than the interior layer magnetizations at higher temperatures. This cross-over phenomenon is due to the competition between quantum fluctuations, which dominate the low-T behavior, and the low-lying surface spin-wave modes which strongly diminish the surface magnetization at higher T. Note that the second-layer magnetization makes also a crossover at $T \simeq 0.6$. Similar cross-overs have been observed in quantum antiferromagnetic thin films [57] and quantum superlattices [58].

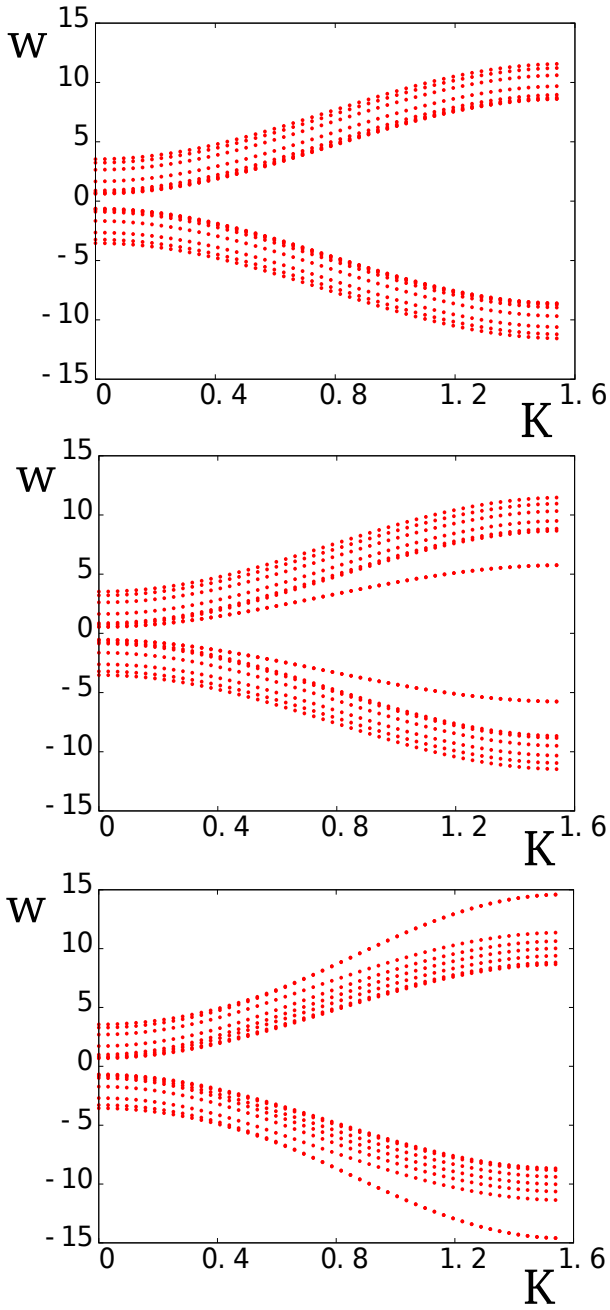

Figure II.6: Spin-wave spectrum versus k=k_x=k_y at T = 0.19, in the case where N_z=8, d=0.1, and J_2=-0.5 for J_S=1 (top), J_s=0.6 (middle) and J_s=1.6 (bottom).

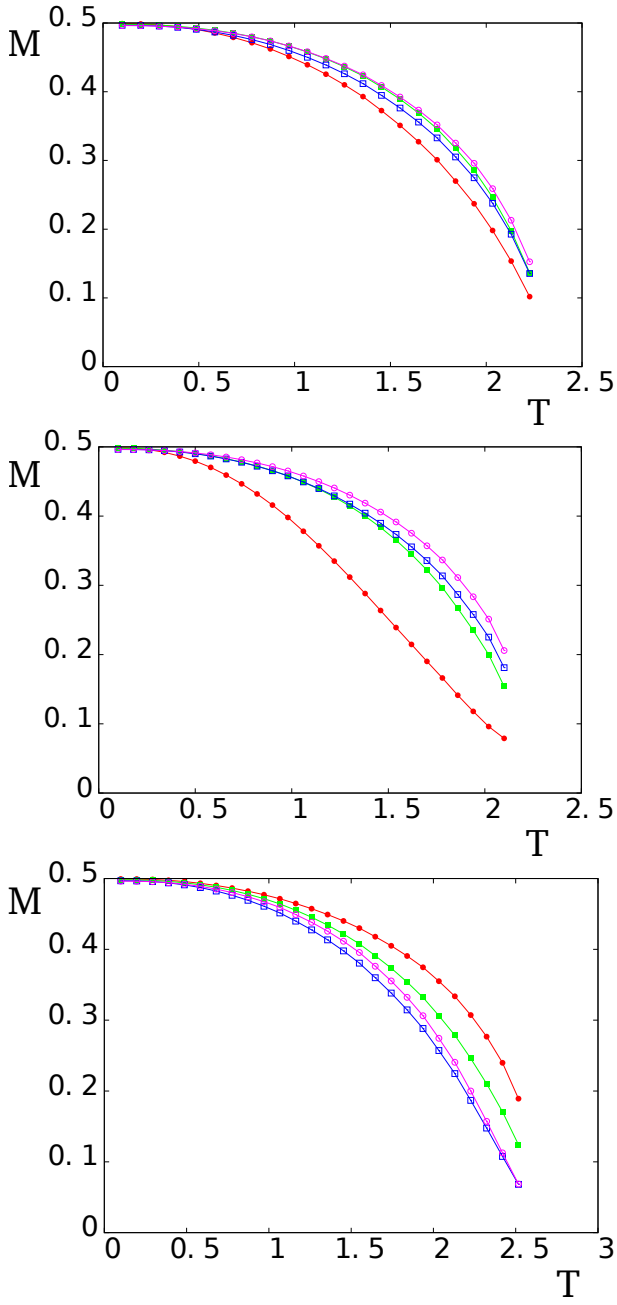

Figure II.7: Layer magnetizations as function of T for J_2=-0.5 with d=0.1, N_z=8: red circles, green squares, blue void squares and magenta void circles are magnetization of the first, second, third and fourth layers, respectively, for J_S=1 (top), J_s=1 (middle), J_s=1.6 (bottom).

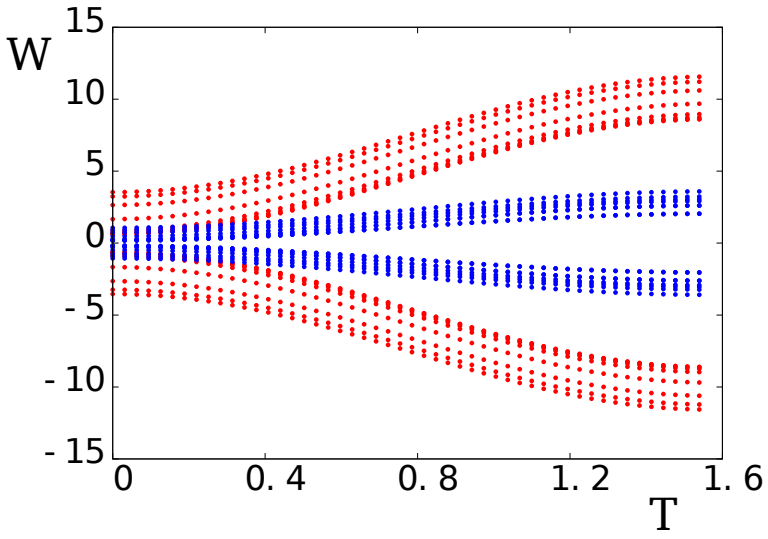

Figure II.8: Spin-wave spectrum versus k=k_x=k_y at T=0.19 (red) and T=2.22 (green), in the case where N_z=8, d=0.1, J_2=-0.5 and J_s=1.

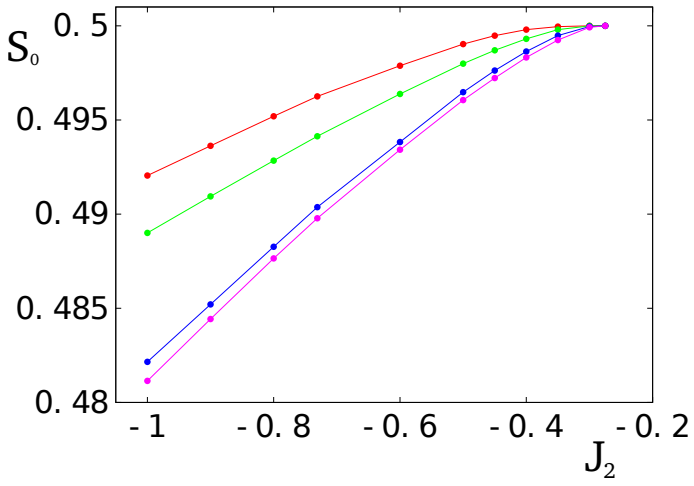

Figure II.9: Spin lengths at $T = 0$ for several values of J_2 with $d = 0.1$, $N_z = 8$, for spins in first (red), second (green), third (blue) and fourth layers (magenta), respectively.

II.4.3 Transition temperature

Layer magnetizations are different at low temperatures, they will tend to zero at a unique transition temperature as seen in Fig. II.11(top). The reason is that as long as an interior layer magnetization is not zero, it will act on the surface spins as an external field, preventing them to become zero.

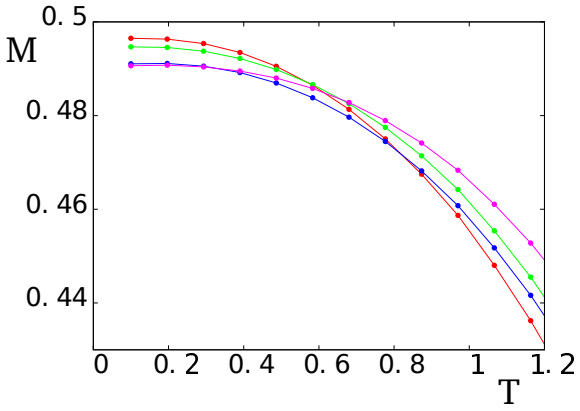

Figure II.10: Layer magnetizations as functions of T for J_2=-0.7 with d=0.1, N_z=8, for spins in first (red), second (green), third (blue) and fourth layers (magenta), respectively.

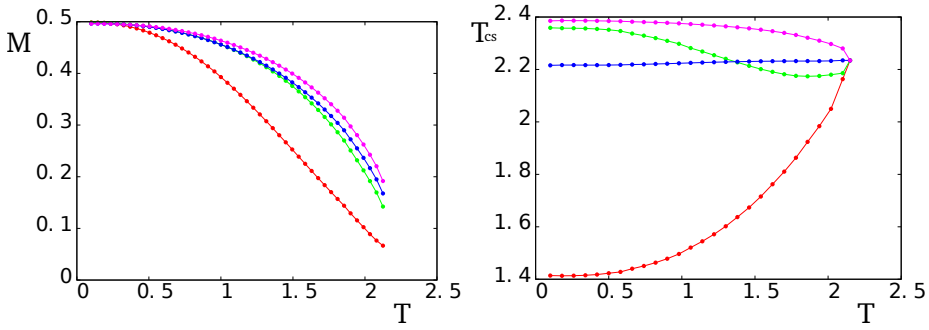

Figure II.11: Layer magnetization (top) and pseudo transition temperatures T_{cs} (bottom) as functions of T for $J_2 = -0.5$ with $J_s = 0.6$, $N_z = 8$, for spins in first (red), second (green), third (blue) and fourth layers (magenta), respectively.

Since the convergence is rather good at low T but it is difficult near T_c, we explain how to determine T_c by another way which is easier. As said earlier, each Eq. (II.33) for a given n gives a pseudo transition T_{cs} as long as T is not close to the temperature where all layers magnetizations vanish. To determine this temperature, we have to use the self-consistent layer magnetizations obtained as described above at a temperature as close as possible to T_c as input for Eq. (II.33), we find four pseudo-transition temperatures T_{cs} as seen in Fig. II.11 (bottom). The convergence of these temperatures to a single one occurs when T=T_c. It is obtained by a short

extrapolation from temperatures when they rather close to each other. T_c is thus obtained with a very small extrapolation error. The results for several J_2/J_1 are shown in Fig. II.12.

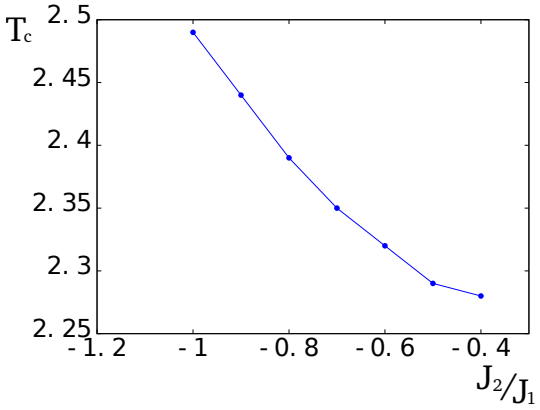

Figure II.12: Transition temperature T_c as a function of J_2/J_1.

II.5 Helimagnetic Thin Films in a Field

In a film, the angles between NN in adjacent planes are not uniform across the film, a strong variation is observed near the surface. An exact determination is made by the numerical steepest descent method explained above. The latter is particularly efficient for complex situations such as the present case where the spins are no longer in the xy planes in an applied magnetic field. The spin in the *i-th* layer is determined by two parameters which are the angle with its NN in the adjacent plane $\alpha_{i,j}$, and the azimuthal angle β_i formed with the *c-axis*. The spins here are supposed to be classical and the Hamiltonian is given by

$$\mathcal{H} = -\sum_{\langle i,j \rangle} J_{i,j} \, \vec{S}_i \, . \, \vec{S}_j - \sum_i H. \, \vec{S}_i \tag{II.35}$$

where $J_{i,j}$ is the interaction between two spins $\mathcal{S}_i$ and $\mathcal{S}_j$ occupying the lattice sites i and j and H denotes an external magnetic field applied along the c-axis. We use the steepest descent method to determine the classical ground state. Note that we have used several different initial conditions to check the convergence to a single GS for each set of parameters. Figures II.13(a) and II.13(b) show that whatever the initial spin configuration is used, one has S_1^z and $S_{N_z}^z$ converge, following different paths, to the same value. Figure II.13(c)

shows the convergence of the energy per spin to the same value whatever the initial condition is. Figure II.13(d) shows that the energy calculated by the steepest descent method at $T = 0$ is on the extrapolation of the energy calculated by MC simulation at finite T. There is thus no problem of metastability: the spin configuration obtained by the steepest descent method is the GS.

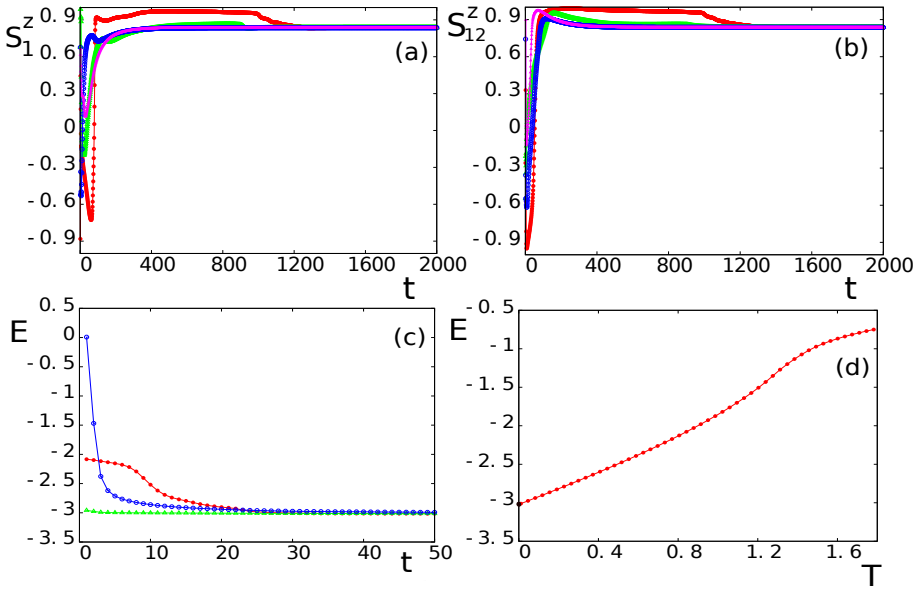

Figure II.13: Time evolution of (a) S_1^z, (b) $S_{N_z}^z$, (c) energy for different spin configuration, (d) energy versus temperature T.

We show in Fig. II.15 the GS configuration obtained for $J_2 = -1$ and $H = 0.2$. The circles in the xy planes with radius equal to 1 are plotted to help identify the orientation of each spin. We describe qualitatively the spin configuration in a field:

i) First of all, the spin configuration depends on the film thickness even in the case where all interactions are the same.

ii) Several planes have negative z spin components.This may be surprising at the first sight since all spins do not turn themselves to the field direction. However, this can be understood by examining the competition between the magnetic field which tends to align spins in the c direction, and the antiferromagnetic interaction J_2 which tries to preserve the antiferromagnetic ordering. This is very similar to the the case of collinear antiferromagnet: in weak magnetic field the spins remain antiparallel, and in a moderate field, the so called "spin flop" occurs: the neighboring spins stay antiparallel with each other but turn themselves perpendicular to the field direction to reduce

the field effect [59].

iii) Due to the symmetry of the two surfaces, their z components are identical (see Fig. II.18), i.e. $S_1^z = S_{N-z}^z$. The same is observed for any two symmetrical planes with respect to the middle of the film, for example $S_2^z = S_{N_z-1}^z$, $S_3^z = S_{N_z-2}^z$ etc. Note that while le z components are equal, the x and y components are antiparallel (see Fig. II.14) $S_1^y = -S_{N_z}^y$, $S_1^x = -S_{N_z}^x$. The spins preserve their antiferromagnetic interaction for the transverse components. Only at a very strong field that all spins turn into the field direction.

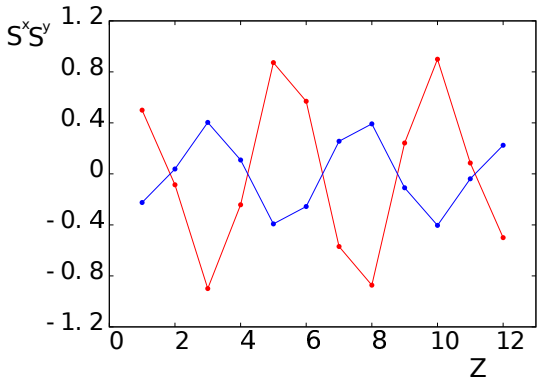

Figure II.14: Spin components across the film in the case where H=0.2. S^x (red), S^y (blue).

A full view of the "chain" of N_z spins along the *c-axis* between the two surfaces is shown in Fig. II.15. Note that the angle in the xy plane is determined by the NNN interaction J_2. Without field, the symmetry is about the c-axis, so x and y spin components are equivalents. Under the field, due to the surface effect, the spins make different angles with the c-axis, giving rise to different z components for the layers across the film as shown in Fig. II.18. Of course, the symmetry axis is still the c-axis, so all S^x and S^y are invariant under a rotation around the c-axis. Figure II.14 is thus an instantaneous configuration of S^x and S^y for each layer across the film. As the simulation time is going on these components rotate about the c axis but their symmetry remains at any time. The xy spin modulus S^{xy} shown in Fig II.18, on the other hand, is time-invariant.

The z components are quite different from plane to plane with the symmetry mentioned above. The reason comes from the fact that the local fields acting on spins near the surface are very different due to the lack of neighbors. The finite "chain" of N_z spins along the c-axis between the two surfaces have a particular symmetry: the z components at the two ends are symmetric

and the spins between these two ends form a non-collinear domain-wall-like configuration.

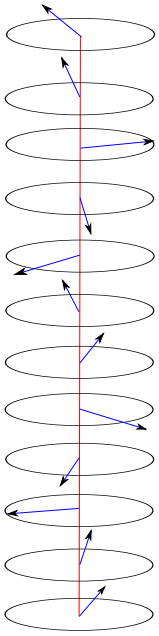

Figure II.15: Spin configuration in the case where H=0.2, J2=-1, N_z=12.

The ground state spin configuration depends on the field magnitude H. If H increases, we observe an interesting phenomenon: Fig. II.16 shows the spin configuration projected on the xy plane (top view) for increasing magnetic field. We see that the spins of each chain tend progressively to lie in the same plane perpendicular to the xy planes [see Fig. II.16(a-b-c)]. The "planar zone" observed in Fig. II.16(c) occurs between $H \simeq 0.05$ and 0.35. For stronger fields they are no more planar [Fig. II.16(d-e-f)]. Note that the larger the xy component is, the smaller the z component becomes: for example in Fig. II.16(a) the spins are in the xy plane without field ($H = 0$) and in Fig. II.16(f) they are almost parallel to the c axis because of a very high field.

We show in Fig. II.17 the angles α_i between a spin of layer i with its NN in layer (i+1) projected on the xy plane. As seen, for $0.05 \leq H \leq 0.35$ the α angles between NN are 0 or 180 degrees. This is a striking aspect which results certainly from a competition between the action of the field and the antiferromagnetic interaction in analogy with the spin-flop phenomenon in antiferromagnets: spins prefer to align in a way to preserve at least a part of their antiferromagnetic interaction.

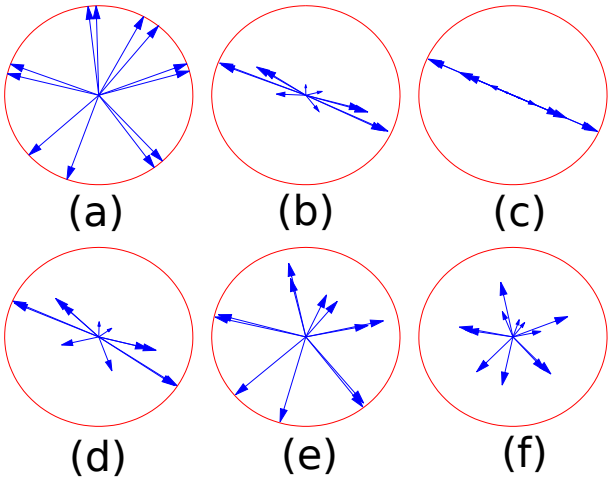

Figure II.16: Top view of S^{xy} (projection of spins on xy plane) across the film for several values of H: (a) 0, (b) 0.03, (c) 0.2, (d) 0.4, (e) 0.7, (f) 1.7. The radius of the circle, equal to 1, is the spin full length. For high fields, spins are strongly aligned along the c-axis, S^{xy} is therefore much smaller than 1.

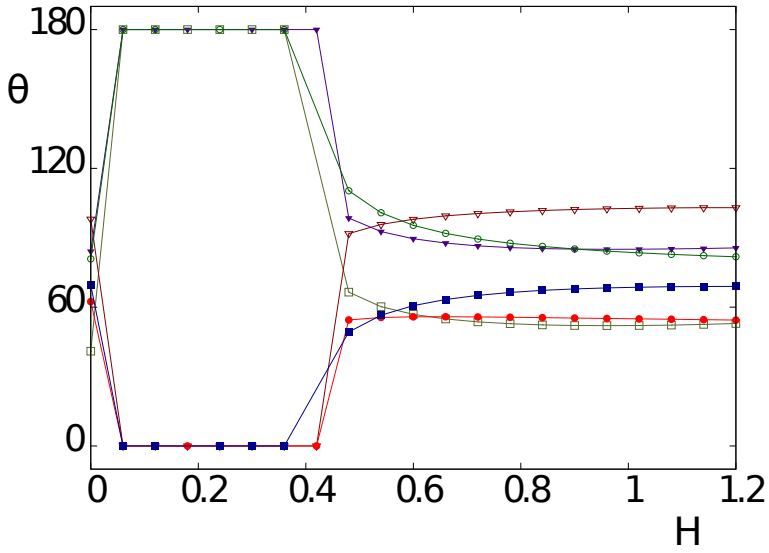

Figure II.17: Projection on the xy plane of the angle α_i between a spin in layer i and its NN in the layer $i+1$ (in degree) as a function of H for $N_z = 12$, J_2=-1. Dark olive green void squares are for α_1, maroon void triangles for α_2, red circles for α_3, indigo triangles for α_4, dark blue squares for α_5, dark void circles for α_6.

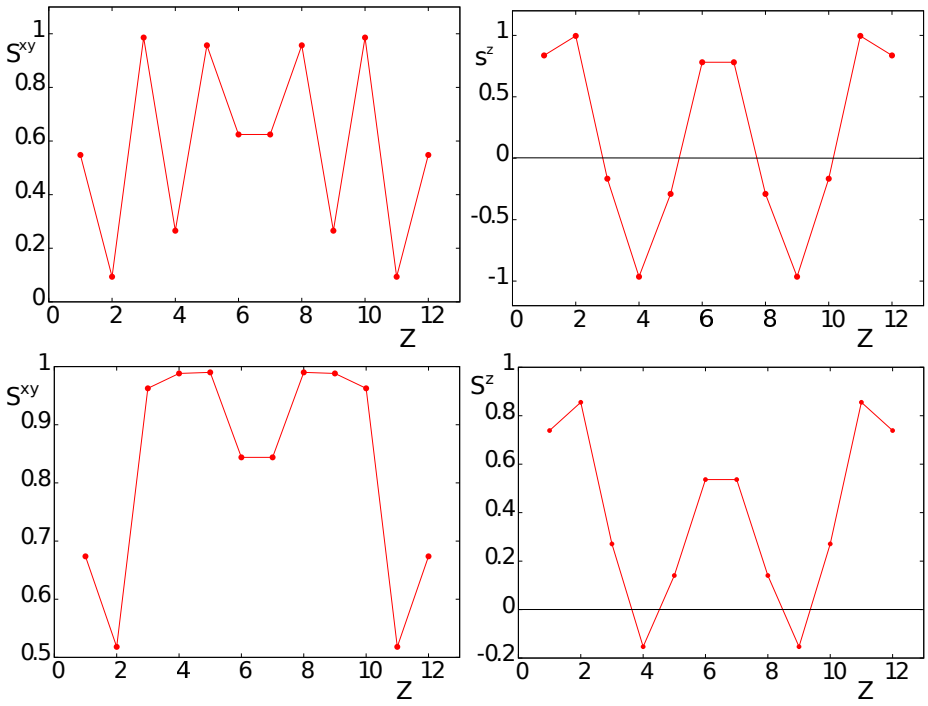

Figure II.18: S^{xy} and S^z components across the film in the case where H=0.2 and 0.7.

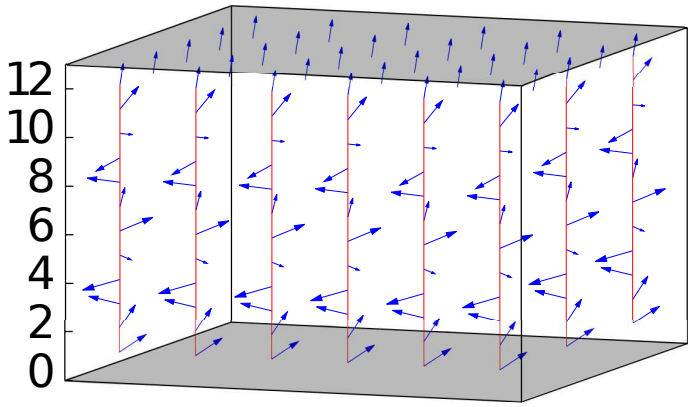

Figure II.19: Spin configuration at $T = 0$ for H=0.6. For clarity only columns at the front edges are shown.

II.5.1 Phase transition

As described above, the planar helical spin configuration in zero field become non planar in a perpendicular field. In order to interpret the phase transition shown below, let us mention that a layer having a large z spin-component

parallel to the field cannot have a phase transition because its magnetization will never become zero. This is similar to a ferromagnet in a field. However layers having large negative z spin-components (antiparallel to the field) can undergo a transition due to the magnetization reversal at higher temperature similarly to an antiferromagnet in a field. In addition, the xy spin-components whose xy fluctuations are not affected by the perpendicular field can make a transition. Having mentioned these, we expect that some layers will undergo a phase transition, while others will not. This is indeed what we observed in MC simulations shown in the following.

For MC simulations, we use the Metropolis algorithm (see Appendix) and a sample size $N \times N \times N_z$ with N=20, 40, 60, 100 for detection lateral size effects and N_z=8, 12, 16 for thickness effects. The equilibrium time is 10^5 MC steps/spin and the thermal average is performed with the following 10^5 MC steps/spin.

In order to appreciate the effect of the applied field, let us show first the case where H=0 in Fig. II.20(top). We see that all layers undergo a phase transition within a narrow region of T.

In an applied, as seen earlier, in the GS all layers do not have the same characteristics so one expects different behaviors. Figure II.20(bottom) shows the layer magnetizations and the layer susceptibility as functions of T for H= 0.2 with J_2= -1, N_z= 12 (only the first six layers are shown, the other six are symmetric). Several remarks are listed below:

(i) Only layer 3 and layer 5 have a phase transition: their magnetizations strongly fall down at the transition temperature. This can be understood from what we have anticipated above: these layers have the largest xy components (see Fig. II.14). Since the correlation between xy components do not depend on the applied field, the temperature destroys the in-plane ferromagnetic ordering causing the transition. It is not the case for the z components which are kept non zero by the field. By symmetry, layers 8 and 10 have the same transition.

(ii) Layers with small amplitudes of xy components do not have a strong transverse ordering at finite T, the absence of pronounced peaks in the susceptibility indicate that they do not make a transition as seen in Fig. II.20(bottom).

(iii) Note that the xy spin components of layers 3 and 5 are disordered at $T_c \simeq 1.275$ as indicated by pronounced peaks of the susceptibility.

Under an applied magnetic field the film can have a partial transition: some layers with large xy spin-components undergo a phase transition (destruction of their transverse xy correlation). This picture is confirmed by several simulations for various field strengths. Another example is shown in the case of a strong field H= 0.7. The GS has been shown in Fig. II.18(bottom) where we observe larger xy spin-components of layers 3, 4 and 5 (and their

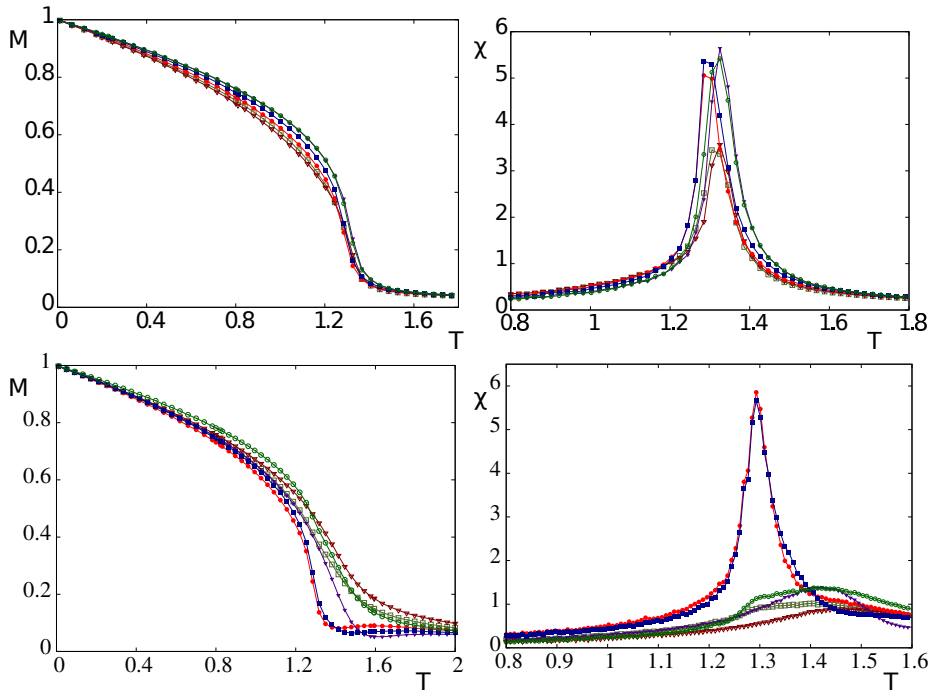

Figure II.20: Layer magnetization and layer magnetic susceptibility as functions of T for H=0 (top) and H=0.2 (bottom), J_2=-1, N_z=12. Dark olive green void squares are for the first layer, maroon void triangles for the second, red circles for the third, indigo triangles for the fourth, dark blue squares for the fifth, dark void circles for the sixth layer.

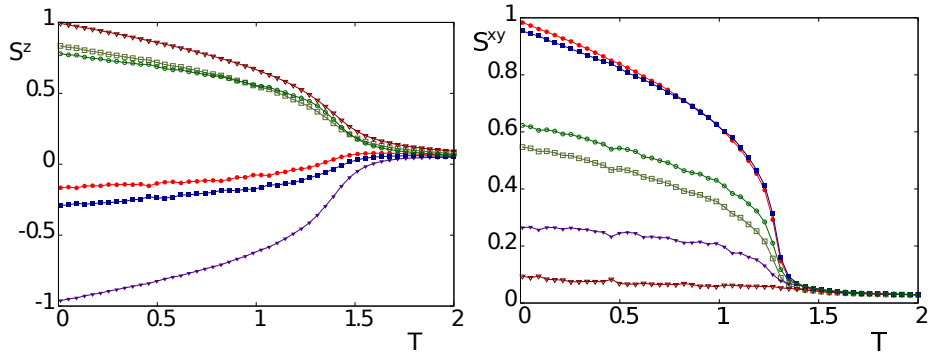

Figure II.21: S^z and S^{xy} of each layer versus T for an applied magnetic field H=0.2. Dark olive green void squares are for the first layer, maroon void triangles for the second, red circles for the third, indigo triangles for the fourth, dark blue squares for the fifth, dark void circles for the sixth layer.

symmetric layers 7, 8 and 9). We should expect a transition of each of these layers. This is indeed the case: we show this transition in Fig. II.22 where sharp peaks of the susceptibilities of these layers are observed. This transition mechanism is also observed for other fields.

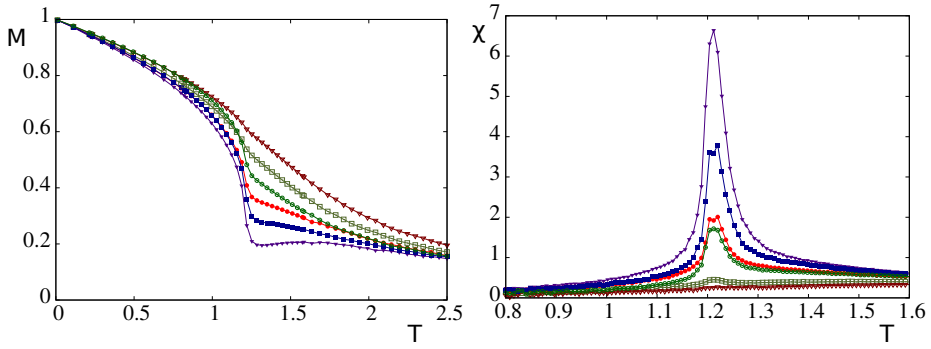

Figure II.22: Layer magnetization and layer magnetic susceptibility as function of T for H=0.7, J_2=-1, N_z=12,Dark olive green void squares for the first layer, maroon void triangles for the second, red circles for the third, indigo triangles for the fourth, dark blue squares for the fifth, dark void circles for the sixth layer.

We close this section by showing some size effects. Figure II.23 shows the effect of the lateral size (xy planes) on the layer susceptibility. As expected in a continuous transition, the peaks of the susceptibilities of the layers undergoing a transition grow strongly with the layer lattice size.

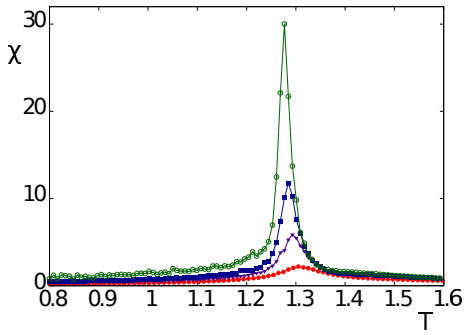

Figure II.23: Magnetic susceptibility of the third layer as a function of T for H=0.2, J_2=-1, N_z=12. Dark green void circles, dark blue squares, indigo triangles, red circles are susceptibilities for layer lattice size 100×100, 60×60, 40×40 and 20×20, respectively.

As for the thickness effects we note that changing the thickness (odd or even number of layers) will change the GS spin configuration so that the

layers with largest xy components are not the same for different thicknesses. As a consequence, the layers which undergo the transition are not the same for different thicknesses. We show in Fig. II.24 the layer susceptibilities for N_z=8 and 16. For N_z=8, the layers which undergo a transition are the first , third and fourth layers with pronounced peaks, while for N_z=16, the layers which undergo a transition are the third, fifth, seventh and eighth layers.

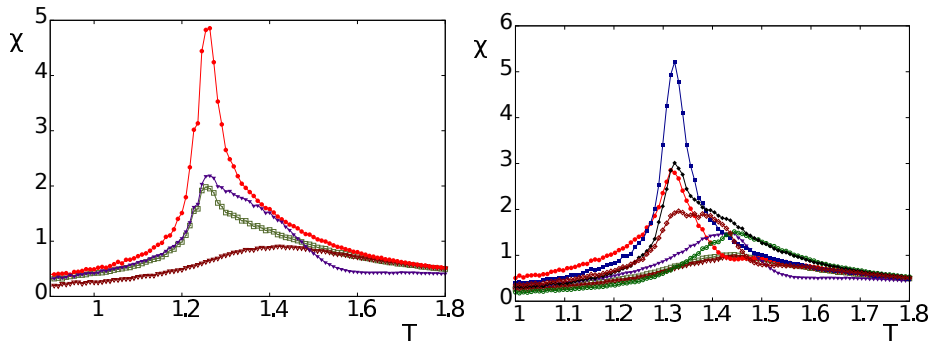

Figure II.24: Magnetic susceptibility as a function of T for two thicknesses with H=0.2, J_2=-1. Left: N_z=8. Right: N_z=16. Dark olive green void squares are for the first layer, maroon void triangles for the second, red circles for the third, indigo triangles for the fourth, dark blue squares for the fifth, dark void circles for the sixth layer, black diamonds for the seventh, dark brown void diamonds for the eight.

Let us show the case of an odd number of layers. Figure II.25 shows the results for N_z=9 with H=0.2, J_2=-1. Due to the odd layer number, the center of symmetry is the middle layer (5th layer). As seen, the layers 1 and 4 and their symmetric counterparts (layers 9 and 6) have largest xy spin modulus as seen in Fig. II.25(middle). The transition argument shown above predicts that these layers have transversal phase transitions. This is indeed seen in Fig. II.25(bottom) where the susceptibility of layer 4 has a strong peak at the transition. The first layer, due to the lack of neighbors, has a weak peak. The other layers do not undergo a transition. They show only a rounded maximum.

II.5.2 Low-temperature quantum fluctuations

We extend here the Green's function used in the above section for zero field to the case where an applied magnetic field is present. The method remains essentially the same except the fact that each spin is defined not only by its angles with the NN in the adjacent layers but also by its azimuthal angle formed with the c-axis. We use in the following Hamiltonian (II.35) but

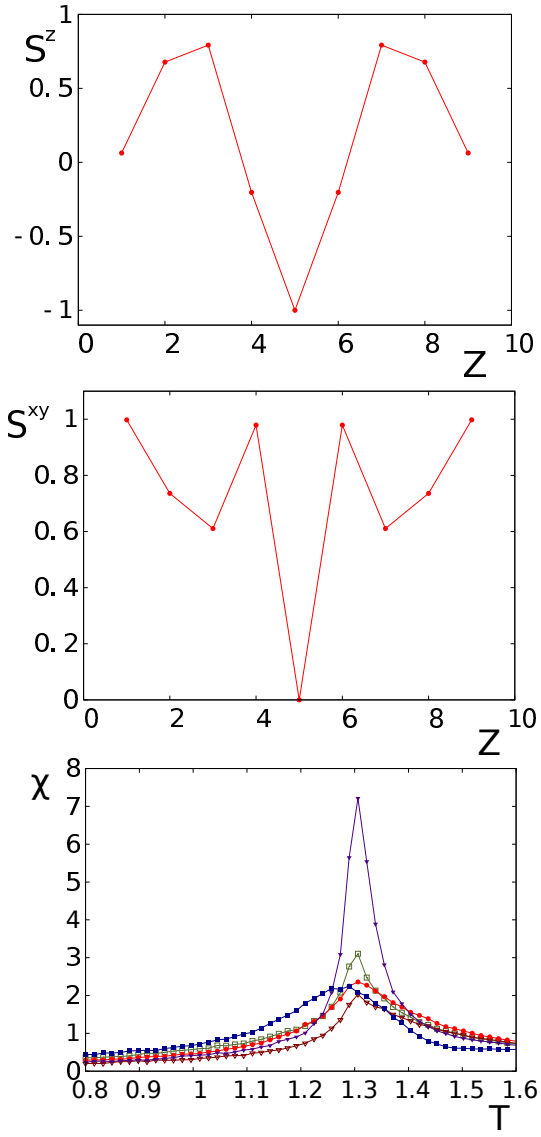

Figure II.25: Case of 9-layer film. Spin components across the film for H=0.2. Top: S_z, middle: S^{xy}, bottom: layer susceptibilities versus T. Dark olive green void squares are for the first layer, maroon void triangles for the second, red circles for the third, indigo triangles for the fourth, dark blue squares for the fifth layer, respectively.

with quantum Heisenberg spins S_i of magnitude 1/2. In addition, we add an anisotropic interaction to stabilize the long-range ordering at finite temperature:

$$\mathcal{H}_a = -I_1 \sum_{<i,j>} S_i^z S_j^z \cos\theta_{ij} \tag{II.36}$$

where I_1 is supposed to be positive, small compared to J_1, and limited to NN. The general method has been described in section II.3. We express the Hamiltonian in the local coordinates of spin S_i:

$$\begin{aligned}\mathcal{H} = &-\sum_{\langle i,j\rangle} J_{i,j}[\frac{1}{4}(S_i^+ S_j^+ + S_i^- S_j^-)(\cos\theta_{ij} - 1) \\ &+ \frac{1}{4}(S_i^+ S_j^- + S_i^- S_j^+)(\cos\theta_{ij} + 1) \\ &+ \frac{1}{2}\sin\theta_{ij}(S_i^+ + S_i^-)S_j^z - \frac{1}{2}\sin\theta_{ij}(S_J^+ + S_j^-)S_i^z + S_i^z S_j^z \cos\theta_{ij}] \\ &- \sum_{\langle i,j\rangle} I_{i,j} S_i^z S_j^z \cos\theta ij - \sum_i H.S_i\end{aligned} \tag{II.37}$$

We define the following two double-time Green's functions in the real space:

$$\begin{aligned} G_{i,j}(t,t') &= << S_i^+(t); S_j^-(t') >> \\ &= -i\theta(t-t') < \left[S_i^+(t), S_j^-(t')\right] > \qquad \text{(II.38)} \\ F_{i,j}(t,t') &= << S_i^-(t); S_j^-(t') >> \\ &= -i\theta(t-t') < \left[S_i^-(t), S_j^-(t')\right] > \qquad \text{(II.39)} \end{aligned}$$

Writing the equations of motion of these functions and using the Tyablikov decoupling scheme to reduce the higher-order functions, we obtain the general equations for non-collinear magnets. We next introduce the following in-plane Fourier transforms $g_{n,n'}$ and $f_{n,n'}$ of the G and F Green's functions, we finally obtain the following coupled equations:

$$\begin{aligned}&D_n^- g_{n-2,n'} + E_n^- f_{n-2,n'} + B_n^- g_{n-1,n'} + C_n^- f_{n-1,n'} \\ &+(\omega + A_n) g_{n,n'} + B_n^+ g_{n+1,n'} + C_n^+ f_{n+1,n'} + D_n^+ g_{n+2,n'} \\ &+E_n^+ f_{n+2,n'} = 2\left\langle S_n^z \right\rangle \delta_{n,n'} \qquad \text{(II.40)} \\ &-E_n^- g_{n-2,n'} - D_n^- f_{n-2,n'} - C_n^- g_{n-1,n'} - B_n^- f_{n-1,n'} \\ &+(\omega - A_n) f_{n,n'} - C_n^+ g_{n+1,n'} - B_n^+ f_{n+1,n'} \\ &-E_n^+ g_{n+2,n'} - D_n^+ f_{n+2,n'} = 0 \qquad \text{(II.41)}\end{aligned}$$

where $n = 1, 2, ..., N_z$, $d_n = I_1/J_1^{\shortparallel}$, $\gamma = (\cos k_x a + \cos k_y a)/2$. The coefficients are given by

$$\begin{aligned}
A_n &= -8J_1^{\shortparallel} < S_n^z > (1 + d_n - \gamma) \\
&\quad -2 < S_{n+1}^z > \cos\theta_{n,n+1}(d_n + J_1^{\perp}) \\
&\quad -2 < S_{n-1}^z > \cos\theta_{n,n-1}(d_n + J_1^{\perp}) \\
&\quad -2J_2 < S_{n+2}^z > \cos\theta_{n,n+2} \\
&\quad -2J_2 < S_{n-2}^z > \cos\theta_{n,n-2} - H\cos\zeta_n \\
B_n^{\pm} &= 2J_1^{\perp} \langle S_n^z \rangle (\cos\theta_{n,n\pm1} + 1) \\
C_n^{\pm} &= 2J_1^{\perp} \langle S_n^z \rangle (\cos\theta_{n,n\pm1} - 1) \\
E_n^{\pm} &= J_2 \langle S_n^z \rangle (\cos\theta_{n,n\pm2} - 1) \\
D_n^{\pm} &= J_2 \langle S_n^z \rangle (\cos\theta_{n,n\pm2} + 1)
\end{aligned}$$

where ω is the spin-wave frequency, k_x and k_y denote the wave-vector components in the xy planes, n is the index of the layer along the c axis with $n = 1$ being the surface layer, $n = 2$ the second layer and so on. The angle ζ_n is the azimuthal angle formed by a spin in the layer n with the c axis. Besides, we have distinguished the in-plane NN interaction $J_1^{\shortparallel}$ from the inter-plane NN one $J_1^{\perp}$. If we write all equations explicitly for $n = 1, ..., N_z$ we can put these equations under a matrix of dimension $2N_z \times 2N_z$. Solving this matrix equation, one gets the spin-wave frequencies ω at a given wave vector and a given T.

We show in Fig. II.26(top) the spin length of different layers at $T = 0$ for N_z=12 and J_2=-1 as a function of H. All spin contractions are not sensitive for H lower than 0.4, but rapidly become smaller for further increasing H. The spin lengths are all saturated at the same value for $H > 2$. Figure II.26(bottom) shows the spin lengths as functions of J_2. When $J_2 \geq -0.4$, the spin configuration becomes ferromagnetic, and as a consequence, the contraction tends to 0. Note that in zero field, the critical value of J_2 is -0.25. The surface layer and third layer have smaller contractions than the other layers. This can be understood by examining the antiferromagnetic contribution of the GS energy of a spin in these layers: they are smaller than those of the other layers.

We show in Fig. II.27(top) the layer magnetizations versus T for the case where J_2=-1 and N_z=12. The low-T region is enlarged in the inset where one observes a cross-over between the magnetizations of layer 1, 3 and 6 at $T \simeq 0.8$: below this temperature $M_1 < M_3 < M_6$ and above they become $M_1 > M_3 < M_6$. This cross-over is due to the competition between several complex factors: for example quantum fluctuations have less effect on the surface magnetization making it larger than the magnetizations of

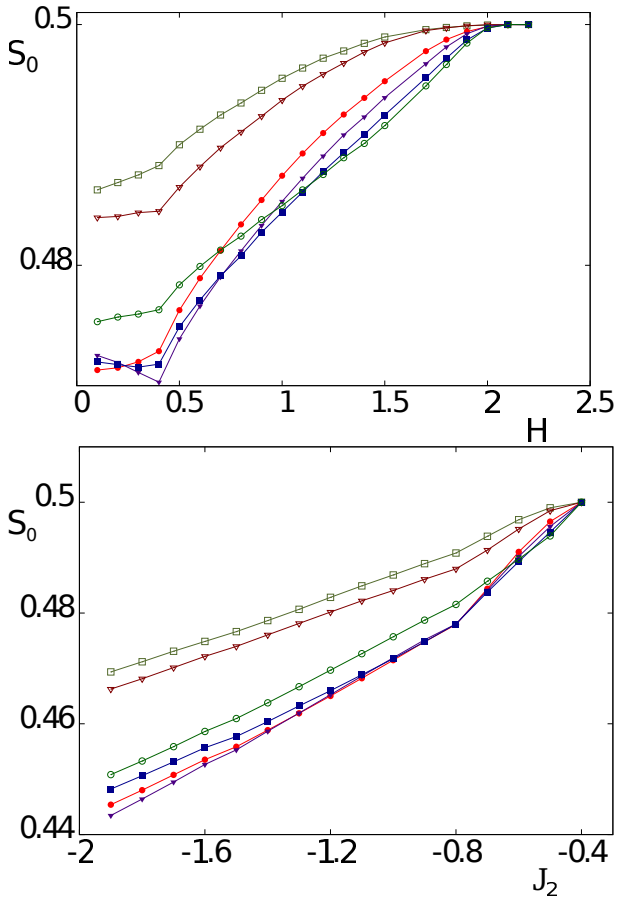

Figure II.26: Spin lengths at T=0 as a function of an applied magnetic field H (top) and versus J_2 (bottom). Dark olive green void squares are for the first layer, maroon void triangles for the second, red circles for the third, indigo triangles for the fourth, dark blue squares for the fifth, dark void circles for the sixth layer.

interior planes at low T, while the missing of neighbors for surface spins tend to diminish the surface magnetization at high T [57, 60]. The case where J_2=−0.5 closer to the ferromagnetic limit is shown in Fig. II.27(middle). The spin length at T=0 is almost 0.5 (very small contraction) and there is no visible cross-over observed in the top figure. Figure II.27(bottom) shows the case J_2=-2 which is the case of a strong helical angle. We observe then a cross-over at a higher T ($\simeq$1.2) which is in agreement with the physical picture given above on the competition between quantum and thermal fluctuations. Note that we did not attempt to get closer to the transition temperature, namely M <0.1 because the convergence of the self-consistency then becomes

bad.

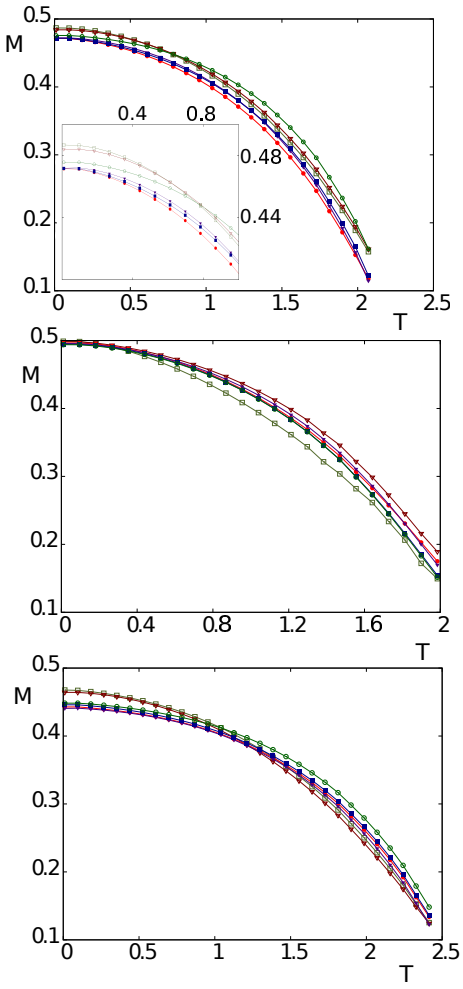

Figure II.27: Layer magnetizations as function of T for several value of J_2 with H=0.2, and N_z=12. TOP: j_2=-1, Middle: J_2 =-0.5, Bottom: j_2=-2. Dark olive green void squares for the first layer, maroon void triangles for the second, red circles for the third, indigo triangles for the fourth, dark blue squares for the fifth, dark void circles for the sixth layer. The inset in the top figure shows an enlarged region at low T.

Let us discuss about the spin-wave spectrum. We remind that to solve self-consistently equation (II.40) at each T, we use as inputs $< S_1^z >, < S_2^z >$ $, ..., < S_{N_z}^z >$ to search for the eigenvalues ω for each vector (k_x, k_y) and then calculate the outputs $< S_1^z >, < S_2^z >, ..., < S_{N_z}^z >$ using equation (II.31). The self-consistent solution is obtained when the outputs are equal to the inputs at a desired convergence precision fixed at the fifth digit, namely

$10^{-}5$. Figure II.28 shows the spin-wave spectrum in the direction $k_x = k_y$ of the Brillouin zone at T=0.353 and T=1.212 for comparison. As seen, as T increases the spin-wave frequency decreases. At the transition it tends to zero.

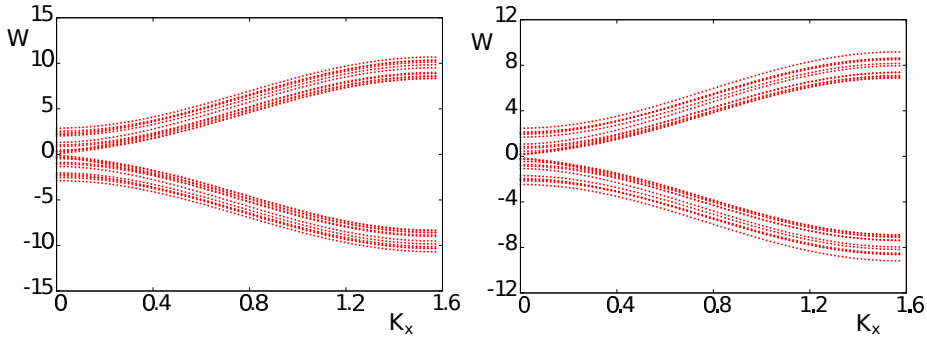

Figure II.28: Spin-wave spectrum versus $k_x = k_y$ where W stands for spin-wave frequency ω, for T=0.353 (left), T=1.212 (right), with H=0.2.

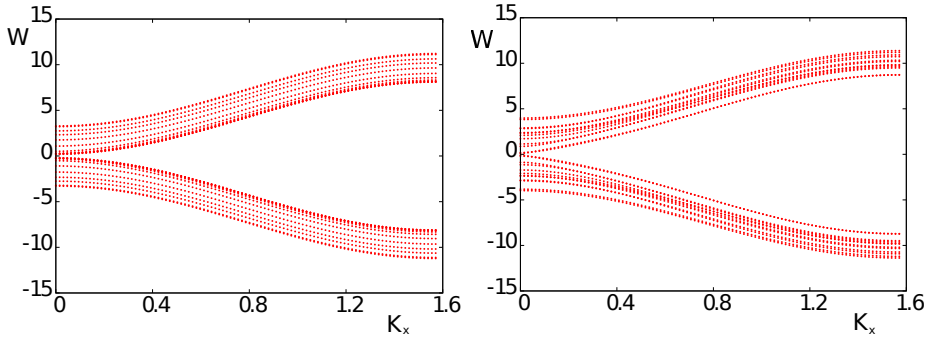

Figure II.29: Spin-wave spectrum versus $k_x = k_y$ at T=0.353 where W stands for spin-wave frequency ω, for J_2=-0.5 (left), J_2=-2 (right), with H=0.2.

Figure II.29 shows the spin-wave spectrum at $T = 0.353$ for J_2=-0.5 and -1, for comparison. Examining them closely, we see that the distribution of the spin-wave modes are quite different for the two cases. When summed up for calculating the layer magnetizations, this results in the difference observed for the two cases shown in Fig. II.27.

II.6 Conclusion

In this chapter, we have studied first the surface effect in a helimagnetic thin film of simple cubic lattice in zero field with quantum Heisenberg spins.

We have found a strong surface spin rearrangement which is experimentally observed on MnSi films and Holmium . We have calculated self-consistently physical quantities such as the spin-wave excitation, the spin length at T=0 and the layer magnetizations as functions of temperature. We have shown that when varying the surface exchange interaction, we observe surface-localized acoustic and optical modes which lie outside the bulk magnon energy band. These modes cause a strong deviation of the surface magnetization with respect to the interior one [49]. Another interesting phenomenon is the cross-over of layer magnetizations at low temperatures due to the competition between quantum fluctuations and thermal effects. Secondly, we have investigated the effect of an applied magnetic field along the c-axis perpendicular to the film using Monte Carlo simulation. We have found that when increasing the temperature, the layers with large xy spin-components undergo a phase transition where the ordering of the transverse (in-plane) xy spin-components is destroyed. This "transverse" transition is possible because the xy spin-components do not depend on the field. Other layers with small xy components, namely large z components, do not make transition because the ordering in S^z is maintained by the applied field. The transition of a number of layers with large xy spin components, not all layers, is a new phenomenon discovered here with our present model. We have also investigated the quantum version of the model by using the Green's function method. The results show that the zero-point spin contraction is different from layer to layer. We also found a cross-over of layer magnetizations which depends on the antiferromagnetic interaction strength, namely on the magnitude of helical angles.

Chapter III

Spin Systems with Dzyaloshinskii Moriya Interaction

Contents

III.1 Introduction

The Dyaloshinskii-Moriya (DM) interaction was proposed to explain the weak ferromagnetism which was observed in antiferromagnetic crystals, such as $MnCO_3$, $CoCO_3$ and α-Fe_2O_3. Based on the lack of inversion symmetry in these kinds of materials I. Dzyaloshinskii has introduced an interaction term [61] which was later microscopically derived by T. Moriya where he found the mechanism behind this interaction which stems from a spin-orbit coupling [62]. Hence, the interaction was named as the Dzyaloshinkii-Moriya interaction. There has been a large number of investigations on the effect

of DM interaction in various materials, both experimentally and theoretically for weak ferromagnetism in perovskite compounds [63–67]. However, the interest in the DM interaction goes beyond the weak ferromagnetism: for example, it has been recently shown in various works that the DM interaction is at the origin of spin spirals and topological skyrmions [9, 68–74] and new kinds of magnetic domain walls [75–79]. The increasing interest in skyrmions results from the fact that skyrmions may play an important role in the electronic transport which is at the heart of technological application devices [80–83].

In this chapter, we are interested in the spin-wave (SW) properties of a system of spins interacting with each other via a DM interaction in addition to the symmetric isotropic Heisenberg exchange interaction. The competition between these interactions gives rise to a non-collinear spin configuration in the ground state (GS). Unlike helimagnets where the helical GS spin configuration results from the competition between the symmetric nearest-neighbor (NN) and next-nearest neighbor (NNN) interactions [28, 29], the DM interaction, as said above, is antisymmetric. This gives rise to a non trivial SW behavior as will be seen below. Note that there has been a number of works dealing with the SW properties in DM systems [84–88].

This chapter is organized as follows. Section III.3 is devoted to the description of the model and the determination of the GS. Section III.4 shows results on the SW spectrum and the magnetization in two dimensions (2D) and three dimensions (3D). The case of thin films with free surfaces is shown in section III.5 where layer magnetizations at finite temperature (T) and the thickness effect are presented.

III.2 Dzyaloshinskii-Moriya Interaction

The Dzyaloshinskii Moriya interaction is related to the lack of inversion symmetry of the compound and a strong spin-orbit coupling. The DM interaction between two spins S_i and S_j is written as

$$\mathcal{H}_{DM} = \mathbf{D}_{i,j} \cdot (\mathbf{S}_i \wedge \mathbf{S}_j) \tag{III.1}$$

The Hamiltonian $\mathcal{H}_{DM}$ contains the cross product $\mathbf{S}_i \wedge \mathbf{S}_j$ which is a vector perpendicular to $\mathbf{S}_i$ and $\mathbf{S}_j$ times the $\mathbf{D}_{i,j}$ vector which results from the displacement of non magnetic ions located between $\mathbf{S}_i$ and $\mathbf{S}_j$, for example in Mn-O-Mn bonds. The direction of $\mathbf{D}_{i,j}$ depends on the symmetry of the displacement [62]. It can be obtained by the cross product $\mathbf{r}_i \wedge \mathbf{r}_j$. This implies that $\mathbf{D}_{ij}$ is perpendicular to the displacement plane (Fig III.1). In the case where the three atoms are aligned $\mathbf{D}_{ij}$=0.

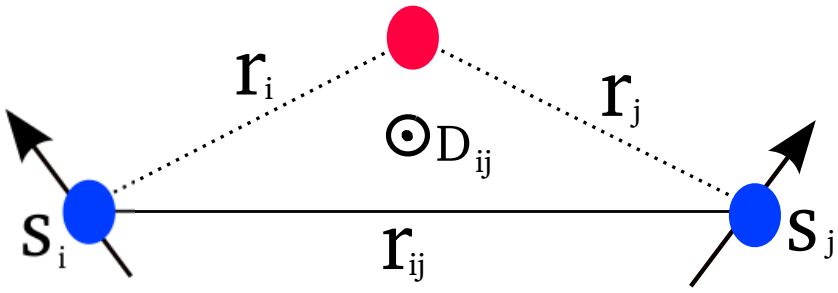

Figure III.1: Schematic view of the DM interaction for two spins.

The DM interaction favors a canted spin structure [61,89], unlike symmetric interaction J which favors a collinear configuration. These two exchange interactions are in competition. J is usually the leading term, that is why in many situations the DM effect is hidden. However, in a recent work it was demonstrated for the first time that on some surfaces the DM interaction dominates the symmetric exchange interaction [90] and induces a spatial rotating magnetic ground state. In ultra-thin magnetic films the DM interaction is crucial for the creation of non-collinear long-range spin order. The resulting structure depends on the direction of the D vector which depends on the symmetry of the displacement.

III.3 Model and Ground State

We consider a thin film of simple cubic (SC) lattice of N layers stacked in the y-direction perpendicular to the film surface. The Hamiltonian $\mathcal{H}$ is given by:

$$\begin{aligned} \mathcal{H} &= \mathcal{H}_e + \mathcal{H}_{DM} \\ \mathcal{H}_e &= -\sum_{\langle i,j \rangle} J_{i,j} \mathbf{S}_i \cdot \mathbf{S}_j \\ \mathcal{H}_{DM} &= \sum_{\langle i,j \rangle} \mathbf{D}_{i,j} \cdot \mathbf{S}_i \wedge \mathbf{S}_j \end{aligned} \tag{III.2}$$

where $J_{i,j}$ and $\mathbf{D}_{i,j}$ are the exchange and DM interactions, respectively, between two Heisenberg spins $\mathbf{S}_i$ and $\mathbf{S}_j$ of magnitude S=1/2 occupying the lattice sites i and j.

For simplicity, let us consider the case where the in-plane and inter-plane exchange interactions between NN are both ferromagnetic and denoted by $J_{\shortparallel}$ and $J_{\perp}$, respectively. The DM interaction is supposed to be between NN in

the plane with a constant D. Due to the competition between the exchange J term which favors the collinear configuration, and the DM term which favors the perpendicular one, we expect that the spin $\mathbf{S}_i$ makes an angle $\theta_{i,j}$ with its neighbor $\mathbf{S}_j$. Therefore, the quantization axis of $\mathbf{S}_i$ is not the same as that of $\mathbf{S}_j$. Let us call $\hat{\zeta}_i$ the quantization axis of $\mathbf{S}_i$ and $\hat{\xi}_i$ its perpendicular axis in the xz plane. The third axis $\hat{\eta}_i$, perpendicular to the film surface, is chosen in such a way to make $(\hat{\xi}_i, \hat{\eta}_i, \hat{\zeta}_i)$ an orthogonal direct frame. Writing $\mathbf{S}_i$ and $\mathbf{S}_j$ in their respective local coordinates, one has

$$\mathbf{S}_i = S_i^x \hat{\xi}_i + S_i^y \hat{\eta}_i + S_i^z \hat{\zeta}_i \tag{III.3}$$

$$\mathbf{S}_j = S_j^x \hat{\xi}_j + S_j^y \hat{\eta}_j + S_j^z \hat{\zeta}_j \tag{III.4}$$

We choose the vector $\mathbf{D}_{i,j}$ perpendicular to the xz plane, namely

$$\mathbf{D}_{i,j} = D e_{i,j} \hat{\eta}_i \tag{III.5}$$

where $e_{i,j}$ =+1 (-1) if $j > i$ ($j < i$) for NN on the $\hat{\xi}_i$ or $\hat{\zeta}_i$ axis. Note that $e_{j,i} = -e_{i,j}$.

To determine the GS, the easiest way is to use the steepest descent method. Note that we have used different initial conditions to check the convergence to a single GS for each set of parameters. Choosing $\mathbf{D}_{i,j}$ lying perpendicular to the spin plane (i.e. xz-plane) as indicated in Eq. (III.5), we determine the GS as a function of D. An example is shown in Fig.III.2 for $\theta = \pi/6$ ($D = -0.577$) with $J_{\shortparallel} = J_{\perp} = 1$. We see that each spin has the same angle with its four NN in the plane (angle between NN in adjacent planes is zero). Let us show the relation between θ and $J_{\shortparallel}$, the energy of the spin $\mathbf{S}_i$ is written as

$$E_i = -4J_{\shortparallel} S^2 \cos\theta - 2J_{\perp} S^2 + 4DS^2 \sin\theta \tag{III.6}$$

where $\theta = |\theta_{i,j}|$ and care has been taken on the signs of $\sin\theta_{i,j}$ and $e_{i,j}$ when counting NN, namely two opposite NN have opposite signs. The minimization of E_i yields

$$\frac{dE_i}{d\theta} = 0 \quad \Rightarrow \quad -\frac{D}{J_{\shortparallel}} = \tan\theta \quad \Rightarrow \quad \theta = \arctan(-\frac{D}{J_{\shortparallel}}) \tag{III.7}$$

The value of θ for a given $\frac{D}{J_{\shortparallel}}$ is precisely what obtained by the steepest descent method.

In the present model, the DM interaction is supposed in the plane, so in the GS the angle between in-plane NN is not zero. We show in Fig. III.2 the relative orientation of the two NN spins in the plane.

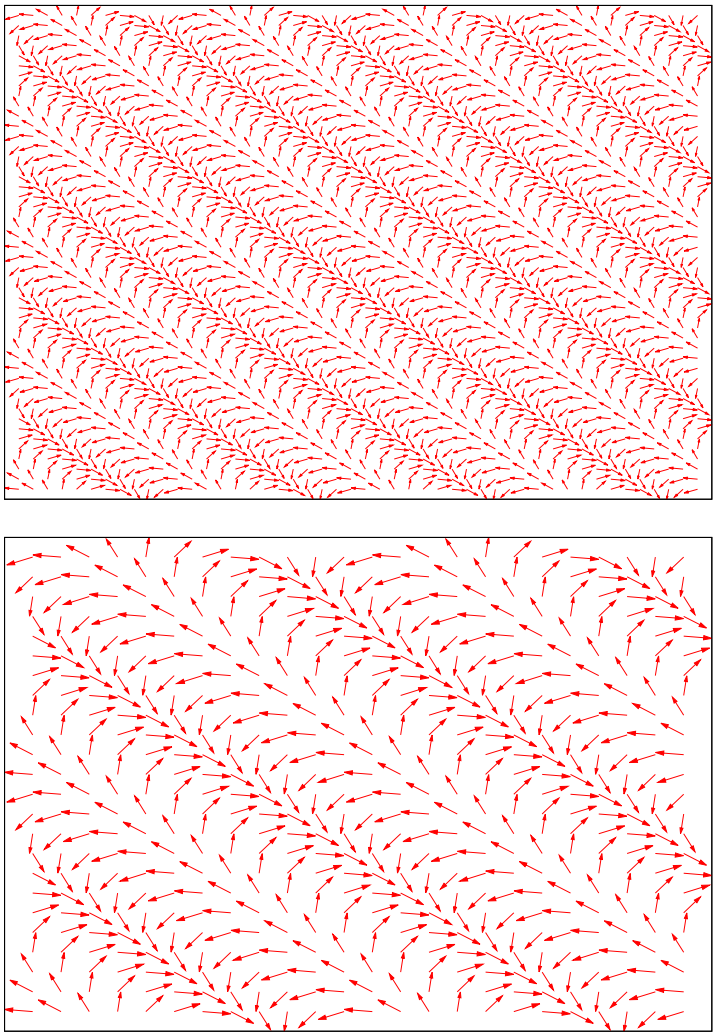

Figure III.2: Top: the ground state is a planar configuration on the xz plane. The figure shows the case where $\theta = \pi/6$ ($D = -0.577$), $J_{\shortparallel} = J_{\perp} = 1$ using the steepest descent method. Bottom: a zoom is shown .

The DM term of Eq. (III.2) can be rewritten in the locale coordinate $(\hat{\xi}_i, \hat{\eta}_i, \hat{\zeta}_i)$ of spin $\mathbf{S}_i$ as

$$\begin{aligned} \mathbf{S}_i \wedge \mathbf{S}_j &= (-S_i^z S_j^y - S_i^y S_j^x \sin\theta_{i,j} + S_i^y S_j^z \cos\theta_{i,j})\hat{\xi}_i \\ &\quad +(S_i^x S_j^x \sin\theta_{i,j} + S_i^z S_j^z \sin\theta_{i,j})\hat{\eta}_i \\ &\quad +(S_i^x S_j^y - S_i^y S_j^z \sin\theta_{i,j} - S_i^y S_j^x \cos\theta_{i,j})\hat{\zeta}_i \end{aligned} \tag{III.8}$$

Using Eq. (III.5), we have

$$\begin{aligned}\mathcal{H}_{DM} &= \sum_{\langle i,j\rangle} \mathbf{D}_{i,j}\cdot\mathbf{S}_i\wedge\mathbf{S}_j \\ &= D\sum_{\langle i,j\rangle}(S_i^xS_j^xe_{i,j}\sin\theta_{i,j}+S_i^zS_j^ze_{i,j}\sin\theta_{i,j}) \\ &= \frac{D}{4}\sum_{\langle i,j\rangle}[(S_i^++S_i^-)(S_j^++S_j^-)e_{i,j}\sin\theta_{i,j} \\ &\quad +4S_i^zS_j^ze_{i,j}\sin\theta_{i,j}]\end{aligned} \tag{III.9}$$

where we have replaced $S^x=(S^+{+}S^-)/2$. Note that $e_{i,j}\sin\theta_{i,j}$ is always positive since for a NN on the positive axis direction, $e_{i,j}=1$ and $\sin\theta_{i,j}=\sin\theta$ where θ is positively defined, while for a NN on the negative axis direction, $e_{i,j}=-1$ and $\sin\theta_{i,j}=\sin(-\theta)=-\sin\theta$.

For non-collinear spin configurations, the local spin coordinates allow one to use the commutation relations between spin operators which are valid only when the spin lies on its quantification axis defined as the z axis. This method has been applied for helimagnets in chapter II. Expressing the Hamiltonian in the local coordinates, we obtain

$$\begin{aligned}\mathcal{H} &= -\sum_{<i,j>}J_{i,j}\Bigg\{\frac{1}{4}\left(\cos\theta_{i,j}-1\right)\left(S_i^+S_j^++S_i^-S_j^-\right) \\ &+ \frac{1}{4}\left(\cos\theta_{i,j}+1\right)\left(S_i^+S_j^-+S_i^-S_j^+\right) \\ &+ \frac{1}{2}\sin\theta_{i,j}\left(S_i^++S_i^-\right)S_j^z-\frac{1}{2}\sin\theta_{i,j}S_i^z\left(S_j^++S_j^-\right) \\ &+ \cos\theta_{i,j}S_i^zS_j^z\Bigg\} \\ &+ \frac{D}{4}\sum_{\langle i,j\rangle}[(S_i^++S_i^-)(S_j^++S_j^-)e_{i,j}\sin\theta_{i,j} \\ &\quad +4S_i^zS_j^ze_{i,j}\sin\theta_{i,j}]\end{aligned} \tag{III.10}$$

As said in the above, the spins lie in the xz planes, each on its quantization local z axis (see Fig.II.3). Note that unlike the sinus term of the DM Hamiltonian, Eq. (III.9), the sinus terms of $\mathcal{H}_e$, the 3rd line of Eq. (III.10),

are zero when summed up on opposite NN (no $e_{i,j}$ to compensate). The 3rd line disappears therefore in the following.

At this stage it is very important to note that the standard commutation relations between spin operators S^z and $S^{\pm}$ are defined with z as the spin quantization axis. In non-collinear spin configurations, calculations of SW spectrum using commutation relations without paying attention to this are wrong.

It is known that in two dimensions (2D) there is no long-range order at finite temperature (T) for isotropic spin models with short-range interaction [54]. Thin films have small thickness, therefore to stabilize the ordering at finite T it is useful to add an anisotropic interaction. We use the following anisotropy between $\mathbf{S}_i$ and $\mathbf{S}_j$ which stabilizes the angle determined above between their local quantization axes S_i^z and S_j^z:

$$\mathcal{H}_a = -\sum_{<i,j>} I_{i,j} S_i^z S_j^z \cos\theta_{i,j} \tag{III.11}$$

where $I_{i,j}$ is supposed to be positive, small compared to $J_{\shortparallel}$, and limited to NN. Hereafter we take $I_{i,j}$=I_1 for NN pair in the xz-plane, for simplicity. As it turns out, this anisotropy helps stabilize the ordering at finite T in 2D as discussed. It helps also stabilize the SW spectrum at $T = 0$ in the case of thin films but it is not necessary for 2D and 3D at $T = 0$. The total Hamiltonian is finally given by

$$\mathcal{H} = \mathcal{H}_e + \mathcal{H}_{DM} + \mathcal{H}_a \tag{III.12}$$

We use the Green's function (GF) described in chapter II for the calculation of magnetization and the spin wave spectrum, where we define the two double-time GF's G and F depending on two times t and t'. The quantum equations of motion for G and F have the form

$$\begin{aligned} i\hbar\frac{dG_{i,j}(t,t')}{dt} &= <\left[S_i^+(t), S_j^-(t')\right]>\delta(t-t') \\ &\quad - <<\left[\mathcal{H}, S_i^+\right]; S_j^- >> \end{aligned} \tag{III.13}$$

$$\begin{aligned} i\hbar\frac{dF_{i,j}(t,t')}{dt} &= <\left[S_i^-(t), S_j^-(t')\right]>\delta(t-t') \\ &\quad - <<\left[\mathcal{H}, S_i^-\right]; S_j^- >> \end{aligned} \tag{III.14}$$

For the $\mathcal{H}_e$ and $\mathcal{H}_a$ parts, the above equations of motion generate terms such as $<< S_l^z S_i^{\pm}; S_j^- >>$ and $<< S_l^{\pm} S_i^{\pm}; S_j^- >>$. These functions can be

approximated by using the Tyablikov decoupling to reduce to the above-defined G and F functions as explained in chapter II. For the DM term, the commutation relations $[\mathcal{H}, S_i^{\pm}]$ give rise to the following term:

$$D\sum_l \sin\theta[\mp S_i^z(S_l^+ + S_l^-) \pm 2S_i^{\pm}S_l^z] \tag{III.15}$$

Note that we have replaced $e_{i,j}\sin\theta_{i,j}$ by $\sin\theta$ where θ is positive. Using the in-plane Fourier transformation of the G and F, we obtain a chain of coupled equations

$$\begin{aligned}
&(E + A_n)g_{n,n'} + B_n f_{n,n'} \\
&+C_n(g_{n+1,n'} + g_{n-1,n'}) = 2\langle S_n^z\rangle \delta_{n,n'} \qquad \text{(III.16)}\\
&(E - A_n)f_{n,n'} - B_n g_{n,n'} \\
&-C_n(f_{n+1,n'} + f_{n-1,n'}) = 0 \qquad \text{(III.17)}
\end{aligned}$$

which can be rewritten in the following matrix equation

$$\mathbf{M}(E)\,\mathbf{h} = \mathbf{u} \tag{III.18}$$

where $\mathbf{M}(E)$ is a square matrix of dimension $(2N \times 2N)$, $\mathbf{h}$ and $\mathbf{u}$ are the column matrices which are defined as follows

$$\mathbf{h} = \begin{pmatrix} g_{1,n'} \\ f_{1,n'} \\ \vdots \\ g_{n,n'} \\ f_{n,n'} \\ \vdots \\ g_{N,n'} \\ f_{N,n'} \end{pmatrix}, \qquad \mathbf{u} = \begin{pmatrix} 2\langle S_1^z\rangle \delta_{1,n'} \\ 0 \\ \vdots \\ 2\langle S_N^z\rangle \delta_{N,n'} \\ 0 \end{pmatrix}, \tag{III.19}$$

where $E = \hbar\omega$ and $\mathbf{M}(E)$ is given by

$$M(E) = \begin{pmatrix}
E{+}A_1 & B_1 & C_1 & 0 & 0 & 0 & 0 & 0 & 0 \\
-B_1 & E{-}A_1 & 0 & -C_1 & 0 & 0 & 0 & 0 & 0 \\
\cdots & \cdots & \cdots & \cdots & \cdots & \cdots & \cdots & \cdots & \cdots \\
\cdots & 0 & C_n & 0 & E{+}A_n & B_n & C_n & 0 & 0 \\
\cdots & 0 & 0 & -C_n & -B_n & E{-}A_n & 0 & -C_n & 0 \\
\cdots & \cdots & \cdots & \cdots & \cdots & \cdots & \cdots & \cdots & \cdots \\
0 & 0 & 0 & 0 & 0 & C_N & 0 & E{+}A_N & B_N \\
0 & 0 & 0 & 0 & 0 & 0 & -C_N & -B_N & E{-}A_N
\end{pmatrix} \tag{III.20}$$

The coefficients are given by

$$
\begin{aligned}
A_n &= -J_{\shortparallel}[8 < S_n^z > \cos\theta(1+d_n) \\
&\quad -4 < S_n^z > \gamma(\cos\theta + 1)] \\
&\quad -2J_{\perp}(< S_{n-1}^z > + < S_{n+1}^z >) \\
&\quad -4D\sin\theta < S_n^z > \gamma \\
&\quad +8D\sin\theta < S_n^z > \qquad \text{(III.21)} \\
B_n &= 4J_{\shortparallel} < S_n^z > \gamma(\cos\theta - 1) \\
&\quad -4D\sin\theta < S_n^z > \gamma \qquad \text{(III.22)} \\
C_n &= 2J_{\perp} < S_n^z > \qquad \text{(III.23)}
\end{aligned}
$$

where $n = 1, 2, ..., N$, $d_n = I_1/J_{\shortparallel}$, $\gamma = (\cos k_x a + \cos k_z a)/2$, k_x and k_z denote the wave-vector components in the xz planes, a the lattice constant. Note that (i) if $n = 1$ (surface layer) then there are no $n-1$ terms in the matrix coefficients, (ii) if $n = N$ then there are no $n+1$ terms. Besides, we have distinguished the in-plane NN interaction $J_{\shortparallel}$ from the inter-plane NN one $J_{\perp}$. In the case of a thin film, the SW eigenvalues at a given wave vector $\vec{k} = (k_x, k_z)$ are calculated by diagonalizing the matrix.

III.4 Two and Three Dimensions: Spin-Wave Spectrum and Magnetization

Consider just one single xz plane. The above matrix is reduced to two coupled equations

$$
\begin{aligned}
(E + A_n)g_{n,n'} + B_n f_{n,n'} &= 2 < S_n^z > \delta(n, n') \\
-B_n g_{n,n'} + (E - A_n)f_{n,n'} &= 0 \qquad \text{(III.24)}
\end{aligned}
$$

where A_n is given by (III.21) but without $J_{\perp}$ term for the 2D case considered here. Coefficients B_n and C_n are given by (III.22) and (III.23) with $C_n = 0$. The poles of the GF are the eigenvalues of the SW spectrum which are given by the secular equation

$$
\begin{aligned}
&(E + A_n)(E - A_n) + B_n^2 = 0 \\
&[E + A_n][E - A_n] + B_n^2 = 0 \\
&E^2 - A_n^2 + B_n^2 = 0 \\
&E = \pm\sqrt{(A_n + B_n)(A_n - B_n)} \qquad \text{(III.25)}
\end{aligned}
$$

where $\pm$ indicate the left and right SW precessions. Several remarks are in order: (i) if $\theta = 0$, we have $B_n = 0$ and the last three terms of A_n are zero. We recover then the ferromagnetic SW dispersion relation:

$$E = 2ZJ_{\shortparallel} < S_n^z > (1-\gamma) \tag{III.26}$$

where $Z = 4$ is the coordination number of the square lattice (taking $d_n = 0$),

(ii) if $\theta = \pi$, we have $A_n = 8J_{\shortparallel} < S_n^z >$, $B_n = -8J_{\shortparallel} < S_n^z > \gamma$. We recover then the antiferromagnetic SW dispersion relation:

$$E = 2ZJ_{\shortparallel} < S_n^z > \sqrt{1-\gamma^2} \tag{III.27}$$

(iii) in the presence of a DM interaction, we have $0 < \cos\theta < 1$, $(0 < \theta < \pi/2)$. If $d_n = 0$, the quantity in the square root of Eq. (III.25) is always ≥ 0 for any θ. It is zero at $\gamma = 1$. The SW spectrum is therefore stable at the long-wavelength limit. The anisotropy d_n gives a gap at $\gamma = 1$.

As said earlier, the necessity to include an anisotropy has a double purpose: it permits a gap and stabilizes a long-range ordering at finite T in 2D systems.

Figure III.3 shows the SW spectrum calculated from Eq. (III.25) for $\theta = 30$ degrees ($\pi/6$ radian) and 80 degrees (1.396 radian). The spectrum is symmetric for positive and negative wave vectors and for left and right precessions. Note that for small θ (i.e. small D) E is proportional to k^2 at low k [Fig.III.3(Left)], as in ferromagnets. However, as θ increases, we observe that E becomes linear in k as seen in Fig. III.3(Right). This is similar to antiferromagnets. The change of behavior is progressive with increasing θ, we do not observe a sudden transition from k^2 to k behavior. This feature is also observed in three dimensions (3D) and in thin films as seen below.

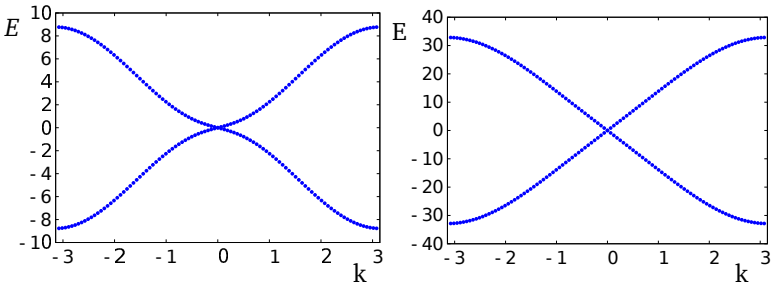

Figure III.3: Spin-wave spectrum $E(k)$ versus $k \equiv k_x = k_z$ for $\theta = 0.524$ radian (Left) and $\theta = 1.393$ (Right) in two dimensions at $T = 0.1$. Positive and negative branches correspond to right and left precessions. A small d $(= 0.001)$ has been used to stabilize the ordering at finite T in 2D.

It is noted that, thanks to the existence of the anisotropy d, we avoid the logarithmic divergence at $k = 0$ so that we can observe a long-range ordering at finite T in 2D. We show in Fig. III.4 the magnetization $M \equiv < S^z >$

calculated by Eq. (II.31) for one layer using $d = 0.001$. It is interesting to observe that M depends strongly on θ: at high T, larger θ yields stronger M. However, at $T = 0$ the spin length is smaller for larger θ due to the spin contraction calculated by Eq. (II.32). As a consequence, there is a cross-over of magnetizations calculated with different θ at low T as shown in Fig. III.4.

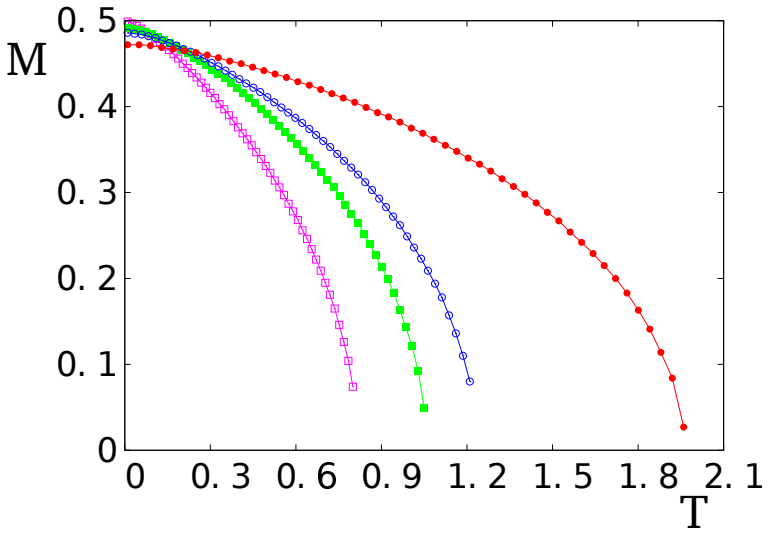

Figure III.4: Magnetizations M versus temperature T for a monolayer (2D) $\theta = 0.175$ (radian), $\theta = 0.524$, $\theta = 0.698$, $\theta = 1.047$ (void magenta squares, green filled squares, blue void circles and filled red circles, respectively). A small d ($= 0.001$) has been used to stabilize the ordering at finite T in 2D.

Let us study the 3D case. The crystal is periodic in three directions. We can use the Fourier transformation in the y direction, namely $g_{n\pm1} = g_n \mathrm{e}^{\pm ik_y a}$ and $f_{n\pm1} = f_n \mathrm{e}^{\pm ik_y a}$. The matrix is reduced to two coupled equations of g and f functions, omitting index n,

$$\begin{aligned} (E + A')g + Bf &= 2 < S^z > \\ -Bg + (E - A')f &= 0 \end{aligned} \qquad \text{(III.28)}$$

where

$$\begin{aligned} A' &= -J_{\shortparallel}[8 < S^z > \cos\theta(1+d) \\ &\quad -4 < S^z > \gamma(\cos\theta + 1)] \\ &\quad +4J_{\perp} < S^z > \cos(k_y a) \\ &\quad -4D\sin\theta < S^z > \gamma \\ &\quad +8D\sin\theta < S^z > \qquad \text{(III.29)} \\ B &= 4J_{\shortparallel} < S^z > \gamma(\cos\theta - 1) \\ &\quad -4D\sin\theta < S^z > \gamma \qquad \text{(III.30)} \end{aligned}$$

The spectrum is given by

$$E = \pm\sqrt{(A'+B)(A'-B)} \qquad \text{(III.31)}$$

If $\cos\theta = 1$ (ferromagnetic), one has $B = 0$. By regrouping the Fourier transforms in three directions, one obtains the 3D ferromagnetic dispersion relation $E = 2Z < S^z > (1-\gamma^2)$ where $\gamma = [\cos(k_x a)+\cos(k_y a)+\cos(k_z a)]/3$ and $Z = 6$, coordination number of the simple cubic lattice. Unlike the 2D case where the angle is inside the plane so that the antiferromagnetic case can be recovered by setting $\cos\theta = -1$ as seen above, one cannot use the above formula to find the antiferromagnetic case because in the 3D formulation it was supposed a ferromagnetic coupling between planes, namely there is no angle between adjacent planes in the above formulation.

The same consideration as in the 2D case treated above shows that for $d = 0$ the spectrum $E \geq 0$ for positive precession and $E \leq 0$ for negative precession, for any θ. The limit $E = 0$ is at $\gamma = 1$ ($\vec{k} = 0$). Thus, there is no instability due to the DM interaction. Using Eq. (III.31), we have calculated the 3D spectrum. This is shown in Fig. III.5 for a small and a large value of θ. As in the 2D case, we observe $E \propto k$ when $k \to 0$ for large θ. Main properties of the system are dominated by the in-plane DM behavior.

Figure III.6 displays the magnetization M versus T for several values of θ. As in the 2D case, when θ is not zero, the spins have a contraction at $T = 0$: a stronger θ yields a stronger contraction. This generates a magnetization cross-over at low T shown in the inset of Fig. III.6. The spin length at $T = 0$ versus θ is displayed in Fig. III.7. Note that the spin contraction in 3D is smaller than that in 2D. This is expected since quantum fluctuations are stronger at lower dimensions.

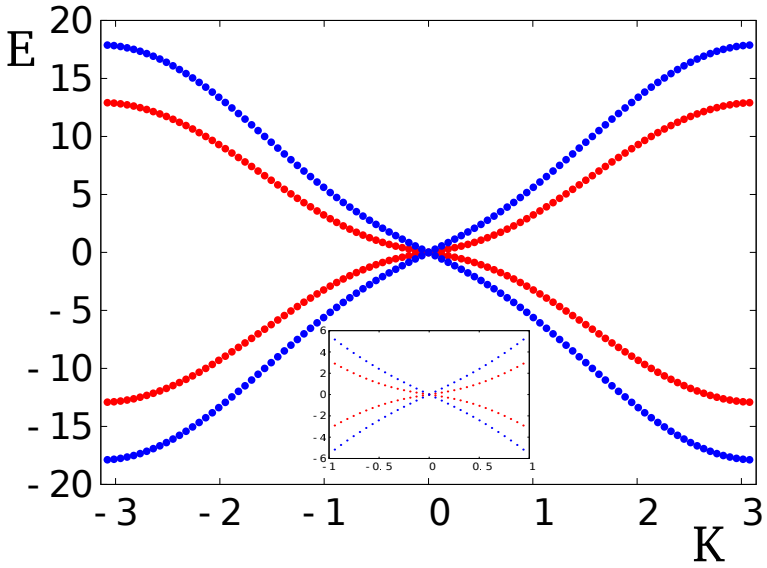

Figure III.5: Spin-wave spectrum $E(k)$ versus $k \equiv k_x = k_z$ for $\theta = \pi/6$ (red circles) and $\theta = \pi/3$ (blue circles) in three dimensions at $T = 0.1$, with $d = 0$. Note the linear-k behavior at low k for the large value of θ (inset).

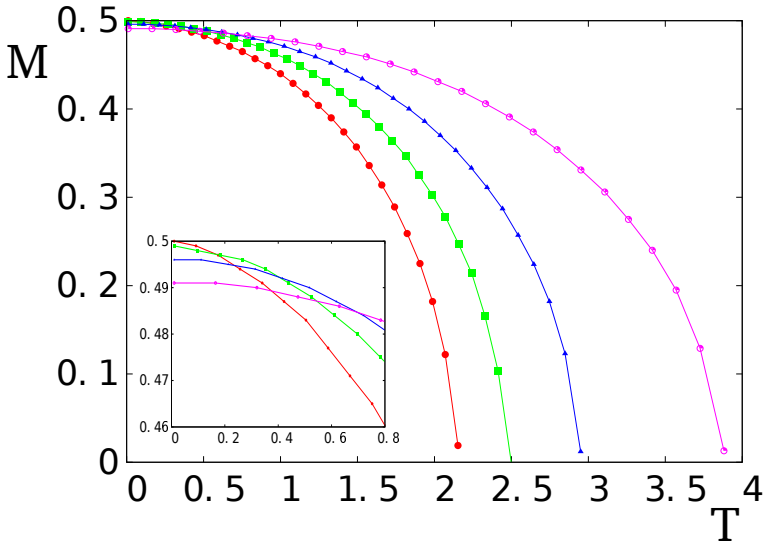

Figure III.6: Magnetization M versus temperature T for a 3D crystal $\theta = 0.175$ (radian), $\theta = 0.524$, $\theta = 0.785$, $\theta = 1.047$ (red circles, green squares, blue triangles and void magenta circles, respectively), with $d = 0$. Inset: Zoom showing the cross-over of magnetizations at low T for different θ.

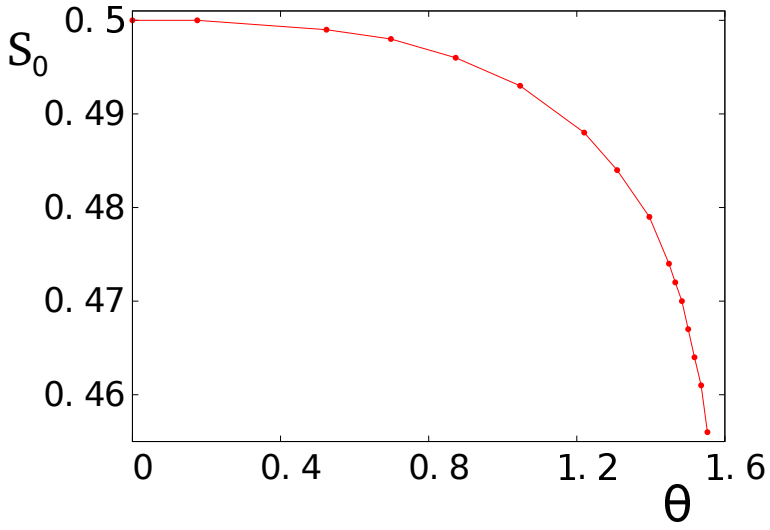

Figure III.7: The spin length S_0 at $T = 0$ versus θ in the 3D case.

III.5 The Case of a Thin Film: Spin-Wave Spectrum, Layer Magnetizations

In the 2D and 3D cases shown above, there is no need at $T = 0$ to use a small anisotropy d. However in the case of thin films shown below, due to the lack of neighbors at the surface, the introduction of a DM interaction destabilizes the spectrum at long wave-length $\vec{k} = 0$. Depending on θ, we have to use a value for d_n larger or equal to a "critical value" d_c to avoid imaginary SW energies at $\vec{k} = 0$. The critical value d_c is shown in Fig. III.8 for a 4-layer film. Note that at the perpendicular configuration $\theta = \pi/2$, no SW excitation is possible: SW cannot propagate in a perpendicular spin configuration since the wave-vectors cannot be defined.

We show now a SW spectrum at a given thickness N. There are $2N$ energy values half of them are positive and the other half negative (left and right precessions): E_i $(i = 1, ..., 2N)$. Figure III.9 shows the case of a film of 8 layers with $J_{\shortparallel} = J_{\perp} = 1$ for a weak and a strong value of D (small and large θ). As in the 2D cases, for strong D, E is proportional to k at small k [cf. Fig. III.9(Right)]. It is noted that this behavior concerns only the first mode. The upper modes remain in the k^2 behavior.

Figure III.10 shows the layer magnetizations of the first four layers in an 8-layer film (the other half is symmetric) for several values of θ. In each case, we see that the surface layer magnetization is smallest. This is a general effect of the lack of neighbors for surface spins even when there is no surface-

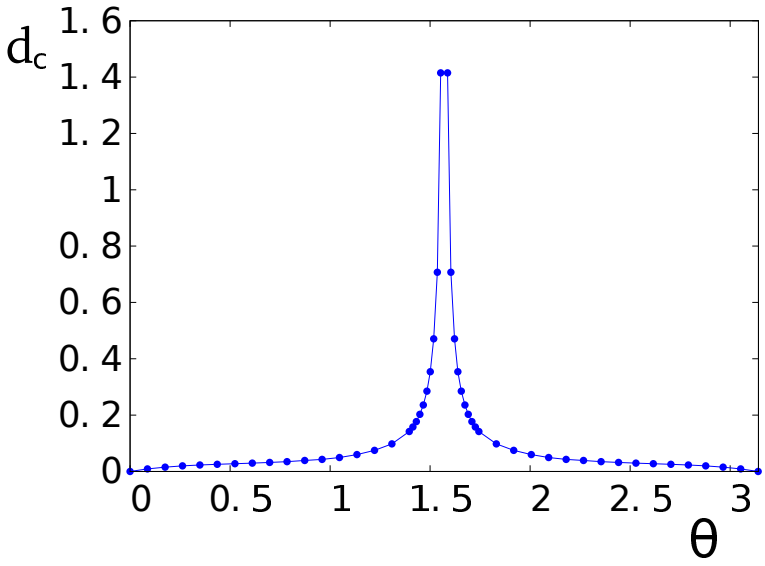

Figure III.8: Value d_c above which the SW energy $E(\vec{k} = 0)$ is real as a function of θ (in radian), for a 4-layer film. Note that no spin-wave excitations are possible near the perpendicular configuration $\theta = \pi/2$.

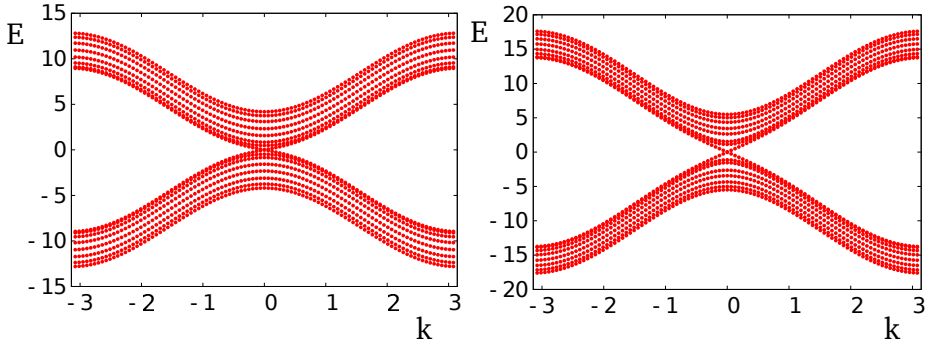

Figure III.9: Spin-wave spectrum $E(k)$ versus $k \equiv k_x = k_z$ for a thin film of 8 layers: $\theta = \pi/6$ (Left), $\theta = \pi/3$ (Right), using $d = d_c$ for each case ($d_c = 0.012$ and 0.021, respectively). Positive and negative branches correspond to right and left precessions. Note the linear-k behavior at low k for the large θ case.

localized SW as in the present simple cubic lattice case [5].

The spin length at $T = 0$ for an 8-layer film is shown in Fig. III.11 as a function of θ. One observes that the spins are strongly contracted with large θ.

Let us touch upon the surface effect in the present model. We know

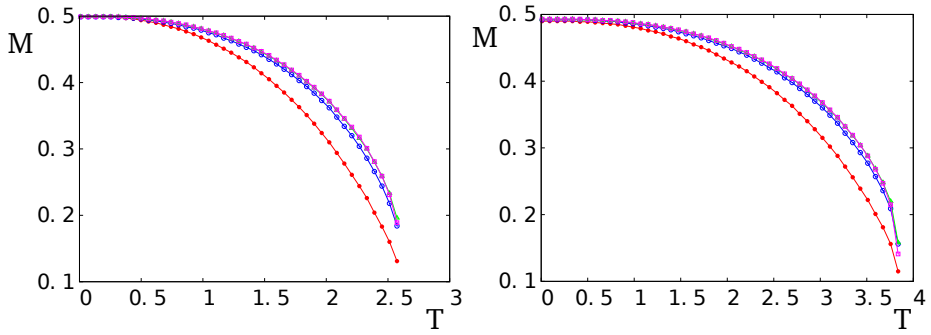

Figure III.10: 8-layer film: layer magnetizations M versus temperature T for (Left) $\theta = \pi/6$, (Right) $\theta = \pi/3$, with $d = 0.1$. Red circles, blue void circles, green void triangles and magenta squares correspond respectively to the first, second, third and fourth layer.

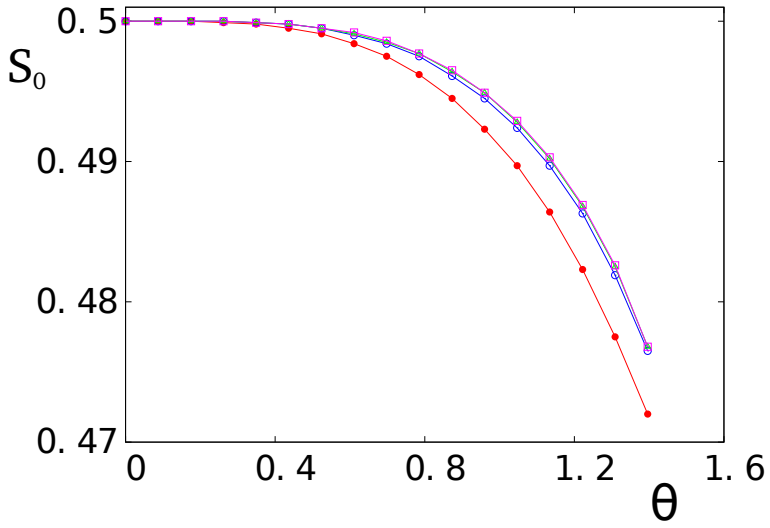

Figure III.11: Spin length S_0 at $T = 0$ of the first 4 layers as a function of θ, for $N = 8$, $d = 0.1$. Red circles, blue void circles, green void triangles and magenta squares correspond respectively to the first, second, third and fourth layer.

that for the simple cubic lattice, if the interactions are the same everywhere in the film, then there is no surface localized mode, and this is true with DM interaction (see spectrum in Fig. III.9) and without DM interaction (see Ref. [91]). In order to create surface modes, we have to take the surface exchange interactions different from the bulk ones. Low-lying branches of surface modes which are "detached" from the bulk spectrum are seen in the SW spectrum shown in Fig. III.12(top) with $J^s_{||} = 0.5$ and $J^s_{\perp} = 0.5$.

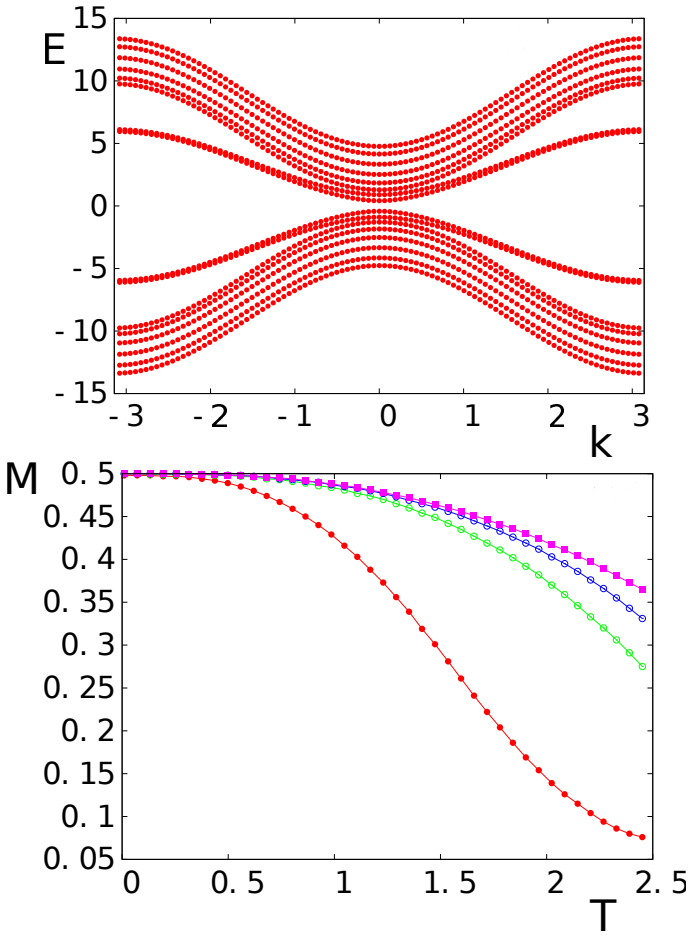

Figure III.12: Surface effect: (Top) spin-wave spectrum $E(k)$ versus $k = k_x = k_z$ for a thin film of 8 layers: $\theta = \pi/6$, $d = 0.2$, $J^s_{\shortparallel} = 0.5$, $J^s_{\perp} = 0.5$, the gap at $k = 0$ is due to d. The surface-mode branches are detached from the bulk spectrum; (Bottom) layer magnetizations versus T for the first, second, third and fourth layers (red circles, green void circles, blue void circles and magenta filled squares, respectively).

These surface modes strongly affect the surface magnetization as observed in Fig. III.12(bottom): the surface magnetization is strongly diminished with increasing T. The role of surface-localized modes on the strong decrease of the surface magnetization as T increases has already been analyzed more than 30 years ago [91].

III.6 Thickness Effect

We show now the effect of the film thickness in the present model. The case of thickness $N = 12$ is shown in Fig. III.13 with $\theta = \pi/6$ where the layer magnetizations versus T are shown in details. The gap at $k = 0$ due to d is shown in Fig. III.14(left) as a function of the film thickness N for $d = 0.1$ and $\theta = \pi/6$, at $T = 0$. We see that the gap depends not only on d but also on the value of the surface magnetization which is larger for thicker films. The transition temperature T_c versus the thickness N is shown in Fig. III.14(right) where one observes that T_c tends rapidly to the bulk value (3D) which is $\simeq 2.82$ for $d = 0.1$.

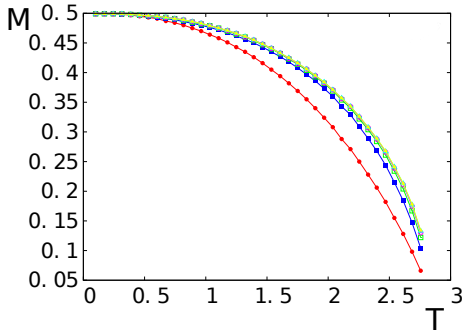

Figure III.13: 12-layer film: Layer magnetizations versus T for $\theta = \pi/6$ and anisotropy $d = 0.1$. Red circles, blue squares, green void squares magenta circles, void turquoise triangles and brown triangles correspond respectively to first, second, third, fourth, fifth and sixth layer.

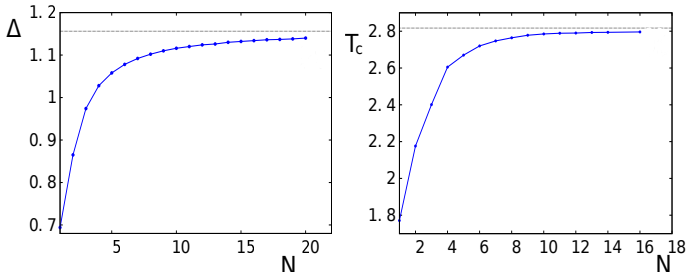

Figure III.14: Left: Gap at $k = 0$ as a function of the film thickness N for $\theta = \pi/6$, $d = 0.1$, at $T = 0.1$. Right: Critical temperature T_c versus the film thickness N calculated with $\theta = \pi/6$ and $d = 0.1$. Note that for the infinite thickness (namely 3D), $T_c \simeq 2.8$.

III.7 Conclusion

By a self-consistent Green's function theory, we obtained the expression of the spin-wave dispersion relation in 2D and 3D as well as in a thin film. Due to the competition between ferromagnetic interaction J and the perpendicular DM interaction D, the GS is non linear with an angle θ which is shown to explicitly depend on the ratio D/J. The spectrum is shown to depend on θ and the layer magnetization is calculated self-consistently as a function of temperature up to the critical temperature T_c.

We have obtained new and interesting results. In particular we have shown that (i) the spin-wave excitation in 2D and 3D crystals is stable at $T = 0$ with the non-collinear spin configuration induced by the DM interaction D without the need of an anisotropy, (ii) in the case of thin films, we need a small anisotropy d to stabilize the spin-wave excitations because of the lack of neighbors at the surface, (iii) the spin-wave energy E depends on D, namely on θ: at the long wave-length limit, E is proportional to k^2 for small D but E is linear in k for strong D, in 2D and 3D as well as in a thin film, (iv) quantum fluctuations are inhomogeneous for layer magnetizations near the surface.

Chapter IV

Phase Transition of Skyrmion Crystals Generated by a DM Interaction - Stretched Exponential Relaxation

Contents

IV.1 Introduction

Skyrmions have been extensively investigated in condensed matter physics since its theoretical formulation by T. H. R. Skyrme [92] in the context of nuclear matter. Their existence in magnetically ordered crystals has been predicted about thirty years ago [93] but it was only recently that skyrmion lattices have been observed in crystals with non-centrosymmetric lattices, in particular in B20 structures such as MnSi [10, 94–96], FeCoSi [11] and FeGe [70] crystals. Although skyrmions are formed only at low temperatures, in recent publications these nanoscale magnetic structures have been observed at room temperature [97,98]. Skyrmions have been identified also in hexagonal Fe monolayers on Ir(111) [99, 100]. It appears that thin magnetic

films are compatible with technology development [101]. There are several mechanisms and interactions leading to the appearance of skyrmions in various kinds of matter, among them the dipole-dipole interaction [102, 103], and the most popular one is certainly the Dzyaloshinskii-Moriya (DM) interaction which was initially proposed to explain the weak ferromagnetism observed in antiferromagnetic Mn compounds. The order of magnitude of DM interaction, D, is very small. However, in many recent papers using the DM interaction, the assumption of small D is not always respected. Therefore, we can think that the demonstration of Moriya [62] is a special case and the general Hamiltonian may have the same form but different microscopic origin. This is similar to the case of the Hubbard model which was initially originated from a second-order perturbation of exchange interaction, but it has been used with liberty for arbitrary ratio t/U. This is also the case of the Ising model if we think of it as a limiting case of the Heisenberg model.

The DM interaction has been shown to generate skyrmions in various kinds of crystals. For example, it can generate a crystal of skyrmions in which skyrmions arrange themselves in a periodic structure [104–107]. Skyrmions have been shown to exist in crystal liquids [108–110] as well as quantum Hall systems [111, 112]. A single skyrmion has also been found [100, 113]. Effects of skyrmions have been investigated in thin films [71, 114]. Artificial skyrmion lattices have been devised for room temperature [115]. Experimental observations of skyrmion lattices have been realized in MnSi in 2009 [9] and in doped semiconductors in 2010 [72] . Needless to say, many potential applications using properties of skyrmions are expected in the years to come. At this stage, it should be noted that skyrmion crystals can also be created by competing exchange interactions without DM interactions [116, 117]. So, mechanisms for creating skyrmions are multiple.

In this chapter, we study a skyrmion crystal created by the competition between the nearest-neighbor (NN) ferromagnetic interaction J and the DM interaction of magnitude D under an applied magnetic field $\vec{H}$. We show by Monte Carlo (MC) simulation that the skyrmion crystal is stable at finite temperatures up to a transition temperature T_c where the topological structure of each skyrmion and the periodic structure of skyrmions are destroyed.

The chapter is organized as follows. Section IV.2 is devoted to the description of the model and the method to determine the ground state (GS).The results from MC simulations are shown in section IV.3. Concluding remarks are given in section IV.4.

IV.2 Model and Ground State

The DM interaction between two spins $\mathbf{S}_i$ and $\mathbf{S}_j$ is written as

$$\mathbf{D}_{i,j} \cdot \mathbf{S}_i \wedge \mathbf{S}_j \tag{IV.1}$$

where $\mathbf{D}_{i,j}$ is a vector which results from the displacement of non magnetic ions located between $\mathbf{S}_i$ and $\mathbf{S}_j$. As said in chapter III, the direction of $\mathbf{D}_{i,j}$ depends on the symmetry of the displacement. For two spins, the DM interaction is antisymmetric with respect to the inversion symmetry. We consider in this chapter the two-dimensional case where the spins are on a square lattice in the xy plane. We are interested in the stability of the skyrmion crystal generated by a DM interaction and a symmetric isotropic Heisenberg exchange interaction in an applied field perpendicular to the xy plane. All interactions are limited to NN. The full Hamiltonian is given by

$$\mathcal{H} = -J\sum_{\langle ij\rangle}\mathbf{S}_i\cdot\mathbf{S}_j + D\sum_i \mathbf{S}_i\wedge\mathbf{S}_{i+x}.\widehat{x} + \mathbf{S}_{i+y}.\widehat{y}) - H\sum_i S_i^z \tag{IV.2}$$

where the DM interaction and the exchange interaction are taken between NN on both x and y directions. Rewriting it in a convenient form, we have

$$\begin{aligned}
\mathcal{H} &= -J\sum_{\langle ij\rangle}\vec{S}_i.\vec{S}_j + D\sum_i [S_i^y S_{i+x}^z - S_i^z S_{i+x}^y - S_i^x S_{i+y}^z \\
&\quad + S_i^z S_{i+y}^x] - H\sum_i S_i^z \\
&= -J\sum_{\langle ij\rangle}\vec{S}_i.\vec{S}_j + D\sum_i [S_i^y(S_{i+x}^z - S_{i-x}^z) \\
&\quad - S_i^z(S_{i+x}^y - S_{i-x}^y) - S_i^x(S_{i+y}^z - S_{i-y}^z) \\
&\quad + S_i^z(S_{i+y}^x - S_{i-y}^x)] - H\sum_i S_i^z
\end{aligned} \tag{IV.3}$$

For the i-th spin, one has

$$\mathcal{H}_i = -S_i^x H_i^x - S_i^y H_i^y - S_i^z H_i^z y$$

where the local-field components are given by

$$\begin{aligned}
H_i^x &= J\sum_{NN} S_j^x + D(S_{i+y}^z - S_{i-y}^z) \\
H_i^y &= J\sum_{NN} S_j^y - D(S_{i+x}^z - S_{i-x}^z) \\
H_i^z &= J\sum_{NN} S_j^z + D(S_{i+x}^y - S_{i-x}^y) - D(S_{i+y}^x - S_{i-y}^x) + H
\end{aligned}$$

To determine the ground state (GS), we minimize the energy of each spin, one after another. This can be numerically achieved as the following. At each spin, we calculate its local-field components acting on it from its NN using the above equations. Next we align the spin in its local field, i. e. we take $S_i^x = H_i^x/\sqrt{H_i^x * *2 + H_i^y * *2 + H_i^z * *2}$ etc. The denominator is the modulus of the local field. In doing so, the spin modulus is normalized to 1. As seen from Eq. (IV.4), the energy of the spin $\mathbf{S}_i$ is minimum. We take another spin and repeat the same procedure until all spins are visited. This achieves one iteration. We have to do a sufficient number of iterations until the system energy converges. For the skyrmion case, it takes about one thousand iterations to have a fifth-digit convergence. An example of GS are shown in Fig. IV.1 using $D = 1$ and $H = 0.5$ (in unit of $J = 1$): a crystal of skyrmions is seen.

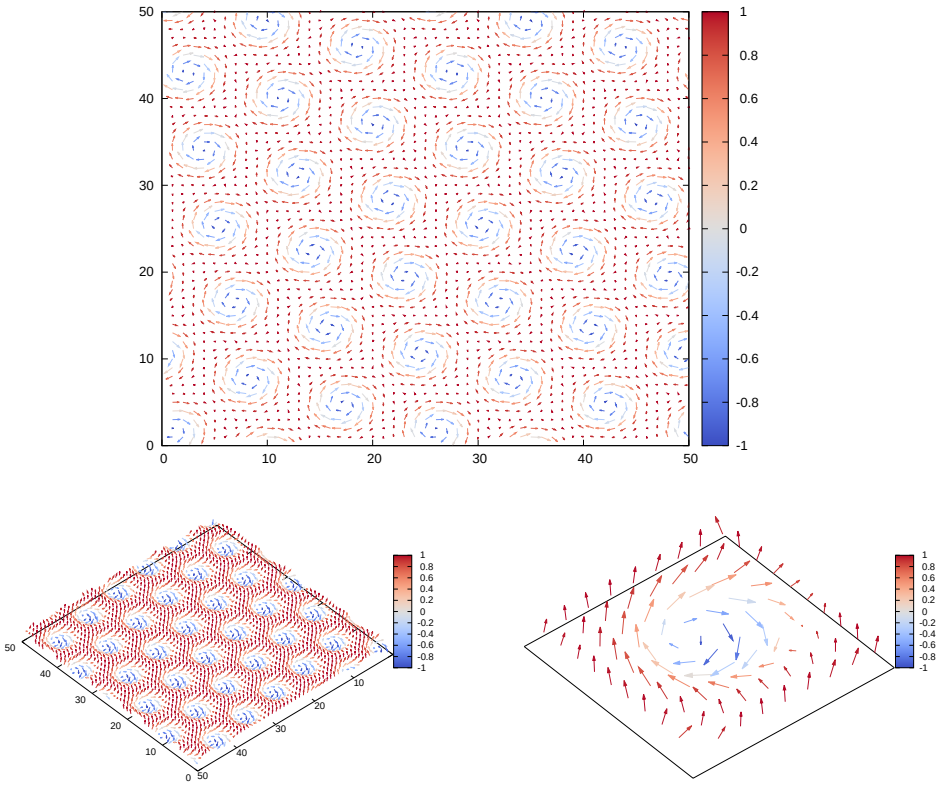

Figure IV.1: Ground state for $D/J = 1$ and $H/J = 0.5$, a crystal of skyrmions is observed (a) skyrmion crystal viewed in the xy plane; (b) a 3D view; (c) zoom of the structure of a single vortex. The value of S_z is indicated on the color scale.

In Fig. IV.2(Left) we show a GS at $H = 0$ where domains of long and round islands of up spins separated by labyrinths of down spins are mixed. When H is increased, vortices begin to appear. The GS is a mixing of long islands of up spins and vortices as seen in Fig. IV.2(Right) obtained with $D = 1$ and $H = 0.25$. This phase can be called "labyrinth phase" or "stripe phase".

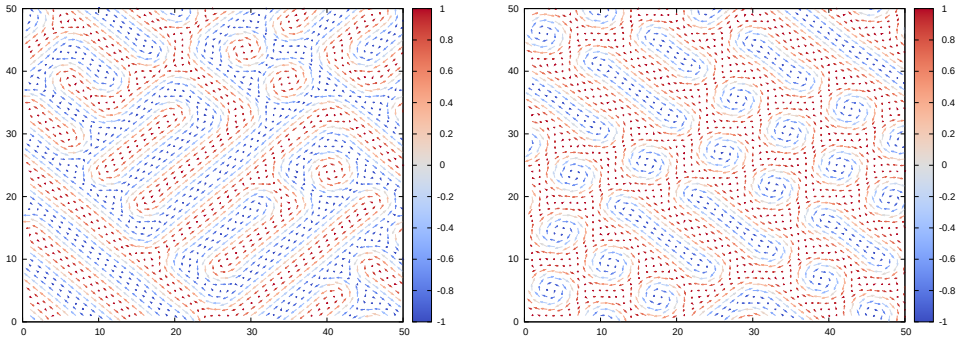

Figure IV.2: (Left) Ground state for $D/J = 1$ and $H/J = 0$: a mixing of domains of long and round islands; (Right) Ground state for $D/J = 1$ and $H/J = 0.25$: a mixing of domains of long islands and vortices. We call these structure the "labyrinth phase".

We have performed the GS calculation for many values in the plane (D, H). The phase diagram is established in Fig. IV.3. Above the blue line is the field-induced ferromagnetic phase. Below the red line is the labyrinth phase with a mixing of skyrmions and rectangular domains. The skyrmion crystal phase is found in a narrow region between these two lines.

Experimentally the TEM images observed for the (001) thin plate of SC-doped barium ferrite [118]) show a magnetic domain Fig. IV.4(A), and a mixed structure of stripe and skyrmions Fig. IV.4(B). The hexagonal structure of skyrmion is observed when we increase the magnetic field Fig. IV.4(C)

In the following section, we are interested in the stability of the skyrmion crystal phase as the temperature (T) is increased from zero.

IV.3 Stability of Skyrmion Crystal at Finite Temperatures

In this section, we show results obtained from MC simulations on a sheet of square lattice of size $N \times N$ with periodic boundary conditions. The first step is to determine the GS spin configuration by minimizing the spin energy

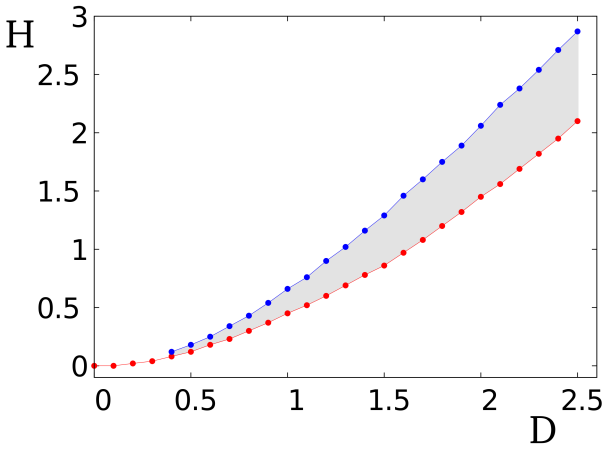

Figure IV.3: Phase diagram in the (D, H) plane for size $N = 100$.

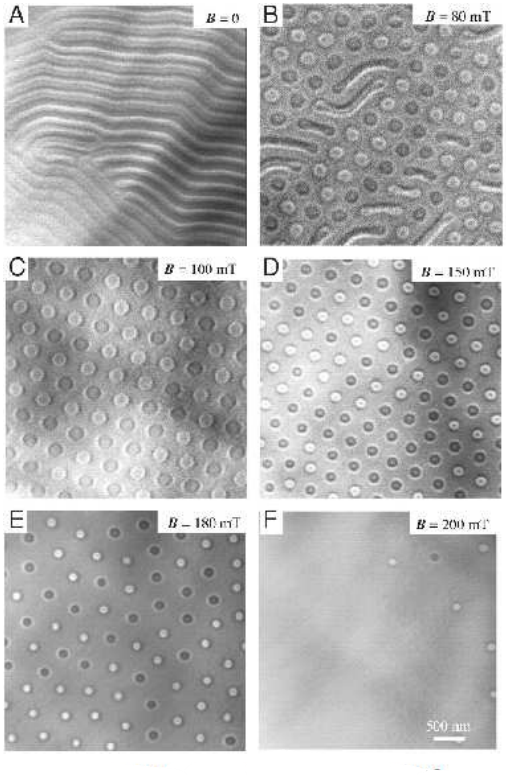

Figure IV.4: TEM images observed for (001) thin plate of Sc-doped barium showing changes in magnetic domain structure produced by a magnetic field normal to the plate (Ref. [118]).

by iteration as described above. Using this GS configuration, we heat the system from $T = 0$ to a temperature T during an equilibration time t_0 before averaging physical quantities over the next 10^6 MC steps per spin. The time t_0 is the "waiting time" during which the system relaxes before we perform averaging during the next t_a steps.

The definition of an order parameter for a skyrmion crystal is not obvious. Taking advantage of the fact that we know the GS, we define the order parameter as the projection of an actual spin configuration at a given T on its GS and we take the time average. This order parameter is thus defined as

$$M(T) = \frac{1}{N^2(t_a - t_0)} \sum_i |\sum_{t=t_0}^{t_a} \mathbf{S}_i(T,t) \cdot \mathbf{S}_i^0(T=0)| \qquad \text{(IV.4)}$$

where $\mathbf{S}_i(T,t)$ is the i-th spin at the time t, at temperature T, and $\mathbf{S}_i(T=0)$ is its state in the GS. The order parameter $M(T)$ is close to 1 at very low T where each spin is only weakly deviated from its state in the GS. $M(T)$ is zero when every spin strongly fluctuates in the paramagnetic state. The above definition of $M(T)$ is similar to the Edward-Anderson order parameter used to measure the degree of freezing in spin glasses [119]: we follow each spin with time evolving and take the spatial average at the end.

We show in Fig. IV.5 the order parameter M versus T (red data points) as well as the average z spin component (blue data points) calculated by the projection procedure for the total time t=10^5+10^6 MC steps per spin. As seen, both curves indicate a phase transition at $T_c \simeq 0.26 J/k_B$. The fact that M does not vanish above T_c is due to the effect of the applied field. It should be said that each skyrmion has a center with spins of negative z components (the most negative at the center), the spins turn progressively to positive z components while going away from the center.

We can also define another order parameter: since the field acts on the z direction. In the GS and in the skyrmion phase we have both positive and negative S_z. In the paramagnetic state, the negative S_z will turn to the field direction. We define thus the following parameters using the z spin-components

$$Q_+(T) = \frac{1}{N^2(t_a - t_0)} \sum_{S_i^z>0} \sum_{t=t_0}^{t_a} S_i^z(T,t) \qquad \text{(IV.5)}$$

$$Q_-(T) = \frac{1}{N^2(t_a - t_0)} \sum_{S_i^z<0} \sum_{t=t_0}^{t_a} S_i^z(T,t) \qquad \text{(IV.6)}$$

Figure IV.6 shows Q_+ and Q_- versus T. As seen, at the transition Q_+

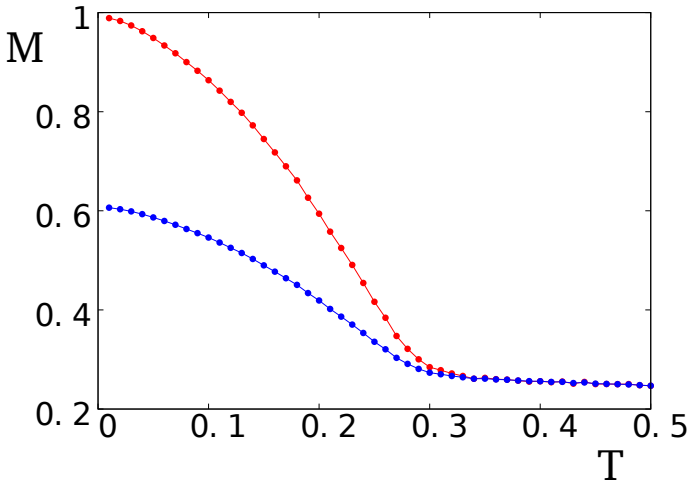

Figure IV.5: Red circles: order parameter defined in Eq. (IV.4) versus T, for $H = 0.5$ and $N = 1800$, averaged during t_a=10^5 MC steps per spin after an equilibrating time t_0=10^5 MC steps. Blue crosses: the projection of the S_z on S_z^0 of the ground state as defined in Eq. (IV.4) but for the z components only.

undergoes a change of curvature and Q_- becomes zero. All spins have positive S_z after the transition due to spin reversal by the field.

At this stage, it is worth to ask ourselves if the results obtained at the end of the simulation depend on the overall time $t = t_0+t_a$. In simple systems, the choices of t_0 and t_a can be guided by testing the time-dependence of physical quantities, and the values of t_0 and t_a are chosen when physical quantities do not depend on these run times. However, in disordered systems such as spin glasses and in complicated systems such as frustrated systems, the relaxation time is very long and often out of the reach of simulation time. In such cases, we have to recourse to some scaling relations in order to deduce the values of physical quantities at equilibrium [120, 121]. We show below how to obtain the value of an order parameter at the infinite time.

In order to detect the dependence of $M(T)$ on the total MC time $t = t_0 + t_a$, we calculate the average of $M(T)$ over 10^6 MC steps per spin, after a waiting time t_0 as said above. We record the values of $M(T)$ in different runs with t_0 varying from 10^4 to 10^6 MC steps per spin. We plot these results as a function of different total time t in Fig. IV.7 for three temperatures. To find the value extrapolated at infinite time we use the stretched exponential relaxation defined by

$$M(T,t) = A\exp\left[-(t/\tau)^{\alpha}\right] + c \qquad \text{(IV.7)}$$

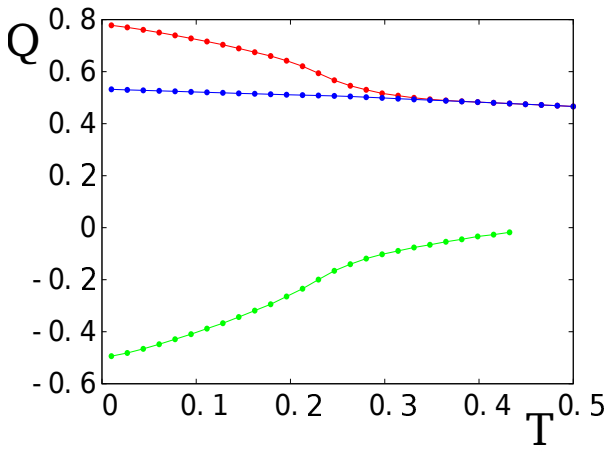

Figure IV.6: Order parameters defined in Eqs. (IV.5)-(IV.6) versus T, for $H = 0.5$ and $N = 800$, $t_0 = 10^5$, $t_a = 10^6$. Red circles: total positive z component $Q_+(T)$. Green circles: total negative z component $Q_-(T)$. Blue circles: total z component.

where t is the total simulation time, α is the stretched exponent, A a temperature-dependent constant, and τ the relaxation time. Note that this definition, without the constant c, has been used by many previous authors in the context of spin glasses [122–126]. We have introduced c which is the infinite-time limit of $M(T)$. We have taken t from 10^4 to 10^6 MC steps per spin in the simulation. At the infinite-time limit, c is zero for $T \gg T_c$, and $c \neq 0$ for $T < T_c$. Figure IV.7 shows $M(T, t)$ as a function of time t in unit of 10^3 MC steps per spin, for three temperatures $T = 0.01$, 0.094 and 0.17. As seen, the fit with Eq. (IV.7) presented by the continuous line is very good for the whole range of t.

Several remarks are in order:

(i) the precision of all parameters are between 1% to 5% depending on the parameter.

(ii) the value of α can vary a little bit according to the choice and the precision of the other parameters in the fitting but this variation is within a very small window of values around the given values. For example, at $T = 0.17$, α can only be in the interval $[0.8 \pm 0.02]$. The value of α can vary with temperature as seen here: at low T, $\alpha = 0.6$, and at a higher T, we have $\alpha = 0.8$. This variation has been seen in other systems, in particular in

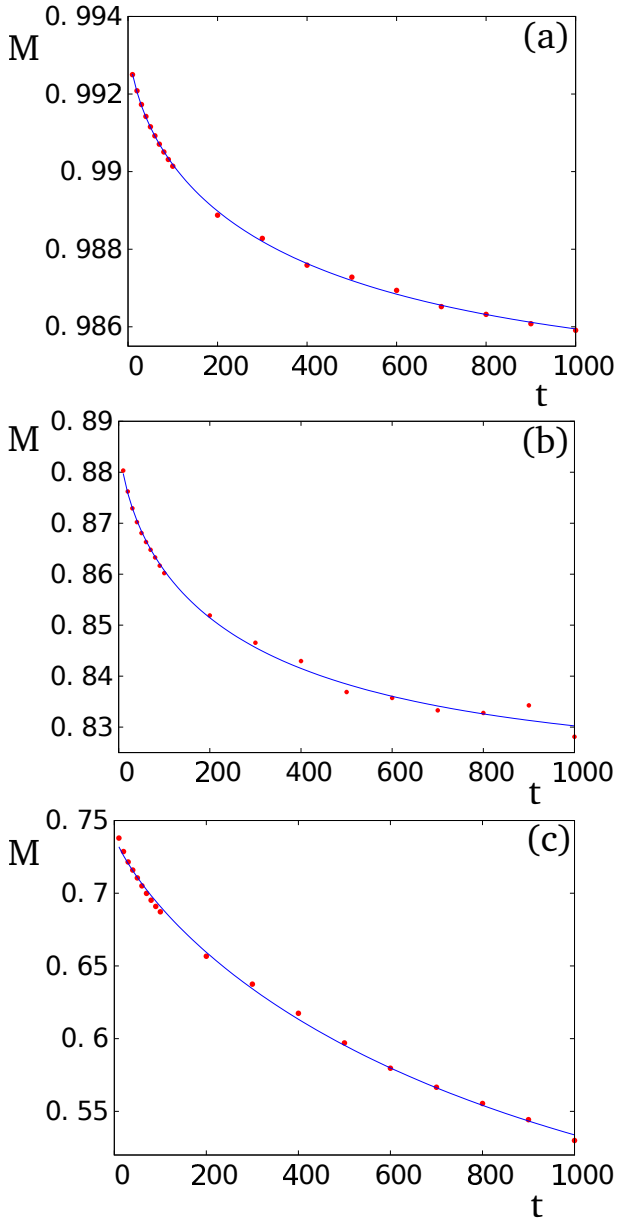

Figure IV.7: The order parameter M defined by Eq. (IV.4) versus MC time t in unit of 1000 MC steps per spin, for $H = 0.5$ and $N = 800$ (a) $T = 0.01$, values of fitting parameters $\alpha = 0.6$, $A = 0.008 \pm 0.00001$, $\tau = (364 \pm 19)10^3$, $c = 0.984505 \pm 0.00012$; (b) $T = 0.094$, $\alpha = 0.6$, $A = 0.0653 \pm 0.0013$, $\tau = (277 \pm 36)10^3$, $c = 0.822 \pm 0.018$); (c) $T = 0.17$, $\alpha = 0.8$, $A = 0.31 \pm 0.01$, $\tau = 891 \pm 100)10^3$, $c = 0.43 \pm 0.017$.

spin glasses [127].

(iii) the relaxation time, within statistical errors, is approximatively constant at low T, but it increases rapidly when T tends to T_c as seen in the value of τ at $T = 0.17$. This increase is a consequence of the so-called "critical slowing-down" when the system enters the critical region.

Let us show $M(T)$ as function of T in Fig. IV.8 using the results of different run times from $t = 10^4 + 10^6$ MC steps per spin to $t = 10^6 + 10^6$. The extrapolated values of at the infinite time for each T deduced from Eq. (IV.7) is also shown. We see that while the total time $10^5 + 10^6$ MC steps per spin is sufficient at low T, it is not enough at higher T. That was the reason why we should use Eq. (IV.7) to find the value of $M(T)$ at the infinite time to be sure that the skyrmion crystal is stable at finite temperatures.

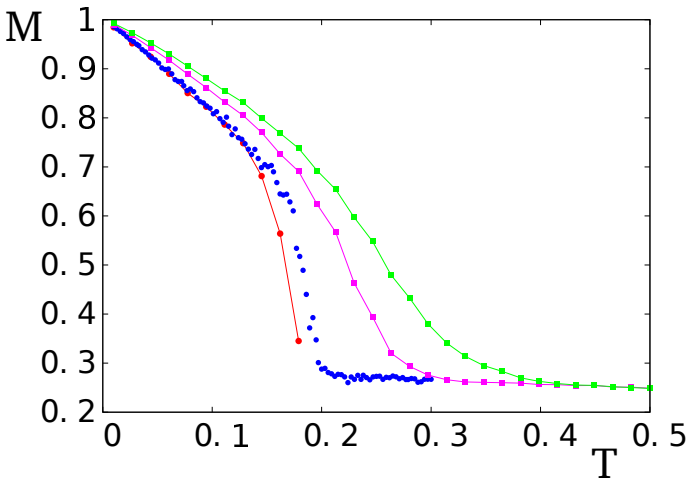

Figure IV.8: The order parameter $M(T)$ versus T for several waiting times t, for $H = 0.5$ and $N = 800$: from above $t = 10^5$, 2×10^5, 10^6, ∞ (by fitting with Eq. (IV.7).

We have studied finite-size effects on the phase transition at T_c and we have seen that from $N = 800$, all curves coincide within statistical errors: there is thus no observable finite size effects for $N \geq 800$. The skyrmion lattice phase remains stable for very large sizes (up to $N = 1800$ used in our simulation), unlike other two-dimensional continuous spin systems such as ferromagnetic XY and Heisenberg spins [54, 128].

IV.4 Conclusion

In this chapter, we have shown that the competition between a ferromagnetic interaction J and a Dzyaloshinskii-Moriya interaction D under an applied magnetic field H in two dimensions generate a skyrmion crystal in a region of the phase space (D, H). The spin model is the classical Heisenberg model. We have numerically determined the ground state by minimizing the energy of spin by spin using an iteration procedure. The skyrmion lattice is then slowly heated to high temperatures by the use of Monte Carlo simulations. We have shown that the skyrmion lattice is stable up to a finite temperature T_c beyond which the system becomes disordered. We have also shown that the relaxation follows a stretched exponential law. This stability is observed in MnSi [9, 10] and FeCoSi [11, 72].

General Conclusion

In this thesis we have studied the phase transition in different spin systems with competing interactions using both Monte Carlo simulations and the Green's function method. Our investigations have been carried out on the BEG model, helimagnetic thin films with and without an applied field, and thin films with an antisymmetric Dzyaloshinshi interaction.

In the first chapter we have investigated the BEG model in a thin film of stacked triangular lattices with a thickness L_z. We have found that the nature of the first order phase transition is conserved when we reduce the film thickness and that the cross-over from second to first order transition observed in the bulk crystal is also conserved when varying the anisotropy. We have investigated also the surface effect on the layer magnetization. We found that the film shows a deficit of He^4 at the surface when we map the BEG model into a mixing of He^3 and He^4.

We have next studied in the second chapter a helimagnetic thin film of simple cubic lattice, this structure results from the competition between ferromagnetic and antiferromagnetic interactions. We have shown that due to the surface effect the helimagnetic structure undergoes a strong surface spin rearrangement. Using the Green's function method we have shown that when varying the surface exchange interaction, the surface localized acoustic and optical modes are detached from the bulk spin wave spectrum. These modes affect the critical temperature and cause a strong deviation of the surface magnetization from the bulk value. We have also investigate the effect of an applied magnetic field H on this spin structure. We have found that for a given value of H the spins of successive planes arrange themselves in a highly non-uniform structure out of the film surface, symmetric around the c axis perpendicular to the film surface. We call it the c-fan phase which results from the competition between the applied field and the antiferromagnetic interaction analogous to the spin flop phenomenon in an antiferromagnetic spin system in a field. Using Monte Carlo simulations, we have shown that the layers with large xy spin-components make a transition at a finite temperature while others do not. This "transverse" transition is possible because

the xy spin-components do not depend on the field applied along the c axis. This transition is a new phenomenon discovered here with our model. Using the quantum version of the model we have investigated the effect of quantum fluctuations. The results show that the zero-point spin contraction is different from layer to layer and there is a cross-over between the layer magnetizations at low temperature.

In the third chapter we have studied spin systems with the competition between the ferromagnetic interaction and a Dzyaloshinskii-Moriya interaction restricted in the xy plane. This competition gives rise to a non-collinear spin structure with a turn angle θ between neighboring spins in the xy planes. Using the Green's function method we have found that the spin-wave excitation in 2D and 3D crystals is stable at $T = 0$ without the need of an anisotropy. However, in the case of thin films we need a small anisotropy to stabilize it because of the lack of neighbors at the surface. Among the results, we have found that the spin-wave energy E depends on the magnitude of DM interaction D and that in the long wave-length limit, E is proportional to k^2 for small D but is linear in k for strong D.

In chapter IV we have investigated the phase diagram of a 2D spin system with a ferromagnetic interaction J, a Dzyaloshinskii-Moriya interaction of strength D and an applied field H perpendicular to the plane. We have found that the competition between these interactions entails the generation of a skyrmion crystal in a region of the phase space (D, H). By Monte Carlo simulations we have shown that the skyrmion lattice is stable up to a finite temperature T_c and that the relaxation follows a stretched exponential law.

The work in this thesis shows that the competition of various interactions between spins in the system gives rise to spectacular phenomena. We have seen in this work that the combination of the frustration and the surface effect enhances the possibility to discover unexpected behaviors in thin films. The next step in our investigations would focus on the spin transport properties of the systems considered in this thesis. This project is motivated by the fact that the transport of itinerant spins in magnetically ordered systems depends on the local spin-spin relaxation, so that our highly non-uniform spin systems found in this thesis would be excellent candidates to find exotic transport properties which are of application interest [80–83].

List of publications

[1] Sahbi El Hog and H. T. Diep, Mod. Phys. Lett. B 30, 1650071 (2016), DOI: 10.1142/S0217984916500718 , https://hal.archives-ouvertes.fr/hal-01138267 , http://arxiv.org/abs/1504.01372

[2] Sahbi El Hog and H. T. Diep, Helimagnetic Thin Films: Surface Reconstruction, Surface Spin-Waves, Magnetization, J. Magn. and Magn. Mater. 400, 276-281 (2016), arXiv:1508.01367; https://hal.archives-ouvertes.fr/hal-01183084.

[3] Sahbi El Hog and H. T. Diep, Partial phase transition and quantum effects in helimagnetic films under an applied magnetic field, J. Magn. and Magn. Mater. 429, 102-109 (2017), https://arxiv.org/abs/1612.06440, https://hal.archives-ouvertes.fr/hal-01415583

[4] Sahbi El Hog, H. T. Diep and Henryk Puszkarski, Theory of magnons in spin systems with Dzyaloshinskii-Moriya interaction, submitted to Phys. Rev. B, arXiv:1612.04147

[5] Sahbi El Hog, A. Bailly-Reyre and H. T. Diep, Stability and Phase Transition of Skyrmion Crystals Generated by Dzyaloshinskii-Moriya Interaction, submitted to Phys. Rev. B, arXiv:1702.06841

Appendices

Appendix A

Monte Carlo Techniques

A.1 Simple Sampling

The goal behind a Monte Carlo (MC) simulation is the calculation of the average value of observable Q, such as magnetization or internal energy. This average value is defined by averaging the quantity of interest over all states μ of the system, weighting each with its own Boltzmann probability:

$$\langle Q \rangle = \frac{\sum_\mu Q_\mu e^{-\beta E_\mu}}{\sum_\mu e^{-\beta E_\mu}} \tag{A.1}$$

The total number of states in a system of N Ising spins is 2^N. This is a huge number when N is large. In most numerical calculations it is only possible to sample a very small set of states among the total number of states. The results depend on the manner in which the subset of states is chosen. The simplest procedure is to choose a subset $\mathcal{C}$ of states in a random manner and average over them:

$$Q_c = \frac{\sum_i^c Q_{\mu_i} e^{-\beta E_{\mu_i}}}{\sum_i^c e^{-\beta E_{\mu_i}}} \tag{A.2}$$

Q_c is called the estimator of $\langle Q \rangle$, it is obvious that, as the number $\mathcal{C}$ of states sample increases the more precise Q_c becomes, and when $\mathcal{C} \to \infty$ we have $Q_c = \langle Q \rangle$. However this is a poor choice, because the probability of obtaining the most important states at a finite temperature is very low, this makes a very inaccurate estimation of the average value $\langle Q \rangle$.

A.2 Importance Sampling

The importance sampling is based on the principle that instead of picking our $\mathcal{C}$ states in a random manner, we pick them using the canonical probability, so that the probability that a particular state μ gets chosen is $P_\mu = Z^{-1}e^{-\beta E_\mu}$, then the average value $\langle Q \rangle$ becomes

$$\langle Q \rangle = \frac{1}{\mathcal{C}} \sum_{\mu}^{c} Q_\mu \tag{A.3}$$

The remaining question is how to generate our states according to the canonical probability. An answer of this question is to generate a series of states in an independent manner called Markov chain.

A.2.1 Markov processes

In all Monte Carlo simulations the generation of states is assured by the Markov processes, which starts from a given state μ and generates a new state ν according to the transition probability $P(\mu \to \nu)$ which depends on the properties of the states μ and ν. This transition probability should not vary over time and should satisfy the constraint $\sum_\nu P(\mu \to \nu) = 1$.

We use this process to generate a Markov chain of states starting from any state of the system. In order to achieve the equilibrium, the Markov process must obey two conditions, the conditions of ergodicity and detailed balance.

A.2.2 Ergodicity and Detailed Balance

The condition of ergodicity is the requirement that any state of the system should be accessible from any other state with non-zero probability. The second condition placed on our Markov process is the condition of detailed balance, it requires that the rate at which the system makes transition into and out of state must be equal:

$$p_\mu P(\mu \to \nu) = p_\nu P(\nu \to \mu) \tag{A.4}$$

This condition guarantees that it is the Boltzmann probability that we generate by the Markov process when our system is in equilibrium. It tells us that the transition probabilities should satisfy the equation:

$$\frac{P(\mu \to \nu)}{P(\nu \to \mu)} = \frac{p_\nu}{p_\mu} = e^{-\beta(E_\nu - E_\mu)} \tag{A.5}$$

A.3 The Metropolis Algorithm

Our computer program is based on the Metropolis algorithm. This algorithm used here uses a single-spin flip dynamics which guarantees the ergodicity, since we can change from any state to another by flipping one spin by which the two states differ. It uses also the transition probability $P(\mu \to \nu)$ which depends on the energy difference between the initial and final states in the following way: if the selected new state has an energy lower than or equal to the present one, we should accept the transition to that state. If not, we accept it with the probability $P(\mu \to \nu) = e^{-\beta(E_\nu - E\mu)}$.

A.3.1 Implementing the Metropolis algorithm

The way the Metropolis algorithm is implemented can be described as follows: to start we should chose the spin model, the lattice system and apply the periodic boundary condition (PBC). Since the simulation is performed on a finite system the PBC ensures that all spins have the same number of neighbors. In the canonical method, we need to fix the temperature at which we want to perform our simulation. We choose the initial spin configuration of the system. although the nature of this initial state μ is not too important, a good choice can reduce the time taken to reach the equilibrium state. The first step in the simulation is to generate a new state ν: this new state differs from the the present by the flip of just one spin. In the second step we calculate the energy difference $\Delta E = E_\nu - E_\mu$ between the two states, then we apply the Metropolis criterion: if $\Delta E \leqslant 0$ we accept the new state and if $\Delta E > 0$, we accept the new state with a probability $e^{-\beta(E_\nu - E\mu)}$. We can do this by comparing the transition probability to a random number "r" between $[0, 1[$: if this number is less than our transition probability we accept the new state, if not we reject it.

We repeat these procedures until the system reaches equilibrium at the selected temperature. As we perform our simulation over a range of temperatures, we use the final state of this simulation as an initial state for the nearby temperature, the justification for doing this is to help our system come to equilibrium much faster than if we start with a random initial state.

A.4 Equilibration

Once the computer program is written, we have to run our simulation during a period of time called "equilibration time" τ_{eq} until our system reaches equilibrium. This means that the probability to find our system in any

particular state is proportional to the Boltzmann weight $e^{-\beta E_\mu}$

To judge if our system has reached equilibrium or not, we can look at the evolution of some quantities like magnetization per spin or the energy as functions of Monte Carlo time.

It is possible that the system is stuck in some metastable region of its state space. To resolve this problem we can perform many different simulations of the same system, starting them in different initial states using different "seeds" for the random generator. This ensures that the system takes different paths to equilibrium: if this is the case, then the magnetization or energy, has the same value within statistical errors for different paths.

Appendix B

Single Histogram Method

The single histogram method proposed by Ferrenberg and Swendsen [129] is a technique which allows us to perform a single Monte Carlo simulation at a specific temperature then extrapolate the results to other nearby temperatures. This method is based on the idea that, from the energy histogram established at temperature T_0 we can estimate the density of states and from this distribution we can calculate the canonical probability $P(T, E)$ at neighboring temperatures T around T_0. Using these probabilities, we can calculate average values of physical quantities as continuous functions of T.

The method is described in the following : we perform a Monte Carlo simulation at $T = T_0$ which generates configurations according to the Boltzmann weight $e^{-\beta_0 E}$. The energy histogram of these states is recorded during the simulation and it provides an estimation of the probability $P(T_0, E) = H(E)/N$, where N is the number of Monte Carlo steps. This estimation becomes exact in the limit of an infinite-length run. We have

$$H(E) = \frac{N}{Z(T_0)} W(E) e^{-\beta_0 E} \tag{B.1}$$

where $Z(T_0)$ is the partition function at T_0 and $W(E)$ is an estimation of the density of states. We invert this equation to determine $W(E)$:

$$W(E) = \frac{Z(T_0)}{N} H(E) e^{\beta_0 E} \tag{B.2}$$

We consider now a temperature T near T_0, the probability $P(T, E)$ is written by

$$P(T, E) = \frac{W(E)}{Z(T)} e^{-\beta E} \tag{B.3}$$

We use equation (B.2) to replace $W(E)$ in equation (B.3), we find the relationship between the histogram $H(E)$ established at $T = T_0$ and the probability distribution for nearby temperatures:

$$P(T, E) = \frac{H(E)e^{(\beta_0 - \beta)E}}{\sum_E H(E)e^{(\beta_0 - \beta)E}} \tag{B.4}$$

From these probabilities we can calculate the average value of any function of E, denoted by $A(E)$, as a continuous function of T:

$$\langle A(E) \rangle = \sum_E A(E)P(T, E) \tag{B.5}$$

In the standard Metropolis Monte Carlo simulation, we calculate this average at discrete temperatures then we extrapolate the results between them. However, near the transition temperature, extrapolation is not possible because thermodynamic derivations such as C_v and χ diverge at the transition temperature. Thus, we cannot find the exact location of their peaks. On the contrary, with the ability to continuously vary T offered by the histogram method we can locate this critical point T_c and study the critical behavior. We have used here the histogram of internal energy, however we can apply also the histogram method to other variables, such as magnetization for example.

We use a very large number of Monte Carlo steps to establish the histogram $H(E)$ at T_0 in order to include as many as possible microscopic states in the sum. The estimation of the histogram of energy at temperature T far from T_0 is calculated by re-weighting the bins of the histogram $H(E)$ with an exponential factor which depends on the difference of temperature. However, if the number of states sampled by a Monte Carlo simulation is relatively small, then we cannot calculate an histogram at T too far from the temperature T_0 of the original simulation. We will have a histogram with large statistical errors leading to unreliable results when we calculate average values of physical quantities.

Bibliography

[1] Mark H. Kryder. Magnetic thin films for data storage. *Thin Solid Films*, 216(1):174 – 180, 1992.

[2] K. Akabli, Y. Magnin, Masataka Oko, Isao Harada, and H. T. Diep. Theory and simulation of spin transport in antiferromagnetic semiconductors: Application to mnte. *Phys. Rev. B*, 84:024428, Jul 2011.

[3] D.C. Ralph and M.D. Stiles. Spin transfer torques. *Journal of Magnetism and Magnetic Materials*, 320(7):1190 – 1216, 2008.

[4] Kai-Shin Li, Yin-Ming Chang, Santhanam Agilan, Jhen-Yong Hong, Jung-Chi Tai, Wen-Chung Chiang, Keisuke Fukutani, P. A. Dowben, and Minn-Tsong Lin. Organic spin valves with inelastic tunneling characteristics. *Phys. Rev. B*, 83:172404, May 2011.

[5] H.T.Diep. Theory of magnetism application to surface physics. *World Scientific, Singapore*, 2014.

[6] H. T. Diep. Frustrated spin systems. *2nd edition, World Scientific (2013).*

[7] J Villain. Spin glass with non-random interactions. *Journal of Physics C: Solid State Physics*, 10(10):1717, 1977.

[8] J Vannimenus and G Toulouse. Theory of the frustration effect. ii. ising spins on a square lattice. *Journal of Physics C: Solid State Physics*, 10(18):L537, 1977.

[9] S. Mühlbauer, B. Binz, F. Jonietz, C. Pfleiderer, A. Rosch, A. Neubauer, R. Georgii, and P. Böni. Skyrmion lattice in a chiral magnet. *Science*, 323(5916):915–919, 2009.

[10] Akira Tonomura, Xiuzhen Yu, Keiichi Yanagisawa, Tsuyoshi Matsuda, Yoshinori Onose, Naoya Kanazawa, Hyun Soon Park, and Yoshinori

Tokura. Real-space observation of skyrmion lattice in helimagnet mnsi thin samples. *Nano Letters*, 12(3):1673–1677, 2012. PMID: 22360155.

[11] W. Münzer, A. Neubauer, T. Adams, S. Mühlbauer, C. Franz, F. Jonietz, R. Georgii, P. Böni, B. Pedersen, M. Schmidt, A. Rosch, and C. Pfleiderer. Skyrmion lattice in the doped semiconductor $fe_{1-x}co_xSi$. *Phys. Rev. B*, 81:041203, Jan 2010.

[12] M. Blume, V. J. Emery, and Robert B. Griffiths. Ising model for the λ transition and phase separation in he^3-he^4 mixtures. *Phys. Rev. A*, 4:1071–1077, Sep 1971.

[13] Kathie E. Newman and John D. Dow. Zinc-blende¯diamond order-disorder transition in metastable crystalline $(GaAs)_{1-x}ge_{2x}$ alloys. *Phys. Rev. B*, 27:7495–7508, Jun 1983.

[14] M. Schick and Wei-Heng Shih. Spin-1 model of a microemulsion. *Phys. Rev. B*, 34:1797–1801, Aug 1986.

[15] Miron Kaufman and Michael Kanner. Random-field blume-capel model: Mean-field theory. *Phys. Rev. B*, 42:2378–2382, Aug 1990.

[16] A. N. Berker and Michael Wortis. Blume-emery-griffiths-potts model in two dimensions: Phase diagram and critical properties from a position-space renormalization group. *Phys. Rev. B*, 14:4946–4963, Dec 1976.

[17] I. Puha, H. T. Diep, and I. Campbell. Phase diagram for a frustrated disordered blume–emery–griffiths model. *Journal of Applied Physics*, 85(8), 1999.

[18] A. Rachadi and A. Benyoussef. Monte carlo study of the blume-emery-griffiths model at the ferromagnetic-antiquadrupolar-disordered phase interface. *Phys. Rev. B*, 69:064423, Feb 2004.

[19] A. Maciołek, M. Krech, and S. Dietrich. Phase diagram of a model for ^{3}He$-^4$He mixtures in three dimensions. *Phys. Rev. E*, 69:036117, Mar 2004.

[20] N. Farahmand Bafi, A. Maciołek, and S. Dietrich. Phase diagram of fluid phases in ^{3}He $-^4$He mixtures. *Phys. Rev. E*, 91:022138, Feb 2015.

[21] T. Balcerzak and M. Gzik. Phase diagrams of a double layer with spin 1. *physica status solidi (b)*, 199(2):541–548, 2 1997.

[22] X.T. Pham Phu, V. Thanh Ngo, and H.T. Diep. Critical behavior of magnetic thin films. *Surface Science*, 603(1):109 – 116, 2009.

[23] X. T. Pham Phu, V. Thanh Ngo, and H. T. Diep. Crossover from first- to second-order transition in frustrated ising antiferromagnetic films. *Phys. Rev. E*, 79:061106, Jun 2009.

[24] S. B. Kim, J. Ma, and M. H. W. Chan. Phase diagram of $^3-^4$he mixture in aerogel. *Phys. Rev. Lett.*, 71:2268–2271, Oct 1993.

[25] Robert B. Griffiths. Spontaneous magnetization in idealized ferromagnets. *Phys. Rev.*, 152:240–246, Dec 1966.

[26] *Finite-size scaling, Phase Transitions and Critical Phenomena*. Academic Press, London, 1983.

[27] V. G. Ivantsov B. N. Esel'son and Zh. Eksp. Teor. Fiz. A. D. Shvetz. Surface tension of he^3-he^4 solutions. *Sov. Phys.—JETP*, 17:330–332, 1963.

[28] Akio Yoshimori. A new type of antiferromagnetic structure in the rutile type crystal. *Journal of the Physical Society of Japan*, 14(6):807–821, 1959.

[29] J. Villain. La structure des substances magnetiques. *Journal of Physics and Chemistry of Solids*, 11(3):303 – 309, 1959.

[30] V Leiner, D Labergerie, R Siebrecht, Ch Sutter, and H Zabel. Investigation of the magnetism in thin single ho(00.1) films via neutron reflectivity measurements. *Physica B: Condensed Matter*, 283(1–3):167 – 170, 2000.

[31] Dory Hélio A. L. Anselmo, Vamberto D. Mello, and Manoel S. Vasconcelos. Simulation of the magnetocaloric effect in tb nanofilms. *AIP Conference Proceedings*, 1590(1), 2014.

[32] M. B. Salamon, Shantanu Sinha, J. J. Rhyne, J. E. Cunningham, Ross W. Erwin, Julie Borchers, and C. P. Flynn. Long-range incommensurate magnetic order in a dy-y multilayer. *Phys. Rev. Lett.*, 56:259–262, Jan 1986.

[33] L.P. Régnault, J. Rossat-Mignod, A. Adam, D. Billerey, and C. Terrier. Inelastic neutron scattering investigation of the magnetic excitations in the helimagnetic state of NiBr2. *Journal de Physique*, 43(8):1283–1290, 1982.

[34] Romhányi J. Onykiienko Y. A. Henschel A. Schmidt M. Cameron A. S. Surmach M. A. Lim J. A. Park J. T. Schneidewind A. Abernathy D. L. Rosner H. van den Brink Jeroen Inosov D. S. Portnichenko, P. Y. Magnon spectrum of the helimagnetic insulator Cu2OSeO3. *Nature Communications*, 7:10725, 1982.

[35] J Beille, J Voiron, F Towfiq, M Roth, and Z Y Zhang. Helimagnetic structure of the fe x co 1-x si alloys. *Journal of Physics F: Metal Physics*, 11(10):2153, 1981.

[36] H Nakamura, N Metoki, S Suzuki, F Takayanagi, and M Shiga. Helimagnetic structure of ymn 2 observed by means of nuclear magnetic resonance and neutron diffraction. *Journal of Physics: Condensed Matter*, 13(3):475, 2001.

[37] V. Thanh Ngo and H. T. Diep. Phase transition in heisenberg stacked triangular antiferromagnets: End of a controversy. *Phys. Rev. E*, 78:031119, Sep 2008.

[38] P Bak and M H Jensen. Theory of helical magnetic structures and phase transitions in mnsi and fege. *Journal of Physics C: Solid State Physics*, 13(31):L881, 1980.

[39] S. V. Maleyev. Cubic magnets with dzyaloshinskii-moriya interaction at low temperature. *Phys. Rev. B*, 73:174402, May 2006.

[40] H. T. Diep. Magnetic transitions in helimagnets. *Phys. Rev. B*, 39:397–404, Jan 1989.

[41] V. Thanh Ngo and H. T. Diep. Stacked triangular xy antiferromagnets: End of a controversial issue on the phase transition. *Journal of Applied Physics*, 103(7), 2008.

[42] Jan Heurich, Jürgen König, and A. H. MacDonald. Persistent spin currents in helimagnets. *Phys. Rev. B*, 68:064406, Aug 2003.

[43] O. Wessely, B. Skubic, and L. Nordström. Spin-transfer torque in helical spin-density waves. *Phys. Rev. B*, 79:104433, Mar 2009.

[44] Isao Harada and Kazuko Motizuki. Effect of magnon-magnon interaction on spin wave dispersion and magnon sideband in mns. *Journal of the Physical Society of Japan*, 32(4):927–940, 1972.

[45] E Rastelli, L Reatto, and A Tassi. Quantum fluctuations in helimagnets. *Journal of Physics C: Solid State Physics*, 18(2):353, 1985.

[46] H. T. Diep. Low-temperature properties of quantum heisenberg helimagnets. *Phys. Rev. B*, 40:741–744, Jul 1989.

[47] R. Quartu and H.T. Diep. Phase diagram of body-centered tetragonal helimagnets. *Journal of Magnetism and Magnetic Materials*, 182(1):38 – 48, 1998.

[48] S. M. Stishov, A. E. Petrova, S. Khasanov, G. Kh. Panova, A. A. Shikov, J. C. Lashley, D. Wu, and T. A. Lograsso. Magnetic phase transition in the itinerant helimagnet MnSi: Thermodynamic and transport properties. *Phys. Rev. B*, 76:052405, Aug 2007.

[49] V. D. Mello, C. V. Chianca, Ana L. Dantas, and A. S. Carriço. Magnetic surface phase of thin helimagnetic films. *Phys. Rev. B*, 67:012401, Jan 2003.

[50] E. Weschke, H. Ott, E. Schierle, C. Schüßler-Langeheine, D. V. Vyalikh, G. Kaindl, V. Leiner, M. Ay, T. Schmitte, H. Zabel, and P. J. Jensen. Finite-size effect on magnetic ordering temperatures in long-period antiferromagnets: Holmium thin films. *Phys. Rev. Lett.*, 93:157204, Oct 2004.

[51] E. A. Karhu, S. Kahwaji, M. D. Robertson, H. Fritzsche, B. J. Kirby, C. F. Majkrzak, and T. L. Monchesky. Helical magnetic order in mnsi thin films. *Phys. Rev. B*, 84:060404, Aug 2011.

[52] V Thanh Ngo and H T Diep. Frustration effects in antiferromagnetic face-centered cubic heisenberg films. *Journal of Physics: Condensed Matter*, 19(38):386202, 2007.

[53] V. Thanh Ngo and H. T. Diep. Effects of frustrated surface in heisenberg thin films. *Phys. Rev. B*, 75:035412, Jan 2007.

[54] N. D. Mermin and H. Wagner. Absence of ferromagnetism or antiferromagnetism in one- or two-dimensional isotropic heisenberg models. *Phys. Rev. Lett.*, 17:1133–1136, Nov 1966.

[55] D N Zubarev. Double-time green functions in statistical physics. *Soviet Physics Uspekhi*, 3(3):320, 1960.

[56] Yu. G. Rudoy. The bogoliubov-tyablikov green's function method in the quantum theory of magnetism. *Theoretical and Mathematical Physics*, 168(3):1318–1329, 2011.

[57] H. T. Diep. Quantum effects in heisenberg antiferromagnetic thin films. *Phys. Rev. B*, 43:8509–8515, Apr 1991.

[58] H. T. Diep. Theory of antiferromagnetic superlattices at finite temperatures. *Phys. Rev. B*, 40:4818–4823, Sep 1989.

[59] A. N. Bogdanov, A. V. Zhuravlev, and U. K. Rößler. Spin-flop transition in uniaxial antiferromagnets: Magnetic phases, reorientation effects, and multidomain states. *Phys. Rev. B*, 75:094425, Mar 2007.

[60] H. T. Diep. Quantum theory of helimagnetic thin films. *Phys. Rev. B*, 91:014436, Jan 2015.

[61] I.E.Dzyaloshinskii. Thermodynamic theory of weak ferromagnetism in antiferromagnetic substances. *Soviet Physics JETP*, 5:1259, 1957.

[62] Tôru Moriya. Anisotropic superexchange interaction and weak ferromagnetism. *Phys. Rev.*, 120:91–98, Oct 1960.

[63] I. A. Sergienko and E. Dagotto. Role of the dzyaloshinskii-moriya interaction in multiferroic perovskites. *Phys. Rev. B*, 73:094434, Mar 2006.

[64] Claude Ederer and Nicola A. Spaldin. Weak ferromagnetism and magnetoelectric coupling in bismuth ferrite. *Phys. Rev. B*, 71:060401, Feb 2005.

[65] Igor Solovyev, Noriaki Hamada, and Kiyoyuki Terakura. Crucial role of the lattice distortion in the magnetism of lamno$_3$. *Phys. Rev. Lett.*, 76:4825–4828, Jun 1996.

[66] Xin-Yi Wang, Lin Gan, Shi-Wei Zhang, and Song Gao. Perovskite-like metal formates with weak ferromagnetism and as precursors to amorphous materials. *Inorganic Chemistry*, 43(15):4615–4625, 2004. PMID: 15257590.

[67] T. Kimura, G. Lawes, T. Goto, Y. Tokura, and A. P. Ramirez. Magnetoelectric phase diagrams of orthorhombic $r$mno$_3$ (r = Gd, tb, and dy). *Phys. Rev. B*, 71:224425, Jun 2005.

[68] Shi-Zeng Lin, Avadh Saxena, and Cristian D. Batista. Skyrmion fractionalization and merons in chiral magnets with easy-plane anisotropy. *Phys. Rev. B*, 91:224407, Jun 2015.

[69] Su Do Yi, Shigeki Onoda, Naoto Nagaosa, and Jung Hoon Han. Skyrmions and anomalous hall effect in a dzyaloshinskii-moriya spiral magnet. *Phys. Rev. B*, 80:054416, Aug 2009.

[70] S. X. Huang and C. L. Chien. Extended skyrmion phase in epitaxial FeGe(111) thin films. *Phys. Rev. Lett.*, 108:267201, Jun 2012.

[71] Y. Onose K. Kimoto W. Z. Zhang S. Ishiwata Y. Matsui X. Z. Yu, N. Kanazawa and Y. Tokura. Near room-temperature formation of a skyrmion crystal in thin-films of the helimagnet FeGe. *Nat Mater*, 10:106, 2011.

[72] Y. Onose K. Kimoto W. Z. Zhang S. Ishiwata Y. Matsui X. Z. Yu, N. Kanazawa and Y. Tokura. Real-space observation of a two-dimensional skyrmion crystal. *Nature*, 465:901, 2010.

[73] S. Seki, X. Z. Yu, S. Ishiwata, and Y. Tokura. Observation of skyrmions in a multiferroic material. *Science*, 336(6078):198–201, 2012.

[74] Masaya Uchida, Yoshinori Onose, Yoshio Matsui, and Yoshinori Tokura. Real-space observation of helical spin order. *Science*, 311(5759):359–361, 2006.

[75] M. Heide, G. Bihlmayer, and S. Blügel. Dzyaloshinskii-moriya interaction accounting for the orientation of magnetic domains in ultrathin films: Fe/w(110). *Phys. Rev. B*, 78:140403, Oct 2008.

[76] S. Rohart and A. Thiaville. Skyrmion confinement in ultrathin film nanostructures in the presence of dzyaloshinskii-moriya interaction. *Phys. Rev. B*, 88:184422, Nov 2013.

[77] Arseni Goussev, J. M. Robbins, Valeriy Slastikov, and Oleg A. Tretiakov. Dzyaloshinskii-moriya domain walls in magnetic nanotubes. *Phys. Rev. B*, 93:054418, Feb 2016.

[78] Han Kheng Teoh, Sarjoosing Goolaup, and Wen Siang Lew. Dzyaloshinskii–moriya interaction induced domain wall depinning anomaly in ferromagnetic nanowire. *Journal of Physics D: Applied Physics*, 50(1):015004, 2017.

[79] André Thiaville, Stanislas Rohart, Émilie Jué, Vincent Cros, and Albert Fert. Dynamics of dzyaloshinskii domain walls in ultrathin magnetic films. *EPL (Europhysics Letters)*, 100(5):57002, 2012.

[80] F. Jonietz, S. Mühlbauer, C. Pfleiderer, A. Neubauer, W. Münzer, A. Bauer, T. Adams, R. Georgii, P. Böni, R. A. Duine, K. Everschor, M. Garst, and A. Rosch. Spin transfer torques in mnsi at ultralow current densities. *Science*, 330(6011):1648–1651, 2010.

[81] V. Cros A. Fert and J. Sampaio. Skyrmions on the track. *Nat Nano*, 8:152, 2013.

[82] Y. Tokura and N. Nagaosa. Orbital physics in transition-metal oxides. *Science*, 288(5465):462–468, 2000.

[83] D. A. Allwood, G. Xiong, C. C. Faulkner, D. Atkinson, D. Petit, and R. P. Cowburn. Magnetic domain-wall logic. *Science*, 309(5741):1688–1692, 2005.

[84] H. Puszkarski and P. E. Wigen. Effect of dzialoshinsky-moriya interactions on propagation of spin waves in ferromagnets: Dynamical canting. *Phys. Rev. Lett.*, 35:1017–1018, Oct 1975.

[85] Kh. Zakeri, Y. Zhang, J. Prokop, T.-H. Chuang, N. Sakr, W. X. Tang, and J. Kirschner. Asymmetric spin-wave dispersion on fe(110): Direct evidence of the dzyaloshinskii-moriya interaction. *Phys. Rev. Lett.*, 104:137203, Mar 2010.

[86] Weiwei Wang, Maximilian Albert, Marijan Beg, Marc-Antonio Bisotti, Dmitri Chernyshenko, David Cortés-Ortuño, Ian Hawke, and Hans Fangohr. Magnon-driven domain-wall motion with the dzyaloshinskii-moriya interaction. *Phys. Rev. Lett.*, 114:087203, Feb 2015.

[87] A. A. Stashkevich, M. Belmeguenai, Y. Roussigné, S. M. Cherif, M. Kostylev, M. Gabor, D. Lacour, C. Tiusan, and M. Hehn. Experimental study of spin-wave dispersion in py/pt film structures in the presence of an interface dzyaloshinskii-moriya interaction. *Phys. Rev. B*, 91:214409, Jun 2015.

[88] Jung-Hwan Moon, Soo-Man Seo, Kyung-Jin Lee, Kyoung-Whan Kim, Jisu Ryu, Hyun-Woo Lee, R. D. McMichael, and M. D. Stiles. Spin-wave propagation in the presence of interfacial dzyaloshinskii-moriya interaction. *Phys. Rev. B*, 88:184404, Nov 2013.

[89] A. N. Bogdanov and U. K. Rößler. Chiral symmetry breaking in magnetic thin films and multilayers. *Phys. Rev. Lett.*, 87:037203, Jun 2001.

[90] K. von Bergmann P. Ferriani S. Heinze G. Bihlmayer A. Kubetzka O. Pietzsch S. Blügel M. Bode, M. Heide and R. Wiesendange. Chiral magnetic order at surfaces driven by inversion asymmetry. *Nature*, 447:190, 05 2007.

[91] J. C. S. Levy, Diep-The-Hung and O. Nagai. Effects of surface spin waves and surface anisotropy in magnetic thin films at finite temperatures. *physica status solidi (b)*, 93(1):351–361, 1979.

[92] T.H.R. Skyrme. A unified field theory of mesons and baryons. *Nuclear Physics*, 31:556 – 569, 1962.

[93] D.A. Yablonskii A.N. Bogdanov. Thermodynamically stable "vortices" in magnetically ordered crystals. the mixed state of magnets. *JETP Lett.*, 68:101, 1989.

[94] Wagner. M Franz. C Bauer. A Pfleiderer. C. Ritz, R Halder. M. Formation of a topological non-fermi liquid in mnsi. *Nature*, 497:231, 1989.

[95] A. Neubauer, C. Pfleiderer, B. Binz, A. Rosch, R. Ritz, P. G. Niklowitz, and P. Böni. Topological hall effect in the *a* phase of mnsi. *Phys. Rev. Lett.*, 102:186602, May 2009.

[96] C. Pappas, E. Lelièvre-Berna, P. Falus, P. M. Bentley, E. Moskvin, S. Grigoriev, P. Fouquet, and B. Farago. Chiral paramagnetic skyrmion-like phase in mnsi. *Phys. Rev. Lett.*, 102:197202, May 2009.

[97] Olivier Boulle and all. Room-temperature chiral magnetic skyrmions in ultrathin magnetic nanostructures. *Nature Nanotechnology*, 11:449, January 2016.

[98] X. Z. White J. S. Rønnow H. M. Morikawa D. Taguchi Y. Tokura Y. Tokunaga, Y. Yu. A new class of chiral materials hosting magnetic skyrmions beyond room temperature. 6, 2015.

[99] Kirsten. Menzel Matthias. Brede Jens. Kubetzka Andre. Wiesendanger Roland. Bihlmayer Gustav. Blugel Stefan Heinze, Stefan. von Bergmann. Spontaneous atomic-scale magnetic skyrmion lattice in two dimensions. *Nat Phys*, 7:713–718, 2011.

[100] Niklas Romming, Christian Hanneken, Matthias Menzel, Jessica E. Bickel, Boris Wolter, Kirsten von Bergmann, André Kubetzka, and Roland Wiesendanger. Writing and deleting single magnetic skyrmions. *Science*, 341(6146):636–639, 2013.

[101] N S Kiselev, A N Bogdanov, R Schäfer, and U K Rößler. Chiral skyrmions in thin magnetic films: new objects for magnetic storage technologies. *Journal of Physics D: Applied Physics*, 44(39):392001, 2011.

[102] Motohiko Ezawa. Giant skyrmions stabilized by dipole-dipole interactions in thin ferromagnetic films. *Phys. Rev. Lett.*, 105:197202, Nov 2010.

[103] N. S. Kiselev, A. N. Bogdanov, R. Schäfer, and U. K. Rößler. Comment on "giant skyrmions stabilized by dipole-dipole interactions in thin ferromagnetic films". *Phys. Rev. Lett.*, 107:179701, Oct 2011.

[104] H. D. Rosales, D. C. Cabra, and Pierre Pujol. Three-sublattice skyrmion crystal in the antiferromagnetic triangular lattice. *Phys. Rev. B*, 92:214439, Dec 2015.

[105] Stefan Buhrandt and Lars Fritz. Skyrmion lattice phase in three-dimensional chiral magnets from monte carlo simulations. *Phys. Rev. B*, 88:195137, Nov 2013.

[106] H. Y. Kwon, S. P. Kang, Y. Z. Wu, and C. Won. Magnetic vortex generated by dzyaloshinskii–moriya interaction. *Journal of Applied Physics*, 113(13):133911, 2013.

[107] H.Y. Kwon, K.M. Bu, Y.Z Wu, and C. Won. Effect of anisotropy and dipole interaction on long-range order magnetic structures generated by dzyaloshinskii–moriya interaction. *Journal of Magnetism and Magnetic Materials*, 324(13):2171 – 2176, 2012.

[108] A. N. Bogdanov, U. K. Rößler, and A. A. Shestakov. Skyrmions in nematic liquid crystals. *Phys. Rev. E*, 67:016602, Jan 2003.

[109] A. O. Leonov, I. E. Dragunov, U. K. Rößler, and A. N. Bogdanov. Theory of skyrmion states in liquid crystals. *Phys. Rev. E*, 90:042502, Oct 2014.

[110] Paul J. Ackerman, Rahul P. Trivedi, Bohdan Senyuk, Jao van de Lagemaat, and Ivan I. Smalyukh. Two-dimensional skyrmions and other solitonic structures in confinement-frustrated chiral nematics. *Phys. Rev. E*, 90:012505, Jul 2014.

[111] N.R. Cooper. Skyrmions in quantum hall systems with realistic force laws. *Physica E: Low-dimensional Systems and Nanostructures*, 1(1–4):62 – 64, 1997.

[112] Skyrmions in quantum hall systems. *International Journal of Modern Physics B*, 17(28):5007–5010, 2003.

[113] Condensed-matter physics: Single skyrmions spotted. *Nature*, 465, 2010.

[114] Mark Vousden, Maximilian Albert, Marijan Beg, Marc-Antonio Bisotti, Rebecca Carey, Dmitri Chernyshenko, David Cortés-Ortuño, Weiwei Wang, Ondrej Hovorka, Christopher H. Marrows, and Hans Fangohr. Skyrmions in thin films with easy-plane magnetocrystalline anisotropy. *Applied Physics Letters*, 108(13):132406, 2016.

[115] Brian B. Balk Andrew L. Kirby Brian J. Fischer Peter. Pierce Daniel T. Unguris John. Borchers Julie A. Liu Kai Gilbert, Dustin A. Maranville. Realization of ground-state artificial skyrmion lattices at room temperature. *Nature Communications*, 6, 2015.

[116] Satoru Hayami, Shi-Zeng Lin, and Cristian D. Batista. Bubble and skyrmion crystals in frustrated magnets with easy-axis anisotropy. *Phys. Rev. B*, 93:184413, May 2016.

[117] Tsuyoshi Okubo, Sungki Chung, and Hikaru Kawamura. Multiple-q states and the skyrmion lattice of the triangular-lattice heisenberg antiferromagnet under magnetic fields. *Phys. Rev. Lett.*, 108:017206, Jan 2012.

[118] Xiuzhen Yu, Maxim Mostovoy, Yusuke Tokunaga, Weizhu Zhang, Koji Kimoto, Yoshio Matsui, Yoshio Kaneko, Naoto Nagaosa, and Yoshinori Tokura. Magnetic stripes and skyrmions with helicity reversals. *Proceedings of the National Academy of Sciences*, 109(23):8856–8860, 2012.

[119] M. Parisi M. Mézard and M. Virasoro. Spin glass theory and beyond an introduction to the replica method and its applications. *World Scientific*, 1986.

[120] J C Phillips. Stretched exponential relaxation in molecular and electronic glasses. *Reports on Progress in Physics*, 59(9):1133, 1996.

[121] Andrew T. Ogielski. Dynamics of three-dimensional ising spin glasses in thermal equilibrium. *Phys. Rev. B*, 32:7384–7398, Dec 1985.

[122] De Dominicis, C., Orland, H., and Lainée, F. Stretched exponential relaxation in systems with random free energies. *J. Physique Lett.*, 46(11):463–466, 1985.

[123] R.M.C. de Almeida, N. Lemke, and I.A. Campbell. Stretched exponential relaxation and independent relaxation modes. *Brazilian Journal of Physics*, 30:701 – 707, 12 2000.

[124] Alain Billoire and I. A. Campbell. Dynamics in the sherrington-kirkpatrick ising spin glass at and above T_g. *Phys. Rev. B*, 84:054442, Aug 2011.

[125] Itsuko S. Suzuki and Masatsugu Suzuki. Stretched-exponential relaxation in the three-dimensional short-range ising spin-glass $cu_{0.5}co_{0.5}cl_2$-$fecl_3$ graphite bi-intercalation compound. *Phys. Rev. B*, 78:214404, Dec 2008.

[126] A. Malinowski, V. L. Bezusyy, R. Minikayev, P. Dziawa, Y. Syryanyy, and M. Sawicki. Spin-glass behavior in ni-doped $la_{1.85}sr_{0.15}cuo_4$. *Phys. Rev. B*, 84:024409, Jul 2011.

[127] Effect of disorder in the frustrated ising fcc antiferromagnet: phase diagram and stretched exponential relaxation. *Modern Physics Letters B*, 28(09):1450067, 2014.

[128] J M Kosterlitz and D J Thouless. Ordering, metastability and phase transitions in two-dimensional systems. *Journal of Physics C: Solid State Physics*, 6(7):1181, 1973.

[129] Alan M. Ferrenberg and Robert H. Swendsen. New monte carlo technique for studying phase transitions. *Phys. Rev. Lett.*, 61:2635–2638, Dec 1988.